Control and Effect of Glial Cell Activation on the Microscale Chronic Neural Interface toward Dynamic Control of Neural Environment

by

Taegyun Moon

A dissertation submitted in partial fulfillment
of the requirements for the degree of
Doctor of Philosophy
(Biomedical Engineering)
in The University of Michigan
2010

Doctoral Committee:

Professor Daryl R. Kipke, Chair
Assistant Professor Anuska Andjelkovic-Zochowska
Associate Professor Jan Stegemann
Associate Professor Shuichi Takayama

Soli Deo Gloria

오직 주님께 영광을
To the only God be glory

ACKNOWLEDGEMENTS

I am finishing my long journey of graduate study. It was all about a story how God worked on my life. My family and I experienced many milestones and challenges during this period: my father got cancer so I returned to Korea for a year and half to care for him, I got married, and my wife is now pregnant. Going through these tough or joyful times, I became closer to God and developed capability to understand and care for other people. This is such a precious experience that I would not exchange with anything else. Specifically, I had very hard time with my father when he got cancer and I stayed with him to support. Our relationship was broken and I came back to Ann Arbor with a broken heart after spending a year and half with him. Celebrating my defense with my father was hard to imagine at that point. However, God worked in a wonderful way to reconcile us by toughing the hearts of both of us. One late night when I was working on my experiments in the lab, I was physically and mentally exhausted because of much pressure. God reminded me how hard time my father had when he took chemotherapies and I had tears in my eyes because I gave him a hard time without understanding his pain of chemotherapy. To make a long story short, my father and I celebrated together after my finishing the oral defense.

I give my thanks to my wife Eun Young who supported and encouraged me through times. I would not be here without her continues love and prayer. Eun Young , you are the most precious gift God ever gave me in my life.

I thank my parents Byoungsoon Moon and Kyungsil Choi and Sukgoo Kang and Junghee Kim. Their sacrifice and prayer made what I am now. Also, I give thanks to my brothers and sisters: Jihye, Yougwook, Soyoung, Snaghyun, and Byoungsun for their encouragement and support.

I would like to thank my advisor, Dr. Daryl Kipke for providing me with the opportunity to work in his lab. I especially appreciate his leadership. He always encouraged me with lots of energy and positive perspective that help me to overcome challenges both in research and personal life. He also is a mentor with great tolerance. When I was returning to lab after a long absence for family issue, he welcomed me from the bottom of the heart. He also was very patient when my research was slow with encouraging me. I appreciate it.

I give my special thanks to my co-advisor, Dr. Anuska Andjelkovic-Zochowska for her support on this project. This project made a stiff curve after I met her a year ago. Her mentorship, expertise on biology and physical help were a tremendous support to me. Most of the biological works on this project were not possible without her support. I also cannot forget the help from Dr. Svetlana Stamatovic of the Andjelkovic-Zochowska's lab. She, not only provided me with advice on biology, but also she encouraged me whenever I had difficulty with cell culture work. She was always there to back me up when I needed her.

I thank Dr. Shuichi Takayama and Dr. Jan Stegemann for serving on my committee. They gave me a new perspective to look at my project, which was very helpful.

I give my thanks to my uncle, Dr. Chul S. Hyun for his mentoring on my carrier and life since my undergraduate, master's, and doctoral studies. Although he was very busy with teaching at Cornell medical school and his practice at doctoral office, he has been always willing to help me. I truly appreciate it.

I give my gratitude to my advisors of my master's study, Dr. Daehie Hong and Dr. Kyu Back Lee for their continued mentorship during my doctoral study. Their encouragement was such a great support to me.

I give my thanks to my tutor for the technical communication, Mimi Adam. She provided not only help for my English but also inspired me by asking me probing questions.

I give thanks to the former and current neural engineering lab friends: Ziya Baghmanli, Eugene Daneshvar, Matt Gibson, Takashi D Yoshida Kozai, Nick Langhals, Paras Patel, Pratik Rohatgi, Azadeh Yazdan, Hirak Parikh, John Seymour, Jongwoo Lee, Greg Gage, Erin Purcell, Timothy Marzullo, Kip Ludwig, Jeyakumar Subbaroyan, Matthew Johnson, Elizabeth Nunamaker, David Pellinen, Rio Vetter, Kevin Otto, Justin Williams, Ruben Rathnasingham, Timothy Becker, Mark Lehmkuhle, Sandeep Bhangoo, Mohammad Abidian, Michael Joseph and David Turer. Also, give thanks to Shayna Bradford and Nikola Sladojevic of the Andjelkovic-Zochowska's lab. I could not do my graduate study without their support.

I thank the great support from the Biomedical Engineering department: Dr. Matthew O'Donnell, Dr. Douglas C. Noll, Dr. Michael Mayer, Dr. Andrew Putnam, Vera

Williams, Lisa Jones, Tonya Y. Thompson, Maria E. Steele, Lauren Pulay, Chuck Nicholas, Jane Mackie, Dana Jackson, Katharine Guarino, Mary Beth Donovan, Susan Bitzer, Brandon J. Baier, and Karen Coulter.

I could stand and move forward with the prayer support from my extended family and friends. Especially I thank my spiritual mentor, Dr. Joseph C. Won for his continued prayer for me. I appreciate his prayer and spiritual encouragement.

Whenever someone calls me Dr. Moon, I will remember: (1) how God helped me through my doctoral study. Since it was not solely made by my efforts, I cannot claim my ownership on the degree and (2) therefore, I should use this degree for Him.

Of all these achievements during my graduate study, the most valuable outcome was the meaningful relationships I established with you. God bless you!

감사의 글　　이제 저는 박사과정 공부의 긴 여정을 마치려 합니다. 돌이켜보면 이 기간은 하나님께서 제 삶에 어떻게 일하셨는지를 직접 보여주신 소중한 시간이었습니다. 박사과정 동안 저와 저희 가족에게 많은 일이 있었습니다. 아버지께서 암이 생기셔서 제가 휴학하고 한국으로 돌아가야 했고, 제 아내를 만나 결혼을 했고, 첫 아이가 유산되었고, 최근에는 아내가 아이를 다시 갖게 되었습니다. 때로는 힘들고 때로는 기쁜 일들을 겪으면서, 하나님과 가까와지게 되었고 다른 사람을 좀 더 이해하고 배려할 수 있게 되었습니다. 이러한 경험들은 너무도 소중한 것이어서 무엇과도 바꾸지 않을 겁니다. 특별히 하나님께서 아빠와 저 사이의 관계를 도와주셨습니다. 항암치료를 받으시는 동안 저는 아빠와 많은 갈등을 겪었고, 저희 관계는 멀어져 갔습니다. 결국 저는 편치 않은 마음으로 아빠와의 관계를 포기하고 Ann Arbor 에 있는 학교로 돌아오게 되었습니다. 그 때를 돌이켜보면, 아빠와 함께 제 졸업을 축하하는 것은 상상조차하기 어려웠습니다. 하지만 하나님께서는 저희 두 사람의 마음을 만져주셔서 저희 관계를 회복시켜 주셨습니다. 늦은 밤 실험하고 있을 때 였습니다. 논문 마감시간을 맞추기 위해 촉박한 실험 스케줄을 맞추느라 몸과 마음이 모두 지쳐있을 때 였습니다. 문득 하나님께서 제게 아빠의 마음을 생각나게 해 주셨습니다. 항암 치료를 받으면서 얼마나 힘드셨을까… 저는 그 때 아빠의 마음은 이해하고 않고 아빠와 갈등하면서 제가 겪는 어려움만 생각하고 있었습니다. 제 눈에 눈물이 고였습니다. 제 박사학위 논문심사에 아빠가 참석하지는 못하셨지만, 전화로 저희는 논문심사를 잘 마치게 해주신 하나님께 같이 감사기도를 드렸습니다. Ann Arbor 에 못오신 이유는 단순한 몸살 때문이었습니다. 새 집 지으시느라 무리를 하셔서…

먼저 그동안 저를 지원해주고 격려해 준 아내에게 제 감사의 마음을 전합니다. 제 아내의 사랑과 기도가 없었더라면 제가 여기까지 오지 못 했을 겁니다. 여보, 당신은 하나님께서 제게 주신 가장 귀한 선물입니다.

부모님들(강석구, 김정희, 문병순, 최경실)께 감사드립니다. 부모님들의 희생과 기도가 있었기에 오늘의 제가 있을 수 있었습니다. 또한 동생들(강병선, 강소영, 김영욱, 문상현, 문지혜)에게도 감사의 마음을 전합니다.

이 논문의 과제들은 National Institute of Health (NIH)의 연구비로 지원되었습니다. 제 지도교수이신 Kipke 교수님께 특별히 감사를 드립니다. 교수님은 항상제게 많은 에너지와 긍정적인 사고로, 제가 연구와 삶에서의 어려움을 이겨나갈 수 있도록 저를 격려해 주셨습니다. 교수님을 넓은 도량을 가진 분이었습니다. 제가 집안일로 1 년이상 떠나있다가 학교로 다시 돌아갈 때에도 진심으로 저를 반겨주셨습니다. 연구가 진행이 잘 않되어 어려울 때도 항상 저를 격려해 주셨습니다.

이 연구를 지원해주신 부 지도교수이신 Andjelkovic-Zochowska 교수님께 감사드립니다. 약 1 년전 Andjelkovic-Zochowska 교수님을 만난 후 연구는 급격한 진전을 이룰 수 있었습니다. 교수님의 조언, 생물학적 전문지식 그리고 실험을 직접 도와주신 것은 제게 큰 도움이 되었습니다. 대부분의 생물학 실험과 분석은 교수님의 도움으로 가능했습니다. 또한 Andjelkovic-Zochowska 교수님 실험실의 Stamatovic 박사님의 도움을 잊을 수 없습니다. 박사님은 제게 생물학적 지원과 조언을 해주신 것 뿐만 아니라 제가 세포 배양 실험이 잘 않되어 힘들어 할 때마다 따뜻한 말로 저를 격려해 주셨습니다. 제가 필요할 때 늘 든든한 지원자로 저와 함께 해 주셨습니다.

제 논문심사 위원으로 수고해주신 Takayama 교수님과 Stegemann 교수님께도 감사드립니다. 두 분 교수님께서는 제가 연구과제를 늘 새로운 시각으로 볼 수 있도록 조언해 주셨습니다.

고모부 현철수 박사님께 감사드립니다. 제가 학부때 부터 제 일과 삶의 멘토가 되어주셨습니다. 코넬 의과대학 교수로, 또 병원에서 환자보시느라 바쁘신 중에도 마다 않으시고 늘 저를 도와주셨습니다. 진심으로 감사드립니다.

제 석사학위 지도교수이신 홍대희, 이규백교수님들께 감사드립니다. 두 분께서는 제가 박사학위를 하는 동안에도 계속해서 제 멘토가 되어주셨습니다. 두 분의 격려와 조언이 제게 큰 힘이 되었습니다.

지난 2 년간 technical communication class 에서 제 tutor 로 저를 도와주신 Mimi Adam 에게 감사를 드립니다. Mimi 에게서 저는 단순히 글쓰기만 배운것이 아니라 생각을 정리하는 방법을 배웠습니다.

저와 같은 연구실에서 저의 친구가 되어주고 저를 도와준 연구실 동기, 선후배들에게도 감사를 전합니다.(Ziya Baghmanli, Eugene Daneshvar, Matt Gibson, Takashi D Yoshida Kozai, Nick Langhals, Paras Patel, Pratik Rohatgi, Azadeh Yazdan, Hirak Parikh, John Seymour, Jongwoo Lee, Greg Gage, Erin Purcell, Timothy Marzullo, Kip Ludwig, Jeyakumar Subbaroyan, Matthew Johnson, Elizabeth Nunamaker, David Pellinen, Rio Vetter, Kevin Otto, Justin Williams, Ruben Rathnasingham, Timothy Becker, Mark Lehmkuhle, Sandeep Bhangoo, Mohammad Abidian, Michael Joseph and David Turer). 특히 Dave Pellinen 은 제가 힘들 때, 큰 형처럼 (사실 나이가 좀 많습니다) 저의 위로가 되어주었습니다. 또한 Andjelkovic-Zochowska 교수님 연구실의 Shayna Bradford and Nikola Sladojevic 에게도 감사드립니다.

저의 연구를 지원해주신 Biomedical Engineering department 의 교수님들과 교직원 여러분에게 감사드립니다(Dr. Matthew O'Donnell, Dr. Douglas C. Noll, Dr. Michael Mayer, Dr. Andrew Putnam, Vera Williams, Lisa Jones, Tonya Y. Thompson, Maria E. Steele, Lauren Pulay, Chuck Nicholas, Jane Mackie, Dana Jackson, Katharine Guarino, Mary Beth Donovan, Susan Bitzer, Brandon J. Baier, and Karen Coulter).

여러 친지분들과 친구들이 기도로 지원해주신 덕분에 제가 견디고 연구에도 진전을 이룰 수 있었습니다. 특별히 자식같이 여기시며 저를 위해 기도해주시고 격려해주신, 제 영적 멘토이신 원종수 목사님께 감사드립니다.

어떤 사람이 저를 '문박사'하고 부르면, 저는 첫째 하나님께서 제 박사학위과정 동안에 어떻게 저를 도와주셨는지를 기억할겁니다. 학위를 제 노력만으로 얻은 것이 아니기 때문에, 제 성취물로 여길 수 없습니다. 둘째, 그래서 저는 이 학위를 주님을 위해 써야하는 것을 기억할겁니다.

박사학위과정 동안에 이룬 여러 가지 가운데 무엇보다도 가장 가치있는 것은 바로 여러분과 제가 맺은 소중한 관계입니다. 하나님의 축복이 함께하시기를 바랍니다.

Table of Contents

List of Figures

ABSTRACT

Control and Effect of Glial Cell Activation on the Microscale Chronic Neural Interface toward Dynamic Control of Neural Environment

by

Taegyun Moon

Chair: Daryl R. Kipke

The limited lifetime of neural implants continues to frustrate the progress of neuroscience research. Despite extensive research into the inflammatory process and the encapsulation cascade, there has been little attention to when functional degradation of the neural probe actually begins. However, the initiation point is critical in determining the optimal time to intervene in the encapsulation process. If onset of signal degradation occurs at the very early stages of encapsulation, inhibition agents could be introduced to prevent glial activation. On the other hand, if onset occurs later in the encapsulation process it might be more advantageous to interrupt the inflammatory process before the formation of scar tissue. To answer these questions, we developed *in vitro* models for injury (thrombin/scratch) and acute inflammatory response (lypopolysaccride, LPS) to investigate the correlation between increasing signal impedance and the activation of

glial cells. Using these *in vitro* models to monitor the impedance of the activated cells, we were able to demonstrate the increased impedance of activated glial cells compared to inactivated cells. This finding suggests that once an optimal strategy to intervene in encapsulation is developed, it should be possible to get stable long term recording/stimulation by controlling encapsulation at acceptable levels. We proved this concept of dynamic control, testing sequential activation/deactivation of glial cells to investigate: 1) if controlling glial activation levels over a short period of time is possible, and 2) the effect of the change of the activation levels on probe functionality by monitoring impedance. The critical implications of our results are that glial activation can be controlled in short periods of time and, hence, the impedance of the probe can be controlled by controlling the activation of the glial cells surrounding the probe.

CHAPTER I

INTRODUCTION AND BACKGROUND

1. Introduction

Neural probes have been widely used to restore brain function through applications such as deep brain stimulation (Obeso, Guridi et al. 2001) and brain computer interfaces (Nicolelis 2001; Wolpaw, Birbaumer et al. 2002; Kipke 2004). However, the unpredictable lifetime of the implanted neural probe has proved a challenge for many promising clinical applications (Normann 2007). The functional degradation of a neural probe, it has been hypothesized, is caused by probe encapsulation, which is an inflammatory response to the probe insertion (Agnew, Yuen et al. 1986; Grill and Mortimer 1994). Considerable efforts have been put into increasing longevity of the neural probe through drug delivery (Spataro, Dilgen et al. 2005), improved probe materials (Rousche, Pellinen et al. 2001), or coatings (Ludwig, Uram et al. 2006). However, maintaining prolonged probe functionality has continued to be a problem.

The encapsulation of neural probes essentially consists of a sheath that is made of microglia and astrocytes. The astrocytes surround the clustered microglia in an encapsulation layer. This sheath of reactive tissue, called a “glial scar”, is a chronic feature of the implant. The thickness of the sheath decreases over time but becomes denser, making a complete glial scar (Schultz and Willey 1976; Edell, Toi et al. 1992; Turner, Shain et al. 1999). Researchers in the 1980’s and 90’s already suspected that glial scarring is responsible for the reduced electrical signal conduction observed over time (Agnew, Yuen et al. 1986; Grill and Mortimer 1994).

Early studies had already determined that the formation of the glial scar is created in two stages: the early acute response to the mechanical injury from insertion (Fig.1.1(a)), and the sustained chronic response which results in the glial scar (Fig.1.1(b)) (Szarowski, Andersen et al. 2003). The early acute response is initiated by the secretion of the proinflammatory cytokines secreted by glial cells secondary to the injury caused by neural probe insertion (Dinarello 2000). These proinflammatory cytokines recruit other glial cells around the inserted neural probe, activating them. The glial scar is then formed by activated astrocytes during the sustained chronic stage (Polikov, Tresco et al. 2005).

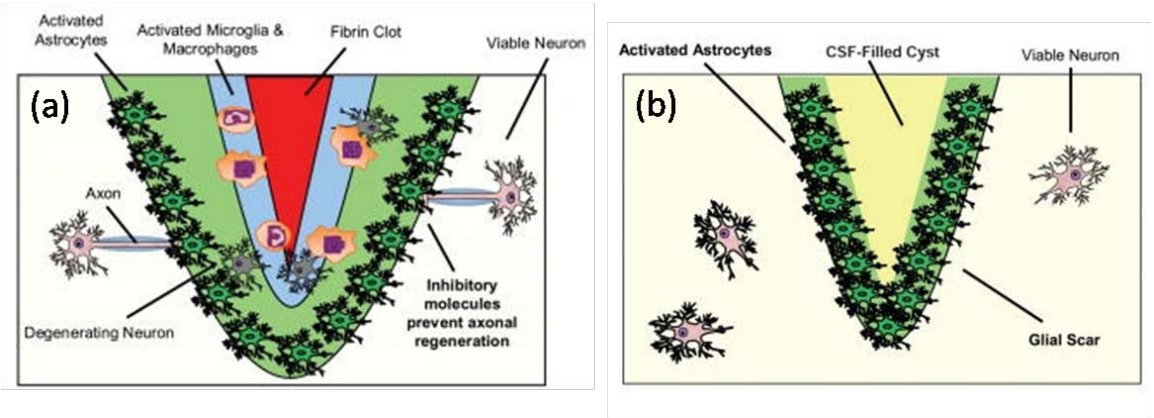

Fig.1.1. Cartoons demonstrating cellular responses during early (a) and chronic (b) reactive responses. (a) In the early inflammation response, microglia and macrophages migrate into the lesion, secreting various cytokines and growth factors while also removing necrotic tissue. Activated astrocytes form a physical barrier around the area of tissue damage, protecting the residential neurons outside the wound from further insult. Inhibitory molecules associated with myelin and produced by astrocytes within the glial scar block regeneration of damaged axons. (b) In the sustained chronic response, the fibrin clot and necrotic tissue is removed by microglia and macrophages. Unlike nonneural tissue, lost tissue is not replaced, leaving a lesion with a cerebral spinal fluid–filled cyst. Astrocytes become denser surrounding the cyst to form a glial scar, protecting the uninjured tissue from further injury (modified from http://www.ncbi.nlm.nih.gov/bookshelf/br.fcgi?book=frimp&part=ch1)

If signal loss could be established in the acute phase, then effective intervention would consist of preventing glial activation, whereas if it occurs in the chronic phase, intervention would have to focus on disrupting the process of scar formation. To determine when the dominant signal loss begins, we investigated if activation at the early stages increases impedance or not, and, if so, at what point. We tested the hypothesis that activated glial cells surrounding the neural probe increase the impedance and signal loss.

In addition to the mechanical injury associated with *in vivo* neural probe insertion, it has been hypothesized that glial cell activation is due to the rupture of small blood vessels which leads to intra-cerebral micro-hemorrhages, bleeding into the extracellular matrix (ECM) of the brain (Power, Henry et al. 2003; Pekny and Nilsson 2005; Polikov, Tresco et al. 2005; Viswanathan and Chabriat 2006). When a neural probe is inserted in the brain tissue, the probe 1) damages glial and neuronal cell processes, and 2) unavoidably ruptures the micro vasculature of the brain, which is very dense (Bjornsson, Smith et al. 2004). Until the damaged vasculature has been restored, there is a large influx of thrombin, as well as other blood components, into the extra cellular matrix of the brain tissue.

Thrombin, a serine protease, is immediately produced in the brain after intracerebral hemorrhage, brain trauma, or the breakdown blood–brain barrier after brain injury (Jiang, Wu et al. 2002). Thrombin stimulates a variety of cells, such as, endothelial cells, neuronal cells, monocytes/macrophages, smooth muscle cells, fibroblasts, platelets and lymphocytes, most of which are important for tissue repair (illustrated in Fig.1.2) (Goldsack, Chambers et al. 1998). Although the trigger mechanism for cytokine secretion is unknown, it is hypothesized that thrombin induces

the cytokine secretion by microglia and astrocytes, initiating inflammatory cascade (see Fig.1.3) with the ensuing formation of glial encapsulation (Suo, Citron et al. 2004).

We were interested in investigating at which point in the encapsulation process signal loss is initiated: at the early inflammation stage or the later scar formation stage. It is important to identify the initiation point in order to determine the optimal time to intervene in the encapsulation process. To test the hypothesis that activated glial cells surrounding the neural probe in the acute phase increase the impedance and signal loss, we decided to test whether impedance increases during glial activation. To do so *in vitro*, however, required that we develop a comparable *in vitro* model that would allow us to activate glial cells (astrocytes and microglia) plated on a microelectrode and monitor for electrical impedance across the plated cell layers. We then had to develop a way to activate the astrocytes and microglia so that we could determine the impedance increase due to activation. This required establishing an adequate control group as well as measuring impedance before and after activation of the experimental group.

Once an optimal strategy to intervene in encapsulation is developed, it should be possible to get stable long term recording/stimulation. We suspect that this optimal strategy will involve dynamic control, i.e., controlling encapsulation levels in an acceptable range. To demonstrate the proof of concept for this control of encapsulation level dynamically for the self-repairing neural probe (SRNP), we opted to test sequential activation/deactivation of glial cells over a short period of time. For each step of the activation/deactivation stage, we would investigate the effect of the change of the activation levels on the probe functionality by monitoring the trans-cellular impedance of the activated/deactivated glial cells.

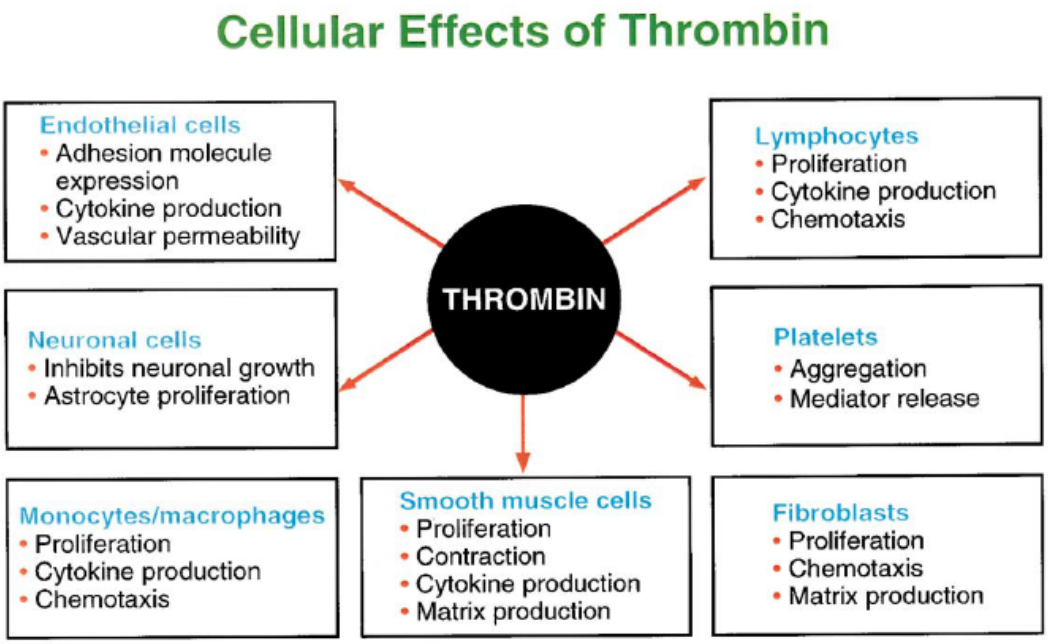

Fig.1.2. Thrombin stimulates variety of cells, activating them, most of which are important for tissue repair (Goldsack, Chambers et al. 1998).

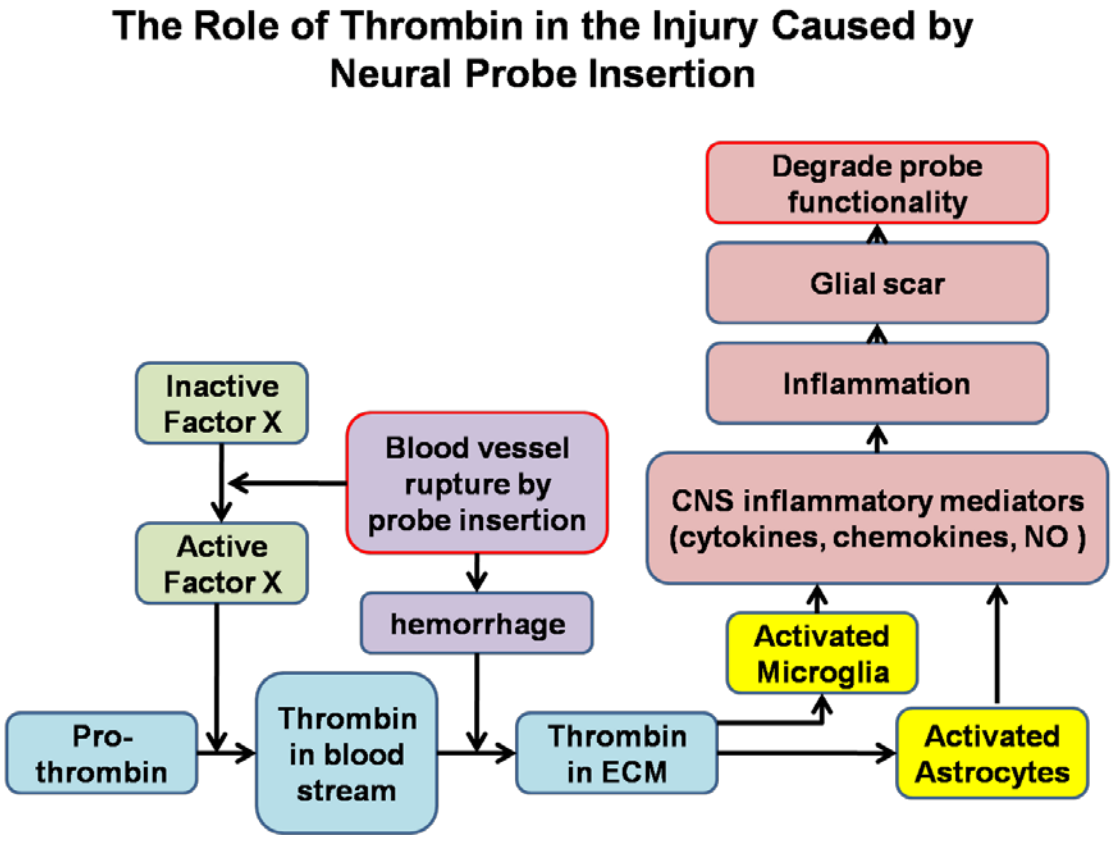

Fig.1.3. Schematic illustration of potential sources of active thrombin in the CNS and its regulation on the injury caused by neural probe insertion

References

Agnew, W. F., T. G. H. Yuen, et al. (1986). "Histopathologic Evaluation of Prolonged Intracortical Electrical-Stimulation." Experimental Neurology **92**(1): 162-185.

Arshady, R. (1991). "Preparation of biodegradable microspheres and microcapsules: 2. Polyactides and related polyesters." Journal of Controlled Release **17**(1): 1-21.

Arvin, B., L. F. Neville, et al. (1996). "The role of inflammation and cytokines in brain injury." Neurosci Biobehav Rev **20**(3): 445-52.

Beck, A., R. Penner, et al. (2008). "Lipopolysaccharide-induced down-regulation of Ca2+ release-activated Ca2+ currents (I CRAC) but not Ca2+-activated TRPM4-like currents (I CAN) in cultured mouse microglial cells." J Physiol **586**(2): 427-39.

Beecher, K. L., T. T. Andersen, et al. (1994). "Thrombin receptor peptides induce shape change in neonatal murine astrocytes in culture." J Neurosci Res **37**(1): 108-15.

Biran, R., D. C. Martin, et al. (2005). "Neuronal cell loss accompanies the brain tissue response to chronically implanted silicon microelectrode arrays." Experimental Neurology **195**(1): 115-126.

Bjornsson, C. S., K. L. Smith, et al. (2004). "Brain vascular damage due to neuroprosthetic insertion: casting and quantitative analysis." Journal of Neurochemistry **90**: 67-67.

Coughlin, S. R. and E. Camerer (2003). "PARticipation in inflammation." J Clin Invest **111**(1): 25-7.

Cui, X., J. Wiler, et al. (2003). "*In vivo* studies of polypyrrole/peptide coated neural probes." Biomaterials **24**(5): 777-87.

Dinarello, C. A. (2000). "Proinflammatory cytokines." Chest **118**(2): 503-508.

Edell, D. J., V. V. Toi, et al. (1992). "Factors Influencing the Biocompatibility of Insertable Silicon Microshafts in Cerebral-Cortex." Ieee Transactions on Biomedical Engineering **39**(6): 635-643.

Frampton, J. P., M. R. Hynd, et al. (2007). "Three-dimensional hydrogel cultures for modeling changes in tissue impedance around microfabricated neural probes." Journal of Neural Engineering **4**(4): 399-409.

Frohman, E. M., T. C. Frohman, et al. (1989). "The induction of intercellular adhesion molecule 1 (ICAM-1) expression on human fetal astrocytes by interferon-gamma, tumor necrosis factor alpha, lymphotoxin, and interleukin-1: relevance to intracerebral antigen presentation." J Neuroimmunol **23**(2): 117-24.

Giaever, I. and C. R. Keese (1993). "A Morphological Biosensor for Mammalian-Cells." Nature **366**(6455): 591-592.

Giaver, I. a. K. C. R. (1993). "A morphological biosensor for mammalian cells." **366**(6455): 591.

Giulian, D., J. Woodward, et al. (1988). "Interleukin-1 injected into mammalian brain stimulates astrogliosis and neovascularization." J Neurosci **8**(7): 2485-90.

Goldsack, N. R., R. C. Chambers, et al. (1998). "Moleculs in focus: Thrombin." Int J Biochem Cell Biol **30**(6): 641-6.

Grill, W. M. and J. T. Mortimer (1994). "Electrical-Properties of Implant Encapsulation Tissue." Annals of Biomedical Engineering **22**(1): 23-33.

He, W., G. C. McConnell, et al. (2007). "A novel anti-inflammatory surface for neural electrodes." Advanced Materials **19**(21): 3529-+.

Jain, R. A. (2000). "The manufacturing techniques of various drug loaded biodegradable poly(lactide-co-glycolide) (PLGA) devices." Biomaterials **21**(23): 2475-90.

Jiang, Y., J. Wu, et al. (2002). "Thrombin-receptor activation and thrombin-induced brain tolerance." J Cereb Blood Flow Metab **22**(4): 404-10.

John, G. R., S. C. Lee, et al. (2003). "Cytokines: powerful regulators of glial cell activation." Neuroscientist **9**(1): 10-22.

Johnson, M. D., K. J. Otto, et al. (2005). "Repeated voltage biasing improves unit recordings by reducing resistive tissue impedances." Ieee Transactions on Neural Systems and Rehabilitation Engineering **13**(2): 160-165.

Jones, A. and C. L. Geczy (1990). "Thrombin and factor Xa enhance the production of interleukin-1." Immunology **71**(2): 236-41.

Kipke, D. R. (2004). "Brain-machine interfaces using thin-film silicon microelectrode arrays." 2004 Ieee International Symposium on Circuits and Systems, Vol 5, Proceedings: 497-499.

Leborgne, S. and M. Graber (1994). "Amidase Activity and Thermal-Stability of Human Thrombin." Applied Biochemistry and Biotechnology **48**(2): 125-135.

Lee, S. J. and E. N. Benveniste (1999). "Adhesion molecule expression and regulation on cells of the central nervous system." Journal of Neuroimmunology **98**(2): 77-88.

Lieberman, A. P., P. M. Pitha, et al. (1989). "Production of tumor necrosis factor and other cytokines by astrocytes stimulated with lipopolysaccharide or a neurotropic virus." Proc Natl Acad Sci U S A **86**(16): 6348-52.

Ludwig, K. A., J. D. Uram, et al. (2006). "Chronic neural recordings using silicon microelectrode arrays electrochemically deposited with a poly(3,4-ethylenedioxythiophene) (PEDOT) film." Journal of Neural Engineering **3**(1): 59-70.

Merrill, D. R. and P. A. Tresco (2005). "Impedance characterization of microarray recording electrodes *in vitro*." Ieee Transactions on Biomedical Engineering **52**(11): 1960-1965.

Merrill, J. E. and E. N. Benveniste (1996). "Cytokines in inflammatory brain lesions: helpful and harmful." Trends Neurosci **19**(8): 331-8.

Meyer, J. U., T. Stieglitz, et al. (2001). "High density interconnects and flexible hybrid assemblies for active biomedical implants." IEEE Trans Adv Packaging **24**(3): 366-375.

Moon, T., D. S. Pellinen, et al. (2007). "Local Drug Delivery System for Dynamic Control of Neural Environment using Parylene-Based Microelectrodes." World Congress on Medical Physics and Biomedical Engineering 2006, Vol 14, Pts 1-6 **14**: 3542-3545.

Nelson, R. B. and R. Siman (1990). "Thrombin and its inhibitors regulate morphological and biochemical differentiation of astrocytes *in vitro*." Brain Res Dev Brain Res **54**(1): 93-104.

Nicholson, C. (2001). "Diffusion and related transport mechanisms in brain tissue." Reports on Progress in Physics **64**(7): 815-884.

Nicole, O., A. Goldshmidt, et al. (2005). "Activation of protease-activated receptor-1 triggers astrogliosis after brain injury." J Neurosci **25**(17): 4319-29.

Nicolelis, M. A. L. (2001). "Actions from thoughts." Nature **409**(6818): 403-407.

Normann, R. A. (2007). "Technology Insight: future neuroprosthetic therapies for disorders of the nervous system." Nature Clinical Practice Neurology **3**(8): 444-452.

Obeso, J. A., J. Guridi, et al. (2001). "Deep-brain stimulation of the subthalamic nucleus or the pars interna of the globus pallidus in Parkinson's disease." New England Journal of Medicine **345**(13): 956-963.

Pekny, M. and M. Nilsson (2005). "Astrocyte activation and reactive gliosis." Glia **50**(4): 427-34.

Pellinen, D. S., T. Moon, et al. (2005). "Multifunctional flexible parylene-based intracortical microelectrodes." 2005 27th Annual International Conference of the IEEE Engineering in Medicine and Biology Society, Vols 1-7: 5272-5275.

Polikov, V. S., M. L. Block, et al. (2006). "*In vitro* model of glial scarring around neuroelectrodes chronically implanted in the CNS." Biomaterials **27**(31): 5368-76.

Polikov, V. S., P. A. Tresco, et al. (2005). "Response of brain tissue to chronically implanted neural electrodes." J Neurosci Methods **148**(1): 1-18.

Power, C., S. Henry, et al. (2003). "Intracerebral hemorrhage induces macrophage activation and matrix metalloproteinases." Ann Neurol **53**(6): 731-42.

Ramakers, G. J. and W. H. Moolenaar (1998). "Regulation of astrocyte morphology by RhoA and lysophosphatidic acid." Exp Cell Res **245**(2): 252-62.

Rousche, P. J. and R. A. Normann (1998). "Chronic recording capability of the Utah Intracortical Electrode Array in cat sensory cortex." J Neurosci Methods **82**(1): 1-15.

Rousche, P. J., D. S. Pellinen, et al. (2001). "Flexible polyimide-based intracortical electrode arrays with bioactive capability." Ieee Transactions on Biomedical Engineering **48**(3): 361-371.

Saura, J. (2007). "Microglial cells in astroglial cultures: a cautionary note." J Neuroinflammation **4**: 26.

Sawada, M., N. Kondo, et al. (1989). "Production of tumor necrosis factor-alpha by microglia and astrocytes in culture." Brain Res **491**(2): 394-7.

Schultz, R. L. and T. J. Willey (1976). "The ultrastructure of the sheath around chronically implanted electrodes in brain." J Neurocytol **5**(6): 621-42.

Skaper, S. D., L. Facci, et al. (1986). "Morphological modulation of cultured rat brain astroglial cells: antagonism by ganglioside GM1." Brain Res **390**(1): 21-31.

Song, C. X., V. Labhasetwar, et al. (1997). "Formulation and characterization of biodegradable nanoparticles for intravascular local drug delivery." Journal of Controlled Release **43**(2-3): 197-212.

Spataro, L., J. Dilgen, et al. (2005). "Dexamethasone treatment reduces astroglia responses to inserted neuroprosthetic devices in rat neocortex." Experimental Neurology **194**(2): 289-300.

Subbaroyan, J., D. C. Martin, et al. (2005). "A finite-element model of the mechanical effects of implantable microelectrodes in the cerebral cortex " Journal of Neural Engineering **2**(4): 103-113.

Suidan, H. S., C. D. Nobes, et al. (1997). "Astrocyte spreading in response to thrombin and lysophosphatidic acid is dependent on the Rho GTPase." Glia **21**(2): 244-52.

Suo, Z., B. A. Citron, et al. (2004). "Thrombin: a potential proinflammatory mediator in neurotrauma and neurodegenerative disorders." Curr Drug Targets Inflamm Allergy **3**(1): 105-14.

Suzumura, A., S. Bhat, et al. (1984). "The isolation and long-term culture of oligodendrocytes from newborn mouse brain." Brain Res **324**(2): 379-83.

Szarowski, D. H., M. D. Andersen, et al. (2003). "Brain responses to micro-machined silicon devices." Brain Research **983**(1-2): 23-35.

Takamiya, M., S. Fujita, et al. (2007). "Simultaneous detections of 27 cytokines during cerebral wound healing by multiplexed bead-based immunoassay for wound age estimation." J Neurotrauma **24**(12): 1833-44.

Turner, J. N., W. Shain, et al. (1999). "Cerebral astrocyte response to micromachined silicon implants." Experimental Neurology **156**(1): 33-49.

Vetter, R. J., J. C. Williams, et al. (2004). "Chronic neural recording using silicon-substrate microelectrode arrays implanted in cerebral cortex." Ieee Transactions on Biomedical Engineering **51**(6): 896-904.

Viswanathan, A. and H. Chabriat (2006). "Cerebral microhemorrhage." Stroke **37**(2): 550-5.

Williams, J. C., J. A. Hippensteel, et al. (2007). "Complex impedance spectroscopy for monitoring tissue responses to inserted neural implants." Journal of Neural Engineering **4**(4): 410-423.

Wolpaw, J. R., N. Birbaumer, et al. (2002). "Brain-computer interfaces for communication and control." Clinical Neurophysiology **113**(6): 767-791.

CHAPTER II

GLIAL CELL ACTIVATION RESULTING FROM TISSUE INJURY: AN *IN VITRO* MODEL

1. Introduction

Encapsulation was first modeled by Merrill and Tresco who built an *in vitro* 2D cell culture chamber and used the electrical impedance of the surrounding tissue as a measure of encapsulation (Merrill and Tresco 2005). Encapsulation was then modeled by Frampton and Shain who built an in-vitro 3D cell culture model mimicking high cell density as found in the brain (Frampton, Hynd et al. 2007). Both studies demonstrated that electrical impedance increased when a neural probe was encapsulated by plated glial cells *in vitro.*

We wanted to further investigate glial encapsulation focusing on the activation level of glial cells in terms of impedance and recorded signal quality. It is well known that glial activation induces cytokine secretion, increases intercellular adhesion and proliferation, and changes the morphology of glial cells. To investigate this relationship, we needed a tissue injury model that could provide glial activation. A good *in vitro* tissue injury model should be able to activate glial cells with a method close to *in vivo* tissue injury and confirm the activation.

Since current encapsulation models do not distinguish between activated and non-activated glial cells, we designed a novel tissue injury model simulating both mechanical

injury and the micro-hemorrhages caused by blood vessel rupture to differentiate between two levels of glial cell activation. A scratch was made on a co-cultured monolayer of mouse astrocytes and microglia to simulate the mechanical tissue injury (Polikov, Block et al. 2006). In addition, thrombin was introduced to the culture media to simulate the microhemorrhages resulting from the blood vessel ruptures during neural probe insertion (Suo, Citron et al. 2004). Thrombin was included in our model because just scratching a cell layer does not simulate micro-hemorrhages since the cultured cells do not include blood vessels. The glial activation was confirmed by demonstrating morphological change, protease-activated receptor-1 (PAR-1) expression, and up regulated proinflammatory cytokines.

2. Method

To mimic the impact of the neural probe insertion, we employed two models: injury and acute inflammation. The injury model has four components: glial cells, a neural probe, thrombin and scratch. The glial cells that were to be activated for the injury model were prepared from the brain of newborn mice using a modified Suzumura protocol (Suzumura, Bhat et al. 1984). The silicon based neural probe was included in the injury model to mimic the environment of neural probe insertion. An actual recording electrode without a printed circuit board (PCB) was used. Glial cells were then plated on the neural probe and subjected to either activation by thrombin/scratch (experimental) or no treatment (control). On the other hand, the acute inflammation model has three components: glial cells, a neural probe and lipo-polysaccharide (LPS), a component of the outer membrane of gram-negative bacteria. LPS was applied to the glial cells in the culture to activate the cells.

2.1. Experimental setup

Cells were cultured in Dulbecco's modified Eagle's medium (DMEM), supplemented with 10% fetal bovine serum (FBS), 100 U/mL penicillin and 100 mg/mL streptomycin (Invitrogen, Rockville, MD). Medium was changed every 3-4 days. This mixed culture mainly contained astrocytes and microglia. These cells were allowed to grow and proliferate for 2-3 weeks based on the state of confluence and then plated on a 24-well tissue culture plate. Each plated well had a dummy silicon electrode placed on the bottom. All experiments and animal care were performed in accordance with the University Committee on Use and Care of Animals (UCUCA) guidelines.

Before plating cells, the setup was sterilized by UV light for 1 hour. To enhance the cell attachment, the bottom of the well, where cells were to be plated was coated with fibronectin solution from bovine plasma (5 µg /cm^2, Sigma-Aldrich, Inc. St. Louis, MO) and then the setup was dried under a sterile hood for 45 minutes at room temperature. Mixed cells were plated on the well at a density of $2x10^5$ cells per well (2 cm^2).

The groups of plated cells were allowed to settle and become confluent for 48 hours in 10% fetal bovine serum (FBS) media and then each group was subjected to either activation by thrombin/scratch (experimental) or no treatment (control). For the experimental group, a mechanical scratch was made on the confluent glial cell layer along the shank of the neural probe using a sterile 31-gauge syringe needle and the cells were then supplied with 5 NIH U/mL of thrombin from bovine plasma (Sigma-Aldrich, Inc. St. Louis, MO) in a 1% FBS culture media (see chapter 2 for more details). The control group received only 1% FBS culture media and was not subjected to thrombin or mechanical scratch.

2.2. Verifying that the neural probe material does not activate glial cells

To verify our plated cells had not been activated by the probe material prior to our experiment, we tested if the probe material induces increased cytokine secretion. Our rational for this test was that if the probe material activates cells, we had to be able to differentiate material induced activation from the injury (thrombin/scratch) induced activation.

To determine if cytokines had been secreted in response to the probe material, we plated one group of cells on silicon probes placed on the bottom of the wells of a 24-well

cell culture plate. Each well contained only one silicon neural probe. The control group was plated in the same manner but in wells that did not include silicon probes. The glial cells were plated on the surface of all wells and allowed to settle for 48 hours in 10% FBS media. Then 10% FBS media was removed and supplied with 2% FBS media with 0.5xAnti-anti media. The media were collected at different time points (30 min, day 1, day 7 and day 13) and analyzed by RayBio Mouse Cytokine Antibody Array (Ray Biotech Inc., Norcross, GA) and by ELISA (SABiosciences, Frederick, MD) to quantify the cytokines secreted at different time points.

2.3. Activation of glial cells in the experimental setup

2.3.1. Activation by thrombin

To find the optimum concentration of thrombin for activation of glial cells, we tested three different concentrations of thrombin in cell culture media with four different serum concentrations. The efficacy of different thrombin concentrations was determined by the degree of morphological change of the glial cells. The optimum condition should make the biggest morphological change while making maximum contrast between thrombin concentrations in the same FBS concentration. If the FBS concentration were too high, it would be difficult to differentiate if the cells were activated by thrombin or FBS. If the FBS concentration were too low, the cells might not have had sufficient nutrients for survival.

Mixed brain cells were seeded in a 24 well plate with a density of $2x10^5$ cells per each well. After the culture became confluent, cells were washed twice with PBS and DMEM with 250 µM of dibutyryl-cAMP (dbcAMP, Sigma-Aldrich, Inc. St. Louis, MO)

was applied to the cells for 24 hours. The cells were then washed twice with PBS and subsequently treated with three different concentrations of thrombin (0.1, 5, and 30 NIH U/mL) in four different cell culture media with different fetal bovine serum (FBS) concentrations (0, 0.1, 1, and 10%). In total, we prepared 12 different treatment conditions. Cell morphologies were observed using phase contrast microscopy.

2.3.2. Activation by scratch

To mimic the mechanical injury caused by the neural probe insertion, and the thrombin release resulting from the ensuing micro-hemorrhage, we made a 5mm long scratch on the confluent glial cell layer running a sterile 31-gauge syringe needle along the neural probe, and 5 NIH U/mL of thrombin from bovine plasma (Sigma-Aldrich, Inc. St. Louis, MO) in 1% FBS culture media was supplied to the cells. Only culture media with 1% FBS was supplied for the control group with no thrombin or mechanical scratch.

2.3.3. Activation by acute inflammation

To mimic the acute inflammatory response introduced by the neural probe insertion, we used LPS (10 μg/mL in 1% FBS media) as an activation agent.

2.4. Detection of activated glial cells in the experimental setup

We wanted to confirm that glial cells are activated by the injury (thrombin/scratch) and the acute inflammation (LPS) model. To confirm the presence of activation, we exploited three activation responses: morphological change, PAR-1 expression and cytokine expression.

2.4.1. Morphological change

The degree of activation produced by thrombin was determined by the morphological change of glial cells using phase contrast microscopy (Nelson and Siman 1990). First, glial cells were deactivated in dbcAMP (1mM in 0% FBS media) for 24 hrs and then activated by applying thrombin (5 NIH U/mL in 0% FBS media) for 24 hrs. The cultures were photo documented under microscopy before and after glial activation.

2.4.2. PAR-1 expression

In addition to observing morphological changes, we also used the expression of protease-activated receptor 1 (PAR-1) to confirm the glial activation by thrombin. The introduction of thrombin to glial cells activates PAR-1, which in turn initiates the activation of glial cells. PAR-1, a seven transmembrane domain G-protein–coupled receptor, is activated by proteolysis from thrombin binding (Fig.2.1) (Coughlin and Camerer 2003; Nicole, Goldshmidt et al. 2005).

Cells were plated on 24 well plates with 1% FBS culture media and subjected to one of six different conditions: 1) control cells without neural probe and treatment (control 1), 2) control cells on a neural probe but no treatment (control 2), 3) cells on a neural probe with thrombin (5 NIH U/mL), 4) cells on a neural probe with thrombin (5 NIH U/mL) and scratch, 5) cells on neural probe with LPS (10 µg/mL, control 3), and 6) cells on neural probe with TNF-alpha (10 ng/mL) and IL-1beta (10 ng/mL, control 4). In addition to controls 1 and 2, controls 3 and 4 were added to confirm that PAR-1was not expressed without thrombin.

Samples were fixed at different time points (days 1 and 5) and stained. Cultures were washed with PBS, fixed with prechilled (4°C) 5% acetic acid in methanol for 45 min at 4°C, and followed by washing with PBS. Samples were blocked with 10% BSA in PBS for 1 h at 25°C and then incubated with primary antibodies against PAR-1 (1:100, Santa Cruz Biotechnology Inc., Santa Cruz, CA) in PBS containing 5% BSA and 0.1% Tween-20 for 2 h at 25°C or overnight at 4°C. After washing with PBS containing 1% BSA and 0.1% Tween-20, samples were incubated with secondary antibodies (1:200, Santa Cruz Biotechnology Inc. Santa Cruz, CA) at room temperature for 1 h followed by washes. After staining, samples were mounted with Prolong gold, an antifade, and observed under a microscope.

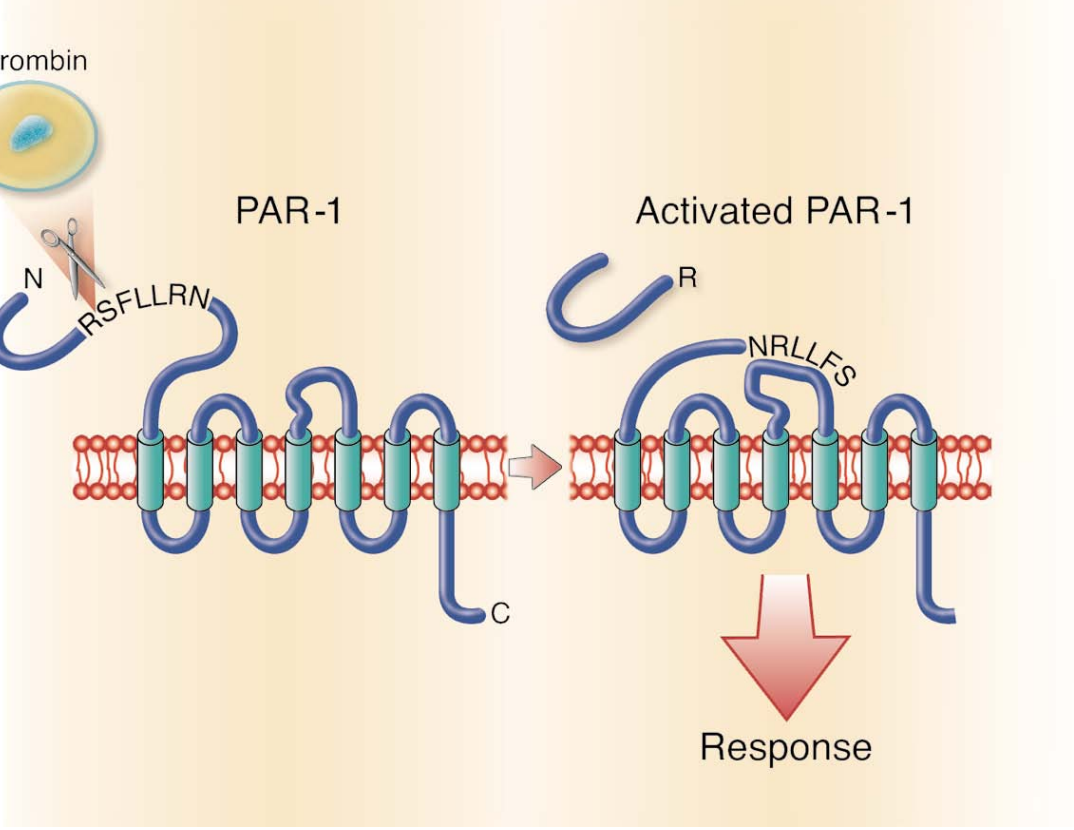

Fig. 2.1. Mechanism of PAR-1 activation. PAR-1, a seven transmembrane domain G-protein–coupled receptor, is activated by proteolysis from thrombin binding from (Coughlin and Camerer 2003)

2.4.3. Detection of expressed cytokines using protein array

Our third method to confirm glial activation used a protein array to detect the up regulated inflammatory cytokines secreted when glial cells are activated. Cells were plated on 24 well plates in 1% FBS culture media and subjected to one of four different conditions: 1) cells without neural probe or treatment (control 1), 2) cells plated on neural probe without treatment (control 2), 3) cells on neural probe with thrombin (5 NIH U/mL), and 4) cells on neural probe with LPS (10 μg/mL). Culture media and cell lysates were collected at different time points (days 1 and 5) and analyzed separately (16 total samples) using RayBio Mouse Cytokine Antibody Array (Ray Biotech Inc., Norcross, GA) and ScanAlyze software (Eisen Lab, Berkeley, CA).

3. Results

Our results demonstrated that glial cells were well plated on the electrode in the experimental setup and successfully activated. We were able to create both injury (thrombin/scratch) and acute inflammation (LPS) models that mimic the *in vivo* conditions of neural probe insertion associated with glial activation. The activation observed in our models confirmed the results of previous studies, i.e., that the glial activation induces morphological change and up-regulated inflammatory cytokine expression.

3.1. Cultured cell layer in the experimental setup

Mixed culture of mice astrocytes and microglia were well plated on the electrode as well as on the bottom surface in the experimental setup (Fig.2.2). Immunohistochemical staining showed plated cells on the electrode and on the bottom of the well surface: Green for astrocyte cell body (GFAP counter staining), red for microglia (Iba-1), and blue for all nuclei (Hoechst).

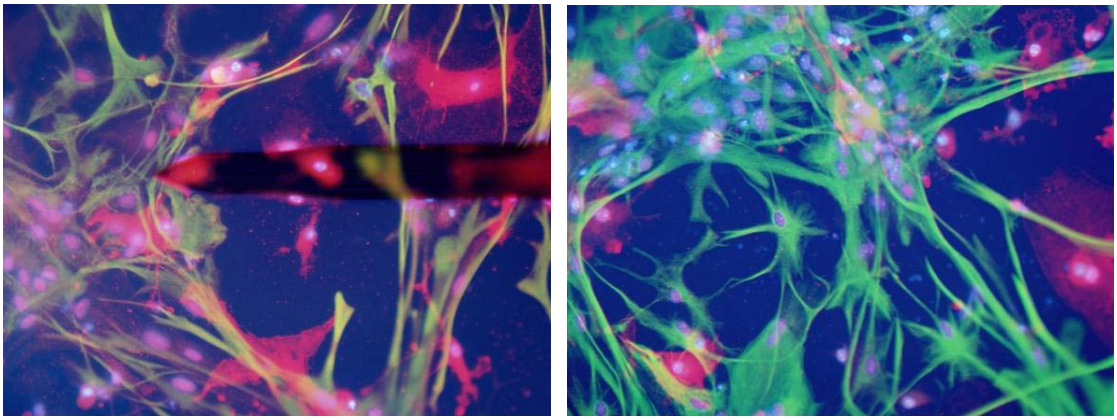

Fig.2.2. Immunohistochemical staining confirmed that cells microglia and astrocytes were successfully plated in the experimental setup. GFAP for astrocytes was stained in red, Iba1 for microglia in green, and Hoechst for all cell nuclei.

3.2. Verifying that the neural probe material does not activate glial cells

Glial cells were not activated by the material of the neural probe itself. Protein array (Fig.2.3) and ELISA (not shown) test results indicated that there was no difference in the amount of secreted cytokines between experimental cells on a neural probe and the control cells. We can deduce that the reactive tissue reaction around the neural probe insertion site may be caused by the injury due to the probe insertion not by the material of the probe. This result is in accordance with *in vivo* result that just one of two adjacent site showed large reactive reaction whereas another site showed very minimal reaction (Rousche and Normann 1998).

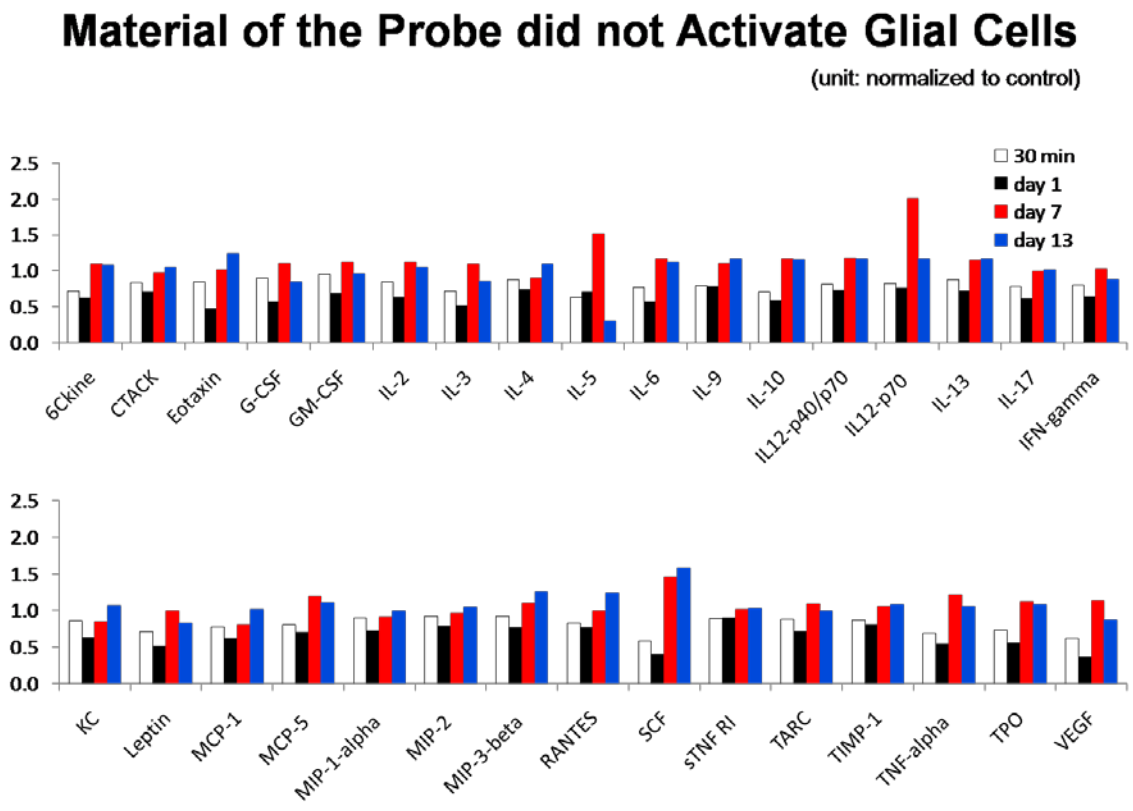

Fig.2.3. Normalized amount of inflammatory cytokines expressed in the cells with a probe at the bottom (experimental) to the control without a probe. Supernatant were collected at different time points (30min, days 1, 7, and 13) and analyzed by a protein array.

3.3 Thrombin concentration test

Cells subjected to 5 NIH U/mL of thrombin (Fig.2.4, second column from left) showed the greatest morphological change. Cells subjected to 1% FBS media (Fig.2.4, third row from the top) were not only viable, but also showed clear differentiation between the morphological changes caused by thrombin and those caused by FBS. Therefore, we decided to use 5 NIH U/mL of thrombin in 1% FBS for our thrombin/scratch model.

Please note that cells subjected to 10% FBS media (Fig.2.4, fourth row from the top) were viable as well. However, it was hard to determine the difference in morphologies between different thrombin concentrations. Cells in all three groups (0.1, 5 and 30 NIH U/mL of thrombin) were flat probably because high serum contents activated cells. In this case, it is hard to differentiate the effect of thrombin on glial activation. Therefore, we decided not to use 10% FBS media.

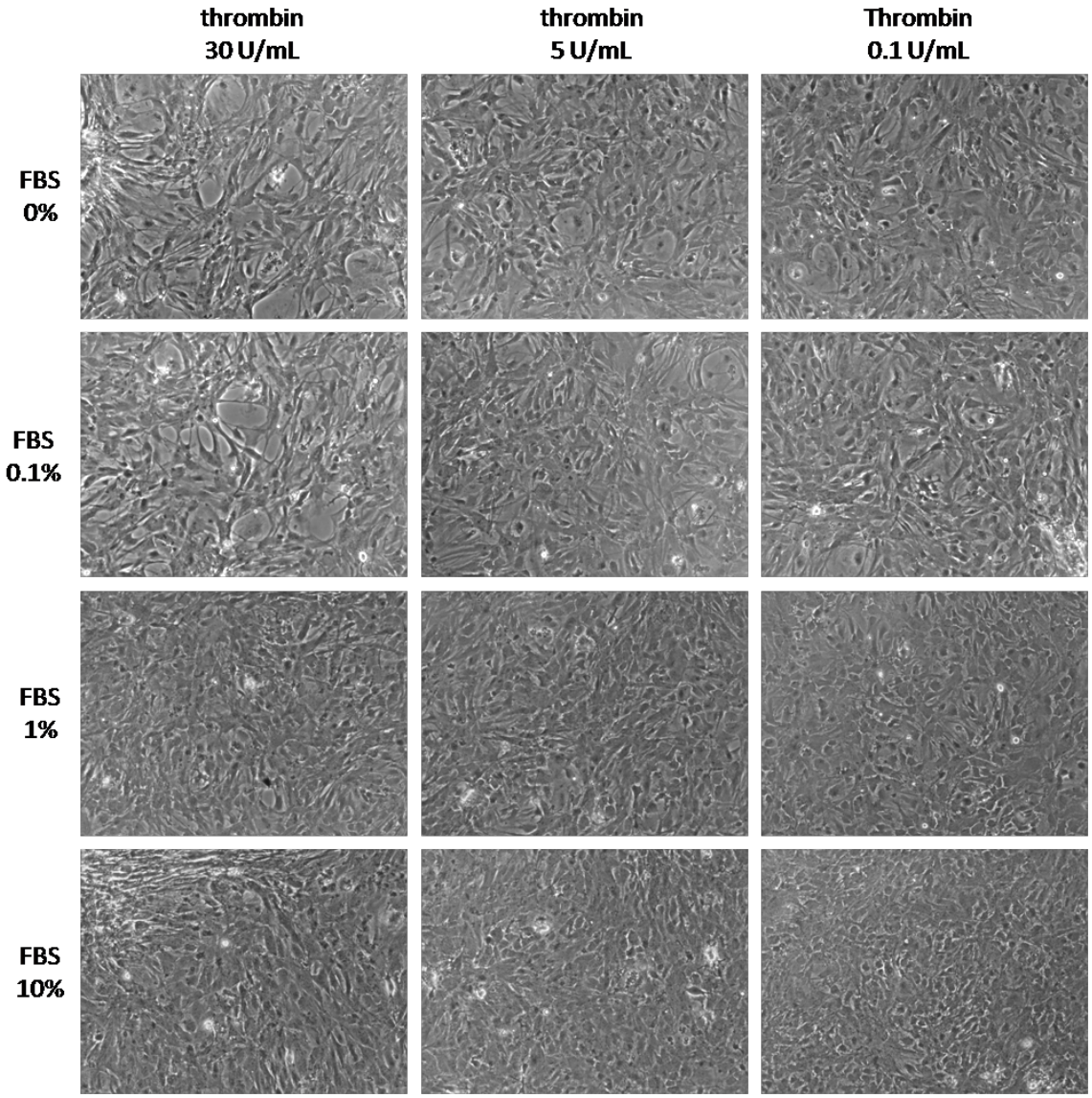

Fig.2.4. Phase contrast microscopic pictures of thrombin concentration test. Four different serum concentrations (0, 0.1, 1 and 10%) and three different thrombin concentrations (0.1, 5 and 30 NIH U/mL) were used. Each rows had same FBS concentration and each column had same thrombin concentration. Cells were deactivated in dbcAMP (250 μM in 0% serum for 24 hrs) and then subjected to one of these conditions.

3.4. Detection of glial activation

3.4.1. Morphological change

Thrombin (in 10% FBS), LPS (in 10% FBS) and 10% FBS all induced morphological changes in glial cells, as shown in Fig.2.5. Fig.2.5(a) shows the cells prior to thrombin treatment (5 NIH U/mL) and (b) shows cells 24 hrs post thrombin treatment. Adding thrombin (5 NIH U/mL in 0% FBS media) to the cells pretreated with dbcAMP (1mM in 0% FBS media for 24 hrs) induced morphological change from stellate to flat. Adding LPS (10 µg/mL in 10% FBS media) to the cells in dbcAMP (1mM in 0% FBS media) for 24 hrs also induced morphological change from stellate to flat. However, control group, adding 10% FBS media to the cells was in 0 dbcAMP (1mM in 0% FBS media) for 24 hrs, also induced the same change and there was no difference between these two groups.

3.4.2. PAR-1 expression

PAR-1 expression was not different between experimental and control groups indicating that activated PAR-1 was not detected more in experimental group. In all groups, PAR-1 was not as highly expressed (figure not shown). This low expression of the activated PAR-1 may be due to rapid internalization and subsequent degradation in the lysosomes (http://datasheets.scbt.com/sc-8202.pdf).

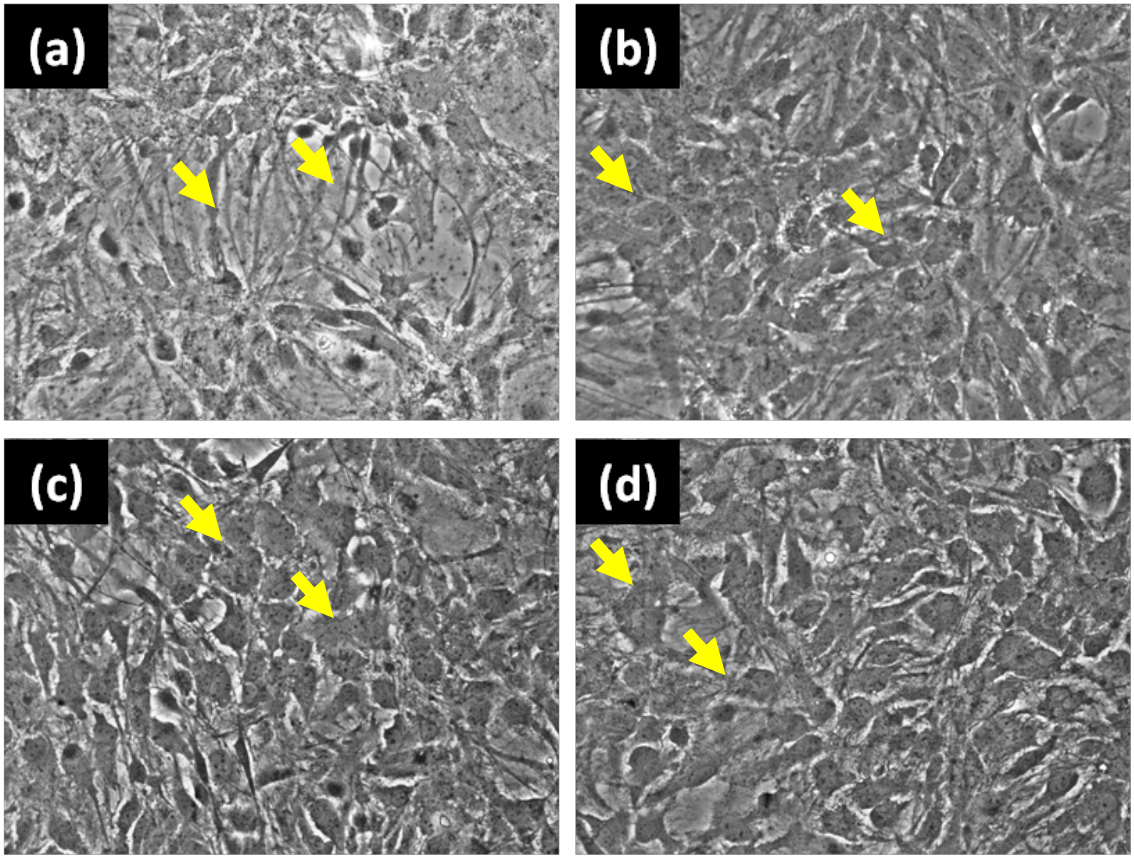

Fig.2.5. Glial cells were (a) treated in dbcAMP (250 µM in 0% serum for 24 hrs) to achieve stellate shape and then subjected to one of three conditions: (b) thrombin (5 NIH U/mL in 0% FBS media), (c) LPS (10 µg/mL in 10% FBS media), and (d) 10% FBS media. All three groups induced morphological changes. Specifically, there is no difference between (c) and (d).

3.4.3. Inflammatory cytokines

As expected, a greater amount of inflammatory cytokines were expressed in the injury (thrombin/scratch) and the acute inflammation (LPS) models compared to the control.

Fig.2.6 and Fig.2.8 shows the cytokines expressed on days 1 and 5 of the injury (thrombin/scratch) model and Fig.2.7 and Fig.2.9 shows the cytokines expressed in the

acute inflammation (LPS) model. To compare the relative expression of the cytokines experimental and control groups, we normalized the expression of experimental group to the control. (Fig.2.7 for thrombin/scratch and Fig.2.9 for LPS). This normalized expression indicated which cytokines were expressed more (by more than 50%) in the experimental group than in the control group. On day 1, 6Ckine, GM-CSF, IL-2, IL-4, IL-5, IL-6, IL-9, IL-10, IL12-p40/p70, IL12-p70, IL-13, IFN-gamma, KC, MCP-1, MIP-1-alpha, MIP-3-beta, RANTES and TNF-alpha were expressed more in the injury (thrombin/scratch) group than the control group (by more than 50%, see Fig.2.6). On day 5, 6Ckine, GM-CSF, IL-9, IL-10, IL12-p40/p70, IL12-p70, IL-13, IL-17, IFN-gamma, KC, MCP-1, MIP-1-alpha, MIP-3-beta, RANTES, sTNF RI, TARC, TNF-alpha, TPO and VEGF were expressed more in the injury (thrombin/scratch) group than the control group (by more than 50%, see Fig.2.8). IL-6 and TNF-alpha, major proinflammatory cytokines were expressed 2 fold more in the injury (thrombin/scratch) model than the control on day 1. TNF-alpha was expressed 9 fold more on day 5. IL-5 was expressed 6 fold more on day1 but was not expressed more on day 5. Please note that (1) IL-5 and IL-6 were more expressed on early stage (day 1) than on later stage (day 5), and (2) GM-CSF, IL-10, IL12-p70, MIP-1-alpha, RANTES and TNF-alpha were more expressed on both early stage (day 1) and later stage (day 5) (see Fig.2.10(a)). These temporal trends of cytokine expression correspond to the *in vivo* trend during cerebral wound healing using a traumatic brain injury model as shown in Fig.2.10(b) (Takamiya, Fujita et al. 2007). Not only proinflammatory cytokines but also antiinflammatory cytokines, such as, IL-10 and IL-13 were expressed more in the injury (thrombin/scratch) model. The antiinflammatory cytokines modulate the inflammation process or decrease the intensity

of the inflammation cascade. These pro- and anti-inflammation cytokines always expressed together with different level. The outcome of a disease is determined by the balance between these two cytokines (Dinarello 2000). Therefore the higher expression of IL-10 and IL-13 should be understood in the context of the balance of the cytokines.

For the acute inflammation (LPS) model, CTACK, GM-CSF, IL-4, IL-5, IL12-p40/p70, IL12-p70, IL-13, KC and RANTES were expressed more in the acute inflammation (LPS) group than the control group (by more than 50%, see Fig.2.9). On day 5, 6Ckine, CTACK, Eotaxin, G-CSF, GM-CSF, IL-2, IL-3, IL-4, IL-10, IL12-p40/p70, IL12-p70, IL-13, IL-17, IFN-gamma, KC, Leptin, MCP-1, sTNF RI, TARC, TNF-alpha, TPO and VEGF were expressed more. In the acute inflammation (LPS) model, the temporal cytokine expression trend was not observed as was found in the injury (thrombin/scratch) model.

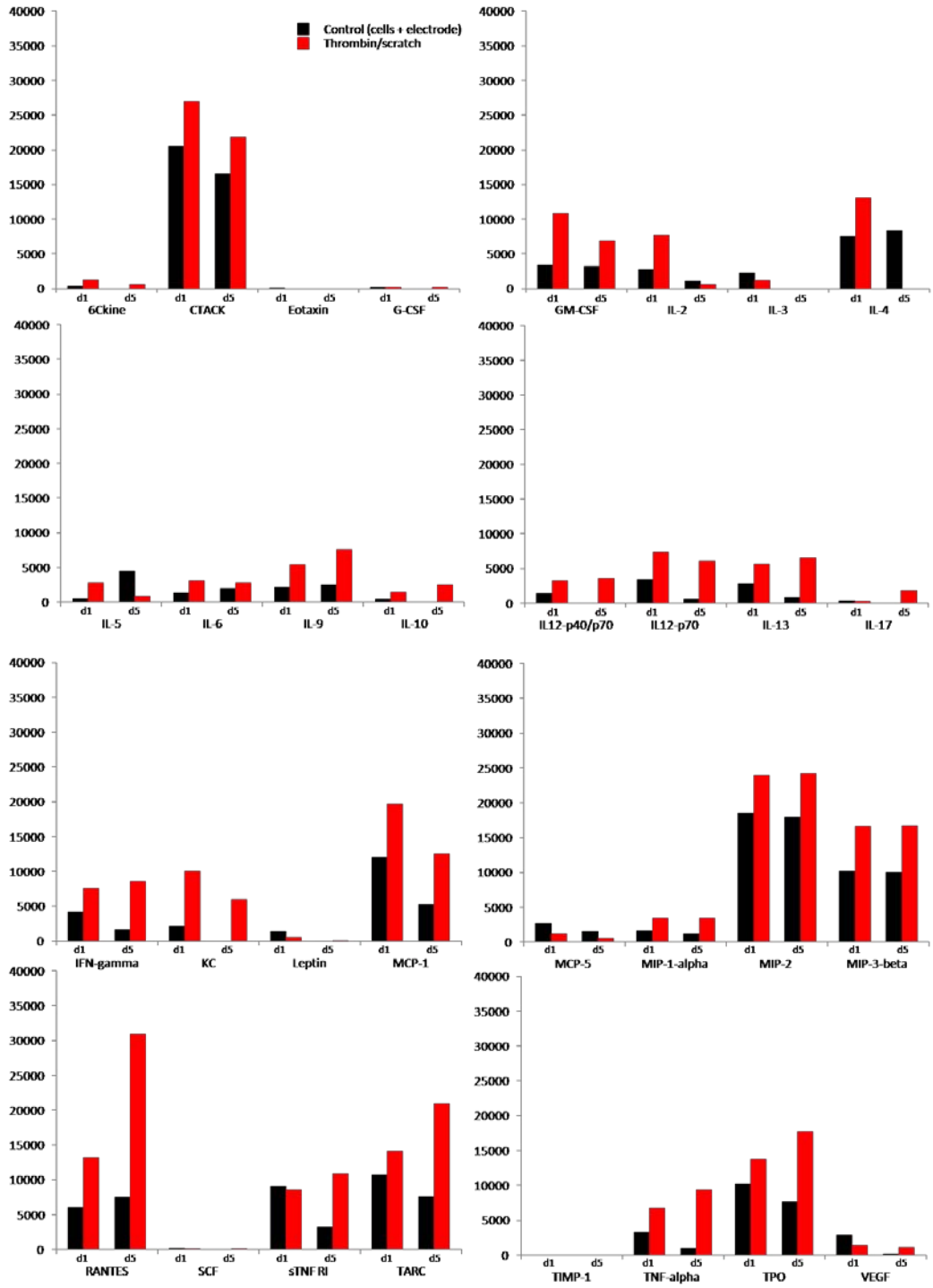

Fig.2.6. Inflammatory cytokines expressed in the injury (thrombin/scratch) group. Cells of the injury group (experimental) were treated with thrombin (5 NIH U/mL) and a scratch was made on the cell layer. Cell lysate samples were collected at days 1 and 5, and analyzed by a protein array. X-axis shows each cytokine at day 1 and day 5 and y-axis indicates arbitrary number for expressed signal intensity. Red bars are for the injury (thrombin/scratch) group and black bars for the control, which had the same condition (cells on a probe) but no treatment.

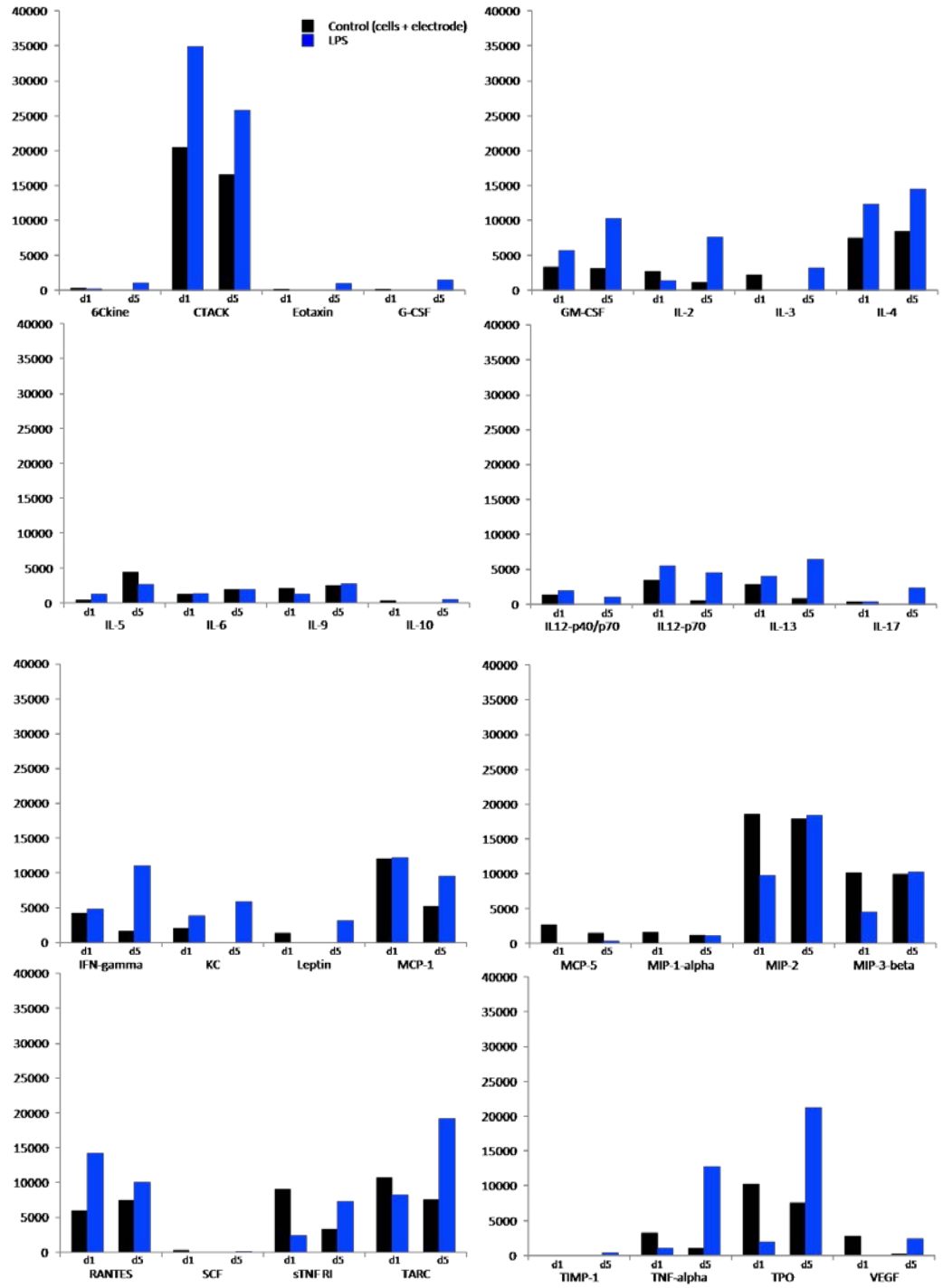

Fig.2.7. Inflammatory cytokines expressed in the acute inflammation (LPS) group. Cells of the acute inflammation group (experimental) were treated with LPS (10 µg/mL). Cell lysate samples were collected at days 1 and 5, and analyzed by a protein array. X-axis shows each cytokine at day 1 and day 5 and y-axis indicates arbitrary number for expressed signal intensity. Blue bars are for the acute inflammation (LPS) group and black bars for the control, which had the same condition (cells on a probe) but no treatment.

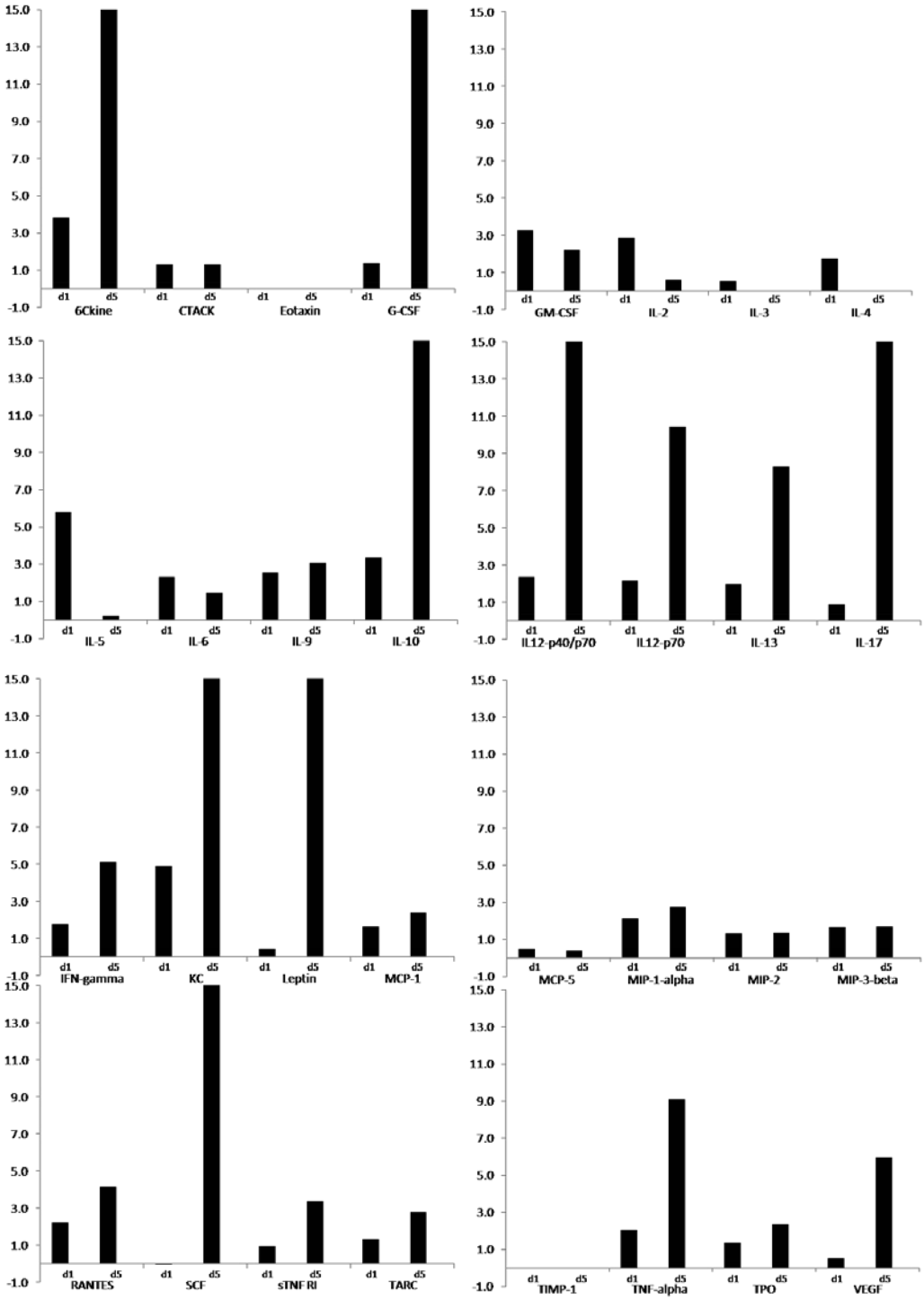

Fig.2.8. Normalized amount of inflammatory cytokines expressed in the injury (thrombin/scratch) group to the control. Normalized values were calculated based on the same data shown in Fig.2.6. Y-axis indicates folds of expression of the injury group compared to the control, which had the same condition (cells on a probe) but no treatment.

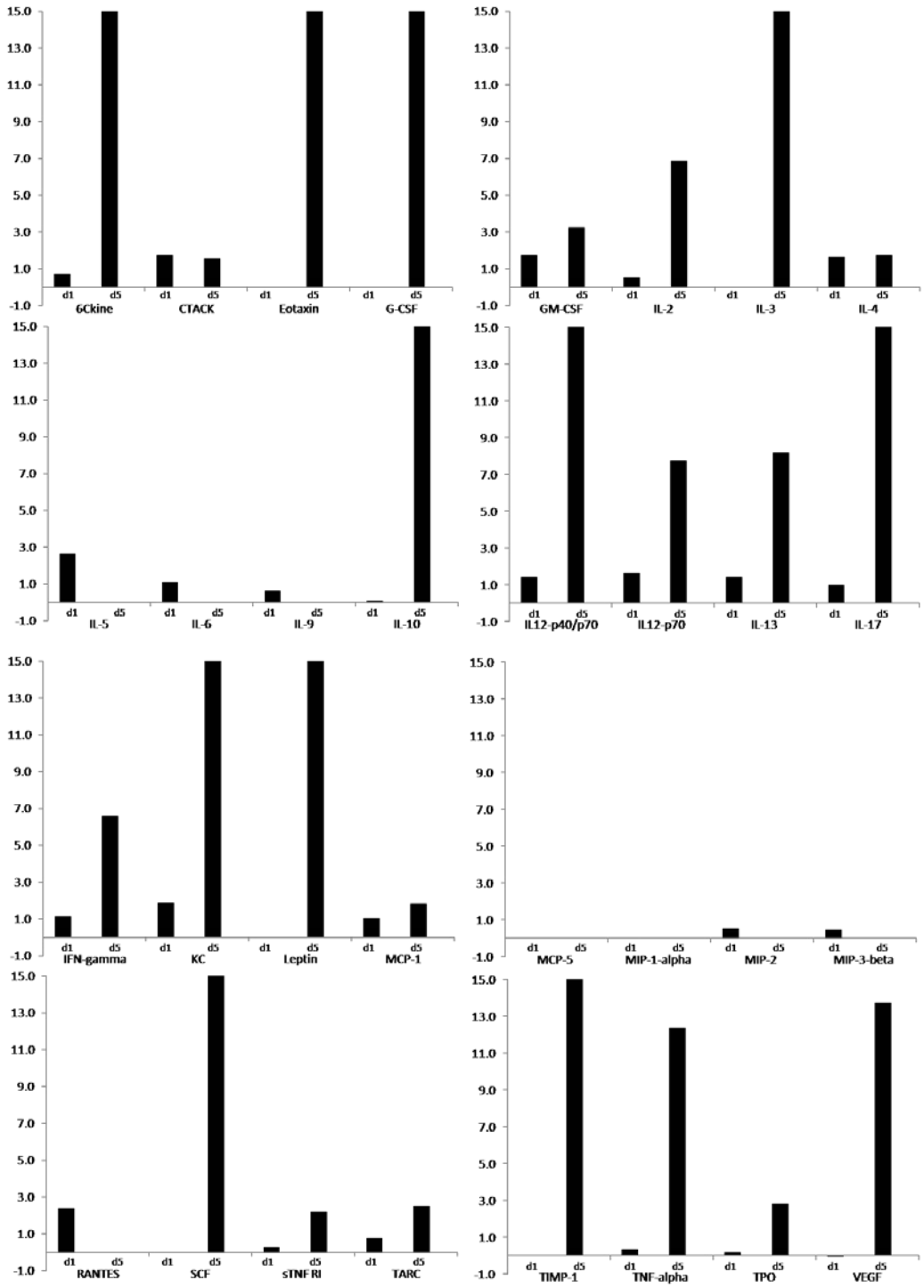

Fig.2.9. Normalized amount of inflammatory cytokines expressed in the acute inflammation (LPS) group to the control. Normalized values were calculated based on the same data shown in Fig.2.7. Y-axis indicates folds of expression of the injury group compared to the control, which had the same condition (cells on a probe) but no treatment.

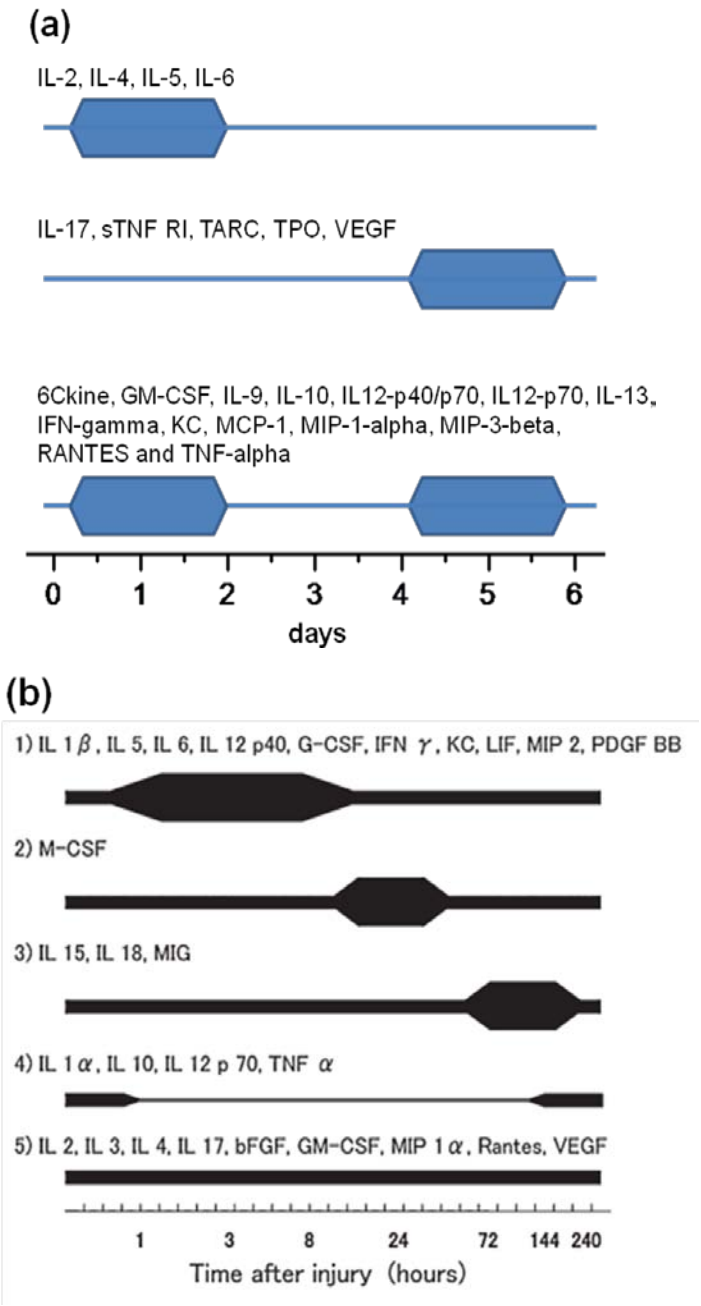

Fig.2.10. Cytokine expression trends during: (a) our *in vitro* injury (thrombin/scratch) model and (b) *in vivo* cerebral wound healing using a traumatic brain injury model from (Takamiya, Fujita et al. 2007). In (a), please note that (1) IL-5 and IL-6 were more expressed on early stage (day 1) than on later stage (day 5), and (2) GM-CSF, IL-10, IL12-p70, MIP-1-alpha, RANTES and TNF-alpha were more expressed on both early stage (day 1) and later stage (day 5). These temporal trends of cytokine expression correspond to the *in vivo* trend in (b). Please note that the time scale in this *in vivo* study could be different from the time scale in the *in vitro* model.

4. Discussion

We proposed and verified a novel tissue injury model to activate glial cells, which simulates both mechanical injury and the micro-hemorrhage by the blood vessel rupture. This injury model was validated by confirming glial activation through demonstrating morphological change and up-regulated proinflammatory cytokines. In addition, acute inflammation model using LPS was characterized by the same protocol. These models are expected to be used for further *in vitro* glial activation studies.

Cellular activation of glial cells by the injury model (thrombin/scratch) and the acute inflammation model (LPS) was confirmed by up-regulated inflammatory cytokine secretion (Fig.2.6, 2.7, 2.8 and 2.9). Cytokines are low molecular weight glycoprotein that activates glial cells and also secreted by activated glial cells (Giulian, Woodward et al. 1988; Lieberman, Pitha et al. 1989; Sawada, Kondo et al. 1989). Proinflammatory cytokines such as IL-1, IL-6, IFN-gamma and TNF-alpha are up-regulated at the site of injury in CNS and activates glial cells (John, Lee et al. 2003). He et al. demonstrated that TNF-alpha is highly expressed in cells at the probe-tissue interface as shown in Fig.2.11 (He, McConnell et al. 2007). Biran et al. observed highly expressed TNF-alpha and MCP-1 from the glial cells of explanted microelectrode at 1 week post implantation (Biran, Martin et al. 2005). These proinflammatory cytokines were also more expressed in the cells of our injury and acute inflammation models than in the control group confirming the glial cells in our model has been activated.

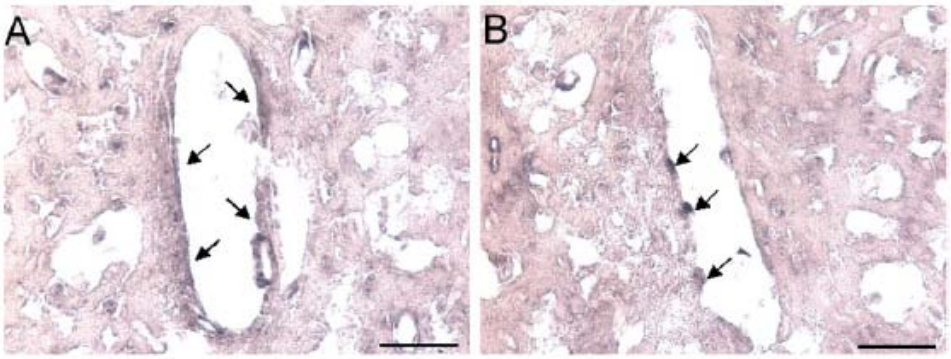

Fig.2.11. In situ hybridization of tissue sections from brain at 1 week post implantation. Arrows indicate TNF-alpha expressing cells (He, McConnell et al. 2007).

Glial cells treated with thrombin/scratch also induced morphological changes. In the injury (thrombin/scratch) group, cellular treatment by dbcAMP (Fig.2.5(a)) induced morphological change from flat into stellate as observed by Skaper et al. (Fig.2.12(b)) (Skaper, Facci et al. 1986) and by Nelson et al. (Fig.2.13(d)) (Nelson and Siman 1990) in rat astrocytes. After treatment by thrombin (Fig.2.5(b)), cells changed their morphology from stellate into flat, similar to the cells treated by thrombin (Fig.2.13(e)) or kept in 10% FBS (Fig.2.13(a)) as observed by Nelson et al. The morphological change by thrombin is mediated via Rho, a small GTP binding protein as demonstrated by Suidan et al. Thrombin also increases proliferation, expression of nerve growth factor (NGF) to promote the survival of astrocytes against environmental challenge (Suidan, Nobes et al. 1997; Ramakers and Moolenaar 1998). As shown in the literature survey by Suo et al., the effect of thrombin on astrocytes *in vitro* is dose dependant (Suo, Citron et al. 2004). At low doses in the pM level, thrombin causes morphological change from stellate into flat and prevents cell death. At high dose in the nM level, thrombin induces proliferation, up-regulation of inducible nitric oxide synthase (iNOS), proinflammatory cytokines and cell death of astrocytes (Jiang, Wu et al. 2002). This dose dependant action of thrombin

on astrocytes was also shown *in vivo*. Pretreatment of low dose thrombin protects astrocytes and neurons whereas high dose thrombin infusion or injury induced thrombin initiated inflammation and resulted in glial scar (Suo, Citron et al. 2004). However, this dose-dependent action of thrombin is specific to the source of thrombin. Experimental results from the Xi group demonstrated that 5 NIH U/mL rat thrombin but not human thrombin caused neuronal death of cultured rat cells (personal communication with Dr. Xi). The dose of thrombin (5 NIH U/mL from bovine plasma) we used in our model was high enough to activate glial cells but not too high to induce the cell death of astrocytes and microglia.

The results suggest that thrombin induced the morphological change in glial cells whereas the morphological change in the acute inflammation (LPS) group may be due to the high serum contents in the media. As shown in Fig.2.14, Beecher et al. observed the flat shaped mouse astrocytes when cells were treated with 10% FBS for 12 hrs (Fig.2.14(a)) and stellate shaped cells in 0% FBS for 12 hrs (Fig.2.14(b)) (Beecher, Andersen et al. 1994). Nelson also observed the same morphological trend in rat astrocytes (Nelson and Siman 1990). Please note, however, that LPS (1 μg/mL) induces morphological change from ramified to amoeboid as observed by Beck et al. in cultured mouse microglia (Fig.2.15). They observed that microglia shows a ramified (resting), 'fried egg'-shaped (fully activated) or intermediate morphology (Fig.2.15(A), left, right and in the middle respectively). From day 1 to day 7 after subculturing, about 90% of the cells represented the ramified (resting) and 10% the 'fried-egg'-shaped (activated) type (Fig.2.15(B)). After adding 1 μg/mL lipopolysaccharide (LPS), 34% of the cells revealed a 'fried egg'-shaped morphology already within 3 h. Within 48 h, the ratio of cell types

completely reversed to just 6% ramified and 94% ‘fried egg’-shaped cells (see Fig.2.15(C)) (Beck, Penner et al. 2008).

A future model may include both injury by thrombin/scratch and acute inflammation by LPS in the same setup because injury is accompanied by acute inflammation as shown in literature survey by Arvin et al. (Arvin, Neville et al. 1996). As Jones and Geczy demonstrated, IL-1 activity of guinea-pig macrophages was greatly increased by the presence of thrombin during the activation by LPS. Although thrombin alone had no effect, inclusion of 1 mU/mL of thrombin with suboptimal levels of LPS produced a 200-fold increase in IL-I activity, and further increase was observed with increasing doses of thrombin (Jones and Geczy 1990).

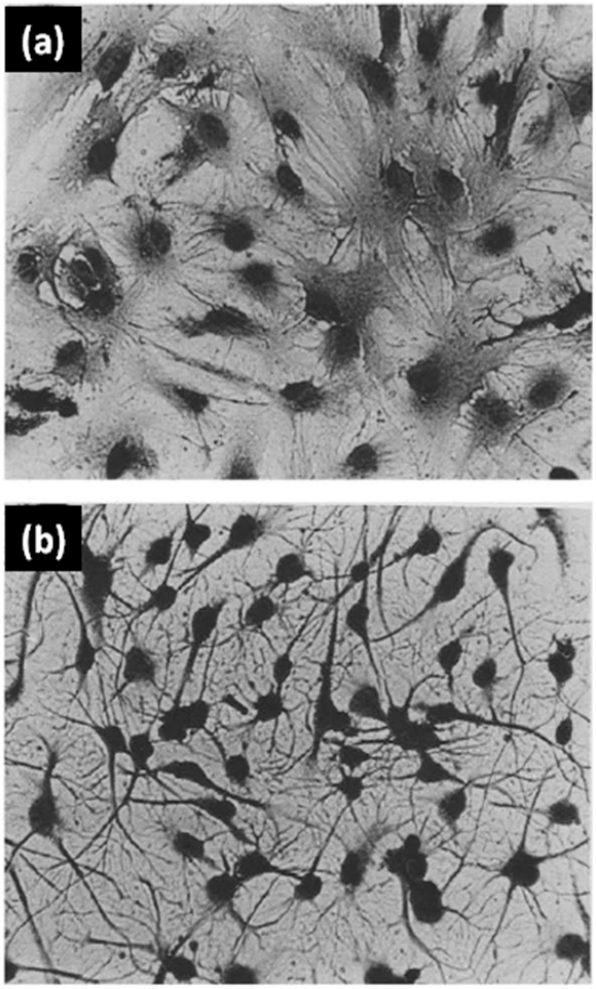

Fig.2.12. Morphological change of astrocytes from flat (a) to stellate (b) shapes. Secondary astrocytes were treated for 24 hrs in serum free media and treated again in serum free media without (a) or with (b) 1 mM dbcAMP for another 24 h (Skaper, Facci et al. 1986).

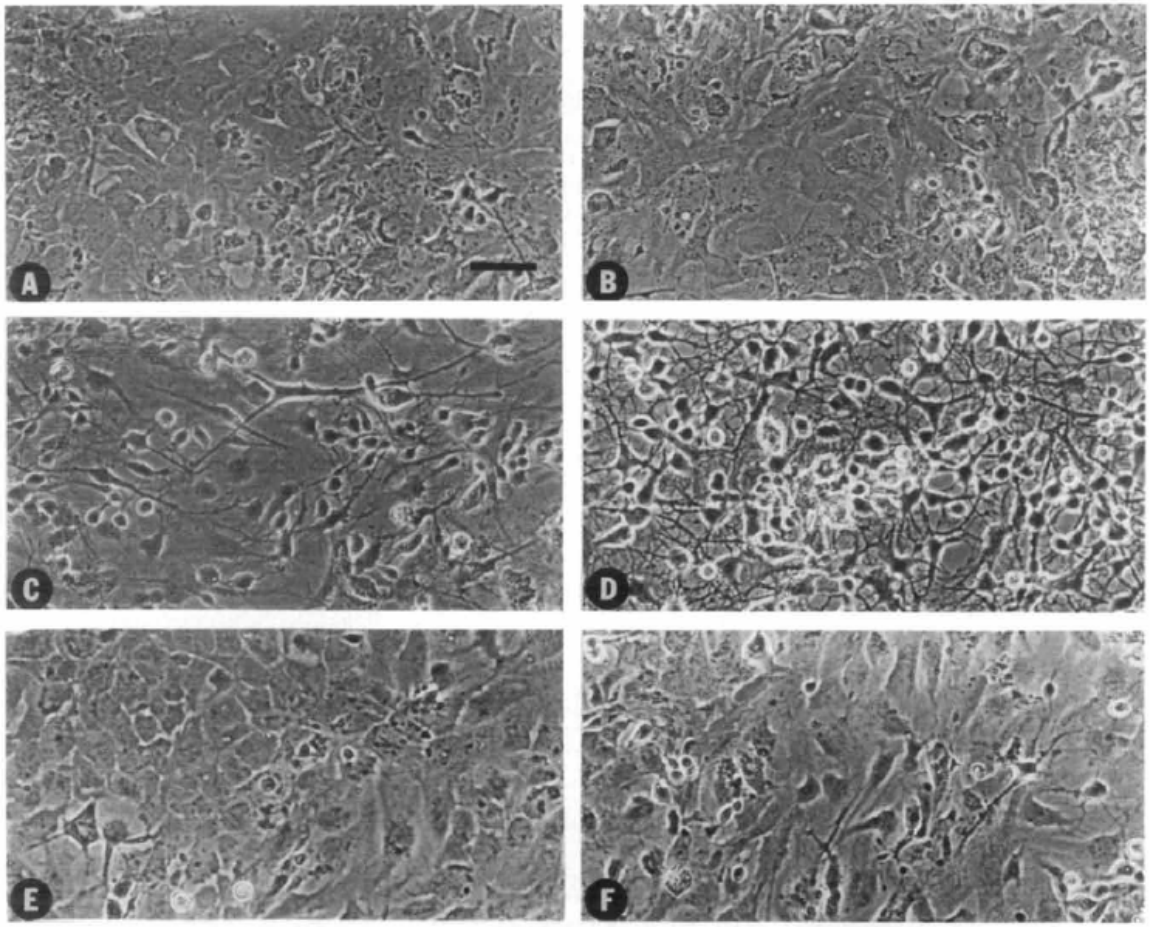

Fig.2.13. Thrombin effects on glial differentiation. 20-day-old mixed glial cultures were incubated in basal medium plus additions listed below, and photographed after 1 h. (A) 10% FBS; (B) 10% FBS+250 µM dbcAMP; (C) 0% FBS; (D) 0% FBS+250 µM dbcAMP; (E) 0% FBS+50 nM thrombin; (F) 0% FBS+50 nM thrombin+250 pM dbcAMP (Nelson and Siman 1990).

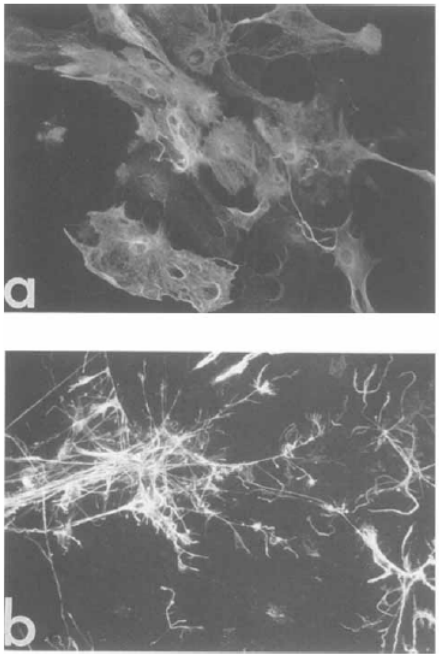

Fig.2.14. Serum effects on astrocyte morphology. Mouse cortical astrocytes were treated for 12 hr in 10% serum media (a), or serum free media (b). Cell treated in 10% serum were flat and cells treated in 0% serum was stellate (Beecher, Andersen et al. 1994).

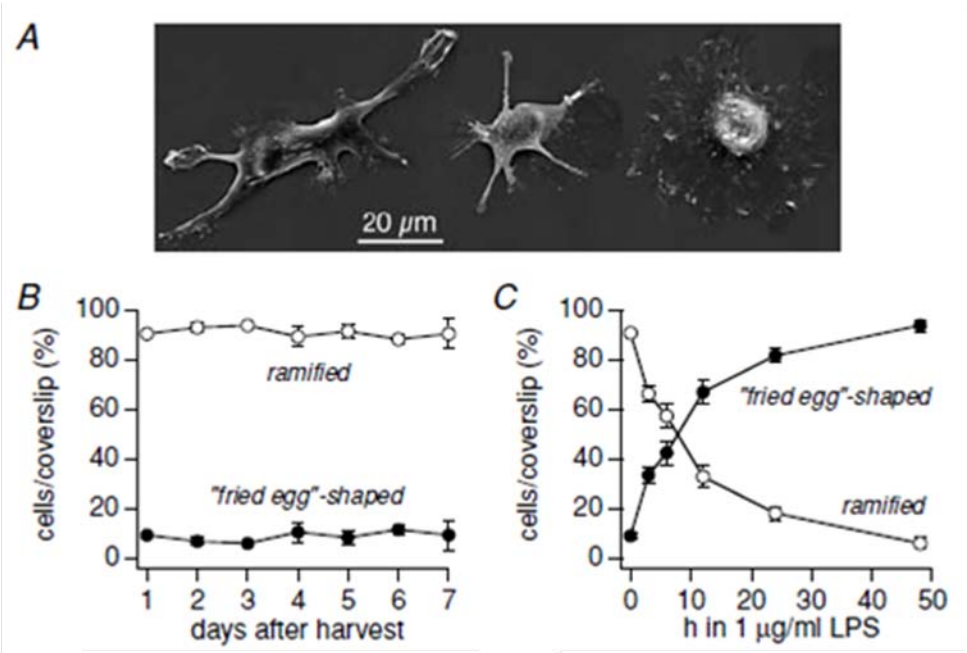

Fig.2.15. Morphology of microglia, (A), composite image of scanning electron micrographs of microglial cells at various stages of activation with 1 µg/mL LPS from non-activated (left cell, arborized) to fully activated (right cell, 'fried egg'-shaped). (B) and (C), percentage of ramified (mean ± S.E.M.) and 'fried egg'-shaped (mean ± S.E.M.) cells per coverslip depending on time in subculture (Beck, Penner et al. 2008).

References

Arvin, B., L. F. Neville, et al. (1996). "The role of inflammation and cytokines in brain injury." Neurosci Biobehav Rev **20**(3): 445-52.

Beck, A., R. Penner, et al. (2008). "Lipopolysaccharide-induced down-regulation of Ca2+ release-activated Ca2+ currents (I CRAC) but not Ca2+-activated TRPM4-like currents (I CAN) in cultured mouse microglial cells." J Physiol **586**(2): 427-39.

Beecher, K. L., T. T. Andersen, et al. (1994). "Thrombin receptor peptides induce shape change in neonatal murine astrocytes in culture." J Neurosci Res **37**(1): 108-15.

Biran, R., D. C. Martin, et al. (2005). "Neuronal cell loss accompanies the brain tissue response to chronically implanted silicon microelectrode arrays." Experimental Neurology **195**(1): 115-126.

Coughlin, S. R. and E. Camerer (2003). "PARticipation in inflammation." J Clin Invest **111**(1): 25-7.

Dinarello, C. A. (2000). "Proinflammatory cytokines." Chest **118**(2): 503-508.

Frampton, J. P., M. R. Hynd, et al. (2007). "Three-dimensional hydrogel cultures for modeling changes in tissue impedance around microfabricated neural probes." Journal of Neural Engineering **4**(4): 399-409.

Giulian, D., J. Woodward, et al. (1988). "Interleukin-1 injected into mammalian brain stimulates astrogliosis and neovascularization." J Neurosci **8**(7): 2485-90.

He, W., G. C. McConnell, et al. (2007). "A novel anti-inflammatory surface for neural electrodes." Advanced Materials **19**(21): 3529-+.

Jiang, Y., J. Wu, et al. (2002). "Thrombin-receptor activation and thrombin-induced brain tolerance." J Cereb Blood Flow Metab **22**(4): 404-10.

John, G. R., S. C. Lee, et al. (2003). "Cytokines: powerful regulators of glial cell activation." Neuroscientist **9**(1): 10-22.

Jones, A. and C. L. Geczy (1990). "Thrombin and factor Xa enhance the production of interleukin-1." Immunology **71**(2): 236-41.

Lieberman, A. P., P. M. Pitha, et al. (1989). "Production of tumor necrosis factor and other cytokines by astrocytes stimulated with lipopolysaccharide or a neurotropic virus." Proc Natl Acad Sci U S A **86**(16): 6348-52.

Merrill, D. R. and P. A. Tresco (2005). "Impedance characterization of microarray recording electrodes *in vitro*." Ieee Transactions on Biomedical Engineering **52**(11): 1960-1965.

Nelson, R. B. and R. Siman (1990). "Thrombin and its inhibitors regulate morphological and biochemical differentiation of astrocytes *in vitro*." Brain Res Dev Brain Res **54**(1): 93-104.

Nicole, O., A. Goldshmidt, et al. (2005). "Activation of protease-activated receptor-1 triggers astrogliosis after brain injury." J Neurosci **25**(17): 4319-29.

Polikov, V. S., M. L. Block, et al. (2006). "*In vitro* model of glial scarring around neuroelectrodes chronically implanted in the CNS." Biomaterials **27**(31): 5368-76.

Ramakers, G. J. and W. H. Moolenaar (1998). "Regulation of astrocyte morphology by RhoA and lysophosphatidic acid." Exp Cell Res **245**(2): 252-62.

Rousche, P. J. and R. A. Normann (1998). "Chronic recording capability of the Utah Intracortical Electrode Array in cat sensory cortex." J Neurosci Methods **82**(1): 1-15.

Sawada, M., N. Kondo, et al. (1989). "Production of tumor necrosis factor-alpha by microglia and astrocytes in culture." Brain Res **491**(2): 394-7.

Skaper, S. D., L. Facci, et al. (1986). "Morphological modulation of cultured rat brain astroglial cells: antagonism by ganglioside GM1." Brain Res **390**(1): 21-31.

Suidan, H. S., C. D. Nobes, et al. (1997). "Astrocyte spreading in response to thrombin and lysophosphatidic acid is dependent on the Rho GTPase." Glia **21**(2): 244-52.

Suo, Z., B. A. Citron, et al. (2004). "Thrombin: a potential proinflammatory mediator in neurotrauma and neurodegenerative disorders." Curr Drug Targets Inflamm Allergy **3**(1): 105-14.

Suzumura, A., S. Bhat, et al. (1984). "The isolation and long-term culture of oligodendrocytes from newborn mouse brain." Brain Res **324**(2): 379-83.

Takamiya, M., S. Fujita, et al. (2007). "Simultaneous detections of 27 cytokines during cerebral wound healing by multiplexed bead-based immunoassay for wound age estimation." J Neurotrauma **24**(12): 1833-44.

CHAPTER III

EFFECT OF GLIAL CELL ACTIVATION ON THE IMPEDANCE OF THE NEURAL PROBE USING AN *IN VITRO* MODEL

1. Introduction

Although the correlation of the full encapsulation and signal quality loss is well known empirically, we still had to determine which step of the encapsulation process decreases signal quality significantly. Better understanding of signal quality loss will make it possible to devise better strategies to resolve the problem.

We were interested in investigating at which point in the encapsulation process signal loss is initiated: at the early inflammation stage or the later scar formation stage. It is important to identify the initiation point in order to determine the optimal time to intervene in the encapsulation process. If it occurs at an early stage, we should focus on preventing glial activation by the thrombin influx caused by the blood vessel rupture. If it occurs only at a later stage, we should focus more on how to disconnect the process between inflammation and scar formation.

In vivo studies showed that there is a rapid increase in impedance between days 3 and 7 post probe insertion (Vetter, Williams et al. 2004; Ludwig, Uram et al. 2006). Vetter et al. observed a significant impedance increase between weeks 0 and 1 of 177 μm^2-site size electrodes and weeks 0 and 2 of 312 μm^2-site size electrodes (Fig.3.1). Ludwig et al. also observed a sharp increase of impedance between days 3 and 7 (Fig.3.2) accompanied with significant decrease in percentage of sites recording low- and high-quality units (Fig.3.3). This increase in impedance is believed to occur because of the

tight intercellular adhesion formed when astrocytes around the probe were activated by inflammation cascade rather than because of the glial scar, which usually is seen between two and four weeks post probe insertion (Turner, Shain et al. 1999; Szarowski, Andersen et al. 2003).

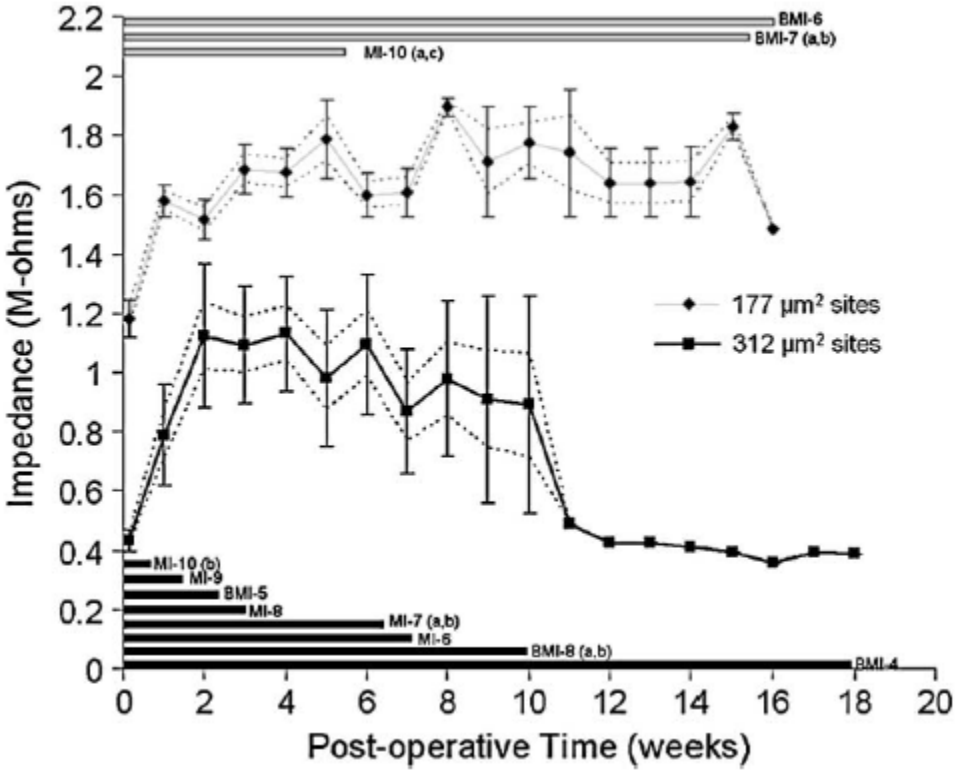

Fig.3.1. Mean impedance values across all implanted probes over time. Data are grouped by the size of the recording sites. Time bars indicate the contribution from each animal. Dotted lines represent the average standard error within each array and the error bars represent the standard error between each array (from (Vetter, Williams et al. 2004).

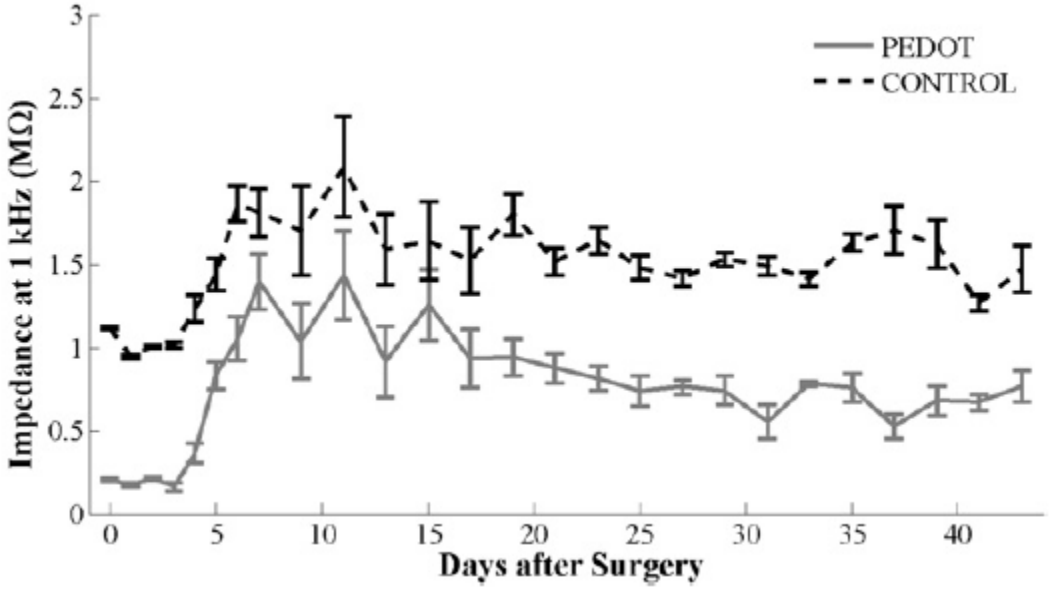

Fig.3.2. Average site impedances at 1 kHz over time. The electrodes were implanted in rat brains. Impedances increased dramatically the third day after implantation, up to a maximum value at the one-week mark (from (Ludwig, Uram et al. 2006).

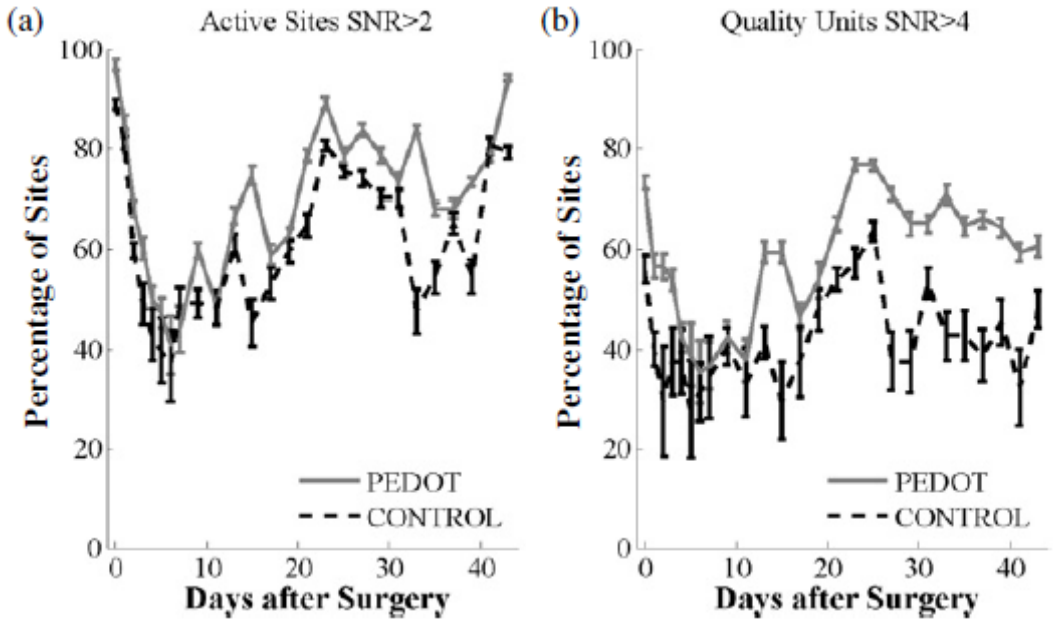

Fig.3.3. Percentage of sites recording low- and high-quality units on a given day. (a) Units with SNR > 2. (b) Quality units with SNR > 4. Unit recordings tended to be unstable over the first two weeks after implantation. During these two weeks, a noticeable drop in measurable units occurred on both PEDOT and control sites (from (Ludwig, Uram et al. 2006).

To investigate if the impedance increase is due to the activation of glial cells in the early inflammation stage, we tested the impedance increase during the glial activation. We prepared an *in vitro* setup, in which astrocytes and microglia cells were plated on the microelectrode, monitoring electrical impedance across the plated cell layers. These astrocytes and microglia were activated by the injury model (thrombin/scratch) or the acute inflammation model (LPS) as described in chapter 2. The impedance increase was monitored before and after activation and compared to the impedance across the glial cell layers without activation (control group).

The second goal of this study is to develop a new in-vitro model that uses recorded signal quality to detect encapsulation and to investigate cellular encapsulation using the new model. Detecting encapsulation by the recorded signal quality gives us more direct understanding of encapsulation because we can analyze which frequency component of the recorded signal is degraded by a specific type of encapsulation, i.e., encapsulation by early reactive response or sustained chronic response. To test the signal conduction through the different thickness and tightness of the sheath, we used the the *in vitro* cellular encapsulation model described in chapter 2. We have also developed an *in vitro* stimulating/recording setup to investigate the relationship between recorded signal quality and cellular encapsulation.

2. Method

To investigate the glial inflammation effect on the performance of the recording electrode, we developed a impedance monitoring setup using the *in vitro* glial activation

model described previously (chapter 2). To create different levels of inflammation, we treated the cultured glial cells on the neural probes under three different conditions: 1) activation by the injury model (thrombin/scratch, experimental), 2) activation by the acute inflammation model (LPS, experimental), and 3) no treatment (control). These three conditions were created to test the hypothesis that the tight encapsulation resulting from the proliferation, changes in morphology, and higher intercellular adhesion, characteristic of cellular activation, is responsible for the reduced performance of the neural probe.

The activated conditions (experimental) represent the injury or the acute inflammation due to probe insertion. The inactivated condition (control) represents the resting state of the glial cells. The performance of the probe was determined by the measured electrical impedance.

To investigate the cellular encapsulation effect on the performance of the recording electrode, we developed and validated an *in vitro* 'stimulation/recording' setup. During the development process, we found that there were daily fluctuations in the recorded signal amplitude even without plated cells on the electrode. Similar fluctuation was observed in the impedance measurements as well. To eliminate these fluctuations, we employed a control electrode array (without plated glial cells) and linear regression model to provide a baseline value for the recorded signal and impedance. Using the new setup, we could determine the net effect of cellular encapsulation on both recorded signal quality and impedance.

2.1. Glial activation effect on impedance

2.1.1. Experimental setup

Primary glial cells were isolated from fetal mouse brain and plated on a 75 cm^2 tissue culture treated flask as described in chapter 2. These cells were allowed to grow and proliferate for 2-3 weeks based on the state of confluence and then plated on the experimental setup, which contains a recording electrode on the bottom of a well. The setup was prepared for cell plating using the same protocol previously describes (see chapter 2 for details). Mixed cells were plated on the well at a density of $2x10^5$ cells per well (2 cm^2). They were allowed to settle and become confluent for 48 hours in 10% fetal bovine serum (FBS) media and then subjected to two different conditions for each setup: 1) activation by thrombin/scratch (experimental), and 2) no treatment (control). For the experimental group, a mechanical scratch was made on the confluent glial cell layer along the shank of the neural probe using a sterile 31-gauge syringe needle and 5 NIH U/mL of thrombin from bovine plasma (Sigma-Aldrich, Inc. St. Louis, MO) in 1% FBS culture media was supplied to the cells (see chapter 2 for more details). Only 1% FBS culture media was supplied for the control group with no thrombin or mechanical scratch.

2.1.2. Neural probes

Microfabricated neural probes (NeuroNexus Technologies, Ann Arbor, MI) with 16 iridium electrodes (each with a surface area of 177 μm^2) were mounted on the bottom of a cell culture treated Petri-dish to serve as a recording electrode. A custom built polystyrene ring was mounted around the neural probe to provide a well to hold cell

culture media around the probe. The function of the well was 1) to confine glial cells just around the neural probe, and 2) to reduce the amount of the activation/deactivation agents (thrombin and LPS) required in the media. Three electrodes were used to measure the impedance: working (microelectrodes), counter (platinum-iridium coil), and reference (miniature Ag/AgCl). The counter and reference electrodes were inserted in the electrolyte on the well only when the impedance measurement was conducted.

62 electrode sites in four independent conditions were used for the injury group (thrombin/scratch), 46 electrode sites in three independent conditions were used for the acute inflammation group (LPS), and 52 electrode sites in four independent conditions were used for the control group with cells but without treatment. To confirm the baseline impedance is constant during the entire period of experiment, we monitored the impedance of the bare electrodes with no cells but in the same condition – coated with fibronectin, soaked in the same cell culture media, temperature and carbon dioxide level.

2.1.3. Impedance measurement

We conducted all the electrophysiological tests in an electrolyte of Hepes-buffered Hanks' saline (HBHS) maintaining the cells in a 37^{o} C and 5% carbon dioxide environment in a tissue culture incubator with electromagnetic shied by copper mesh. HBHS was chosen because basic buffered saline provides the most stable results for our micro scale electrodes compared to DMEM or culture media with serum. Three electrodes were used to measure the impedance: working (microelectrodes), counter (platinum-iridium coil), and reference (miniature Ag/AgCl). Eco Chemie Autolab Potentiostat and Frequency Response Analysis software (Metrohm USA Inc., Riverview,

FL) were used to measure impedance. Impedance measurements were conducted on days 1 and 5 after activation to match the time points of injury model (see chapter 2).

The impedance was measured in a frequency sweep limited to the frequencies typical of *in vivo* recordings. *In vivo* signal recordings are composed of two significant band widths: (1) local field potential (LFP) including alpha (8-12 Hz), beta (12-24 Hz), and gamma (24-70 Hz) bands and (2) neuronal spikes around 1 kHz. To represent these bands, several frequencies were chosen for the impedance spectra: alpha (10 Hz), beta (16 Hz), gamma (47 Hz), and neuronal spikes (300, 650, 1000, 3000 and 5000 Hz).

We took phase contrast microscopic pictures right before the impedance measurements to confirm that the cells were confluent and viable during the impedance measurements.

2.1.4. Statistical analysis

SPSS software package (SPSS Inc. Chicago, IL) was used to conduct student's t-test to compare means of experimental and control groups if they are significantly different.

2.2. Glial encapsulation effect on signal recording

2.2.1. Experimental setup

The setup is composed of three major components: a stimulator, a test chamber (Petri dish setup) and a recording system. The stimulator transmits electrical signals mimicking *in vivo* neuronal spikes to the stimulation electrodes in the test chamber (a Petri-dish setup) filled with phosphate-buffered saline (PBS). In the test chamber, the

signal is propagated in the PBS, received by the recording electrode and then processed. Glial cells were plated on the recording electrode to model cellular encapsulation *in vitro*. With the *in vitro* model in the chamber, electro-physiological (EP) tests were performed in order to investigate the relationship between the recorded signal quality and the encapsulation. Two types of EP tests were conducted: 1) signal quality analysis using the stimulation/recording setup and 2) impedance measurements.

Recording electrodes consisted of two microelectrode arrays (NeuroNexus, Ann Arbor, MI); one for the experimental group and the other for the control group. Each electrode array has 16 electrodes in line made of iridium with 100 μm space between each electrode. Each electrode has 177 μm^2 site area. On top of the electrodes of the experimental group, glial cells were plated to simulate the cellular encapsulation in the brain.

The Petri-dish test chamber allowed us to make an *in vitro* cellular encapsulation model using glial cells, which form a cellular sheath around the implanted recording/stimulation electrode array. Glial cells were kept aseptic in the test chamber while the electro-physiology (EP) tests were being performed to model encapsulation. For the EP tests using the stimulation/recording setup, three types of electrodes were placed in the test chamber: stimulation, recording and reference electrodes. For the EP tests measuring impedances, three types of electrodes were placed in the test chamber: counter, recording and reference electrodes.

2.2.2. Signal recording

A differential recording method was applied to eliminate white noise as illustrated in Fig.3.4. Experimental and control electrodes were used to investigate the actual effect

of encapsulation in signal quality. Recording electrodes and the reference electrode of the recording system receive the signal transmitted by the stimulation electrodes. The received signals were processed using a differential amplifier (TDT, Tampa, FL) to eliminate white noise. These signals were recorded by a 32 channel simultaneous recording system: the experimental group had 16 channels of recording electrodes plated with glial cells and the control group had another 16 channels but without glial cells. The reference electrode was used to eliminate white noise by differential recording. A no-leak Ag/AgCl reference electrode (Cypress systems, Chelmsford, MA) was used in order to prevent possible damage to living cells from the diffusion of the filling solution from the reference electrode into the PBS in the test chamber.

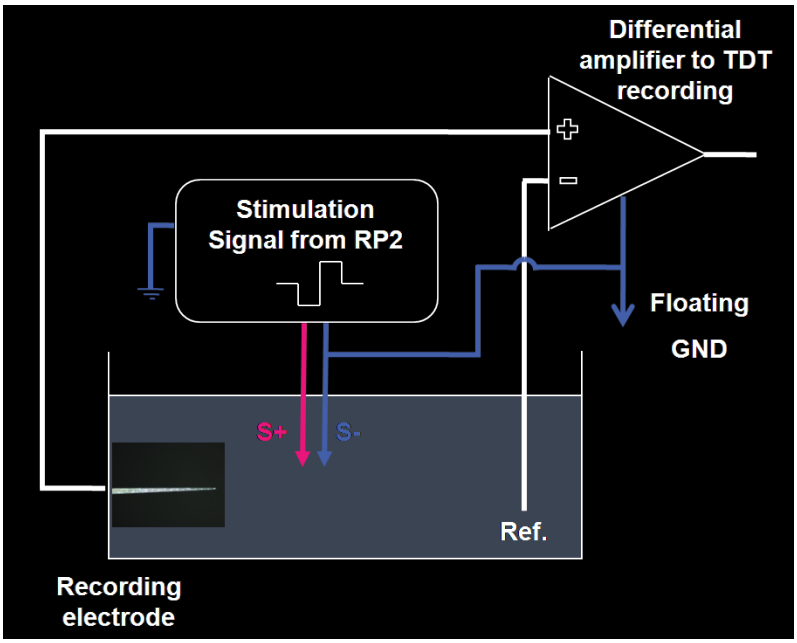

Fig.3.4. The *in vitro* stimulation/recording setup was developed and validated to investigate the cellular encapsulation effect on the performance of recording electrodes. On top of the recording electrodes sitting at the bottom of the Petri-dish, glial cells were plated to model the *in vivo* cellular encapsulation. Another recording electrode array with the same physical properties but without cell plating was used as the control electrodes (not shown in the figure). Three types of electrodes were placed in the test setup: stimulation, recording and reference electrodes. Recording electrodes and the reference

electrode receive the signal transmitted by the stimulation electrodes. The received signals were processed using a differential amplifier to eliminate white noise.

To simulate the cellular encapsulation in the brain, the electrodes of the experimental group were plated with glial cells on top. The rationale for glial cells was that the glial cells were suspected of hindering the signal transmission to the recording electrode. Two types of glial cells were used: primary astrocytes (Lonza, Switzerland), and meningeal fibroblasts (ScienCell, San Diego, CA) from adult male Sprague-Dawley rat cortices. Cells were suspended and plated on the electrodes. All the recording electrodes were coated with bovine plasma fibronectin (20 µg/mL) before being plated with cells to promote adhesion of glial cells on the electrode surface. Cells were cultured in DMEM supplemented with 10% fetal bovine serum (FBS) and antibiotics after being plated. The cells were kept in a humidified incubator at 37ºC and 5% carbon dioxide. Media was exchanged every 24 hrs. The temperature and the carbon dioxide level were maintained during the electro-physiology (EP) tests by performing each test in the incubator with electromagnetic shielding. Cell viability was ascertained by using a live/dead assay (Sigma-Aldrich, St. Louis, MO). Electro-physiology tests were conducted on days 1, 4 and 6 after seeding cells. Along with the recording electrodes for the experimental group, control electrodes were placed in the chamber and the same electro-physiology tests were performed on them. The control electrodes had exactly the same configuration and were kept in the same condition as the experimental electrodes but without plated cells.

The stimulator uses two types of stimulation signals: a single sine wave train and neuronal spike signals previously recorded from a rat brain. The single sine wave train is

used to determine the electrode performance quantitatively whereas the neuronal spike signals are used to determine the electrode performance by a signal similar to that of an actual recording *in vivo*. This stimulation is performed using stimulation electrodes emerged in the PBS, which consist of two adjacent platinum wires (AM-systems, MO) with a diameter of 125 µm. These adjacent two-wire electrodes make dipole stimulation possible, where one electrode functions as a current source and the adjacent electrode functions as a current sink. These dipole electrodes transmit a stimulation signal to be propagated in the test chamber and received by the recording system.

First, recorded signals provided signal amplitude, noise amplitude, signal-to-noise ratio (SNR) and the capability to detect/cluster units. These parameters were used to investigate the effect of cellular encapsulation on the electrode's recording performance. Impedance testing was performed using the above experimental setup to compare the impedance between bare electrodes (control) and glial cell-plated electrodes (experimental). Impedance tests of the electrodes were conducted using an Autolab potentiostat PGSTAT12 (Eco Chemie, Utrecht, The Netherlands) with a built-in frequency response analyzer software (Brinkmann, Westbury, NY). For each impedance test, three types of electrodes were used: reference, recording, and auxiliary electrodes. The latter two electrodes were the same as those used as in the EP tests. For the auxiliary electrode, a coiled platinum wire (125 µm diameter) was used. Impedance tests were conducted with sweep frequencies between 10 Hz and 10 kHz.

2.2.3. Immunohistochemistry (IHC)

Since we wanted to investigate the effect of encapsulation of glial cells on electrode performance, cells were fixed and imaged using an Immunohistochemical (IHC) process

at the end of the EP and the impedance tests to confirm the encapsulation visually. Cells were fixed with 4% paraformaldehyde and then permeabilized with 0.5% Triton (Triton X-100, Sigma, St. Louis, MO). Next, cells were treated with primary antibodies in a blocking solution containing 4% goat serum for 12–18 hrs at 4 C. Antibodies were directed against GFAP, a marker of intermediate filaments, indicating reactive astrocytes (rabbit IgG, 1:1000, Dako, Carpinteria, CA). In addition, vimentin, a marker of intermediate filaments, was used to stain the intermediate cytoskeleton of meningeal fibroblasts and astrocytes (mouse IgG1, 1:1000, Sigma, St. Louis, MO). Cells were then incubated with appropriate secondary antibodies (1:220) conjugated to either Alexa 488 or Alexa 594 fluorescent dye (Molecular Probes, Eugene, OR) for 1 hr at room temperature. All cells were counterstained with DAPI (Molecular Probes) to identify cell nuclei.

A linear regression model was employed for a statistical power analysis 1) to calculate the net effect of the cellular encapsulation on the impedance and 2) to determine if the impedance increases of the glial cell plated electrodes (experimental) are statistically significant. The impedance of an iridium electrode changes over time when the electrode is soaked in an electrolyte. This impedance change is attributed to the change of the electrochemical interface between the electrode and the electrolyte. Because of this electrochemical change, it should be determined if the impedance increases of the experimental group is due to the effect of the plated cells or due to the change of the electrochemical interface. To address this issue, we employed a linear regression model using the impedances of the control group as predictors and the impedances of the experimental group as dependant variables. This model used the

impedance data collected during the soak test before plating cells on the electrodes of experimental group. For the soak test, both the experimental electrode array and the control electrode array were soaked in PBS for a week without plating cells on neither of these arrays and the impedance data were collected on daily bases. Then, the impedance data of these arrays were used to make the linear regression model that provides the expected impedance value of an experimental electrode based on the impedance values of the control electrodes on a given day. This expected impedance represents the baseline value under conditions, which consists of the electrochemical effect alone, without the cell plating effect, i.e., the value for electrochemical effect but not the cell plating effect.

3. Results

3.1. Glial activation effect on impedance

Our results confirmed that neural probe functionality begins to decrease at the early inflammatory stage. Neural probes encapsulated by the activated glial cells by the injury model (thrombin/scratch) or the acute inflammation model (LPS) demonstrated higher impedance than the probes encapsulated by the inactivated cells (control).

3.1.1. Impedance at 1 kHz

Neural probes encapsulated with glial cells activated by the injury model (thrombin/scratch, experimental) demonstrated higher impedance at 1 kHz than the probes encapsulated by the inactivated cells (control) as shown in Fig.3.5.

The group activated by the injury model (thrombin/scratch) demonstrated significantly higher impedance compared to the control group on day 1 ($p<0.05$, student's t-test). On day 5, there was no significant difference between two groups. It is important to note that, as mentioned in method, we monitored the baseline impedance of bare electrodes to confirm the baseline impedance is constant during the period of experiment. The impedance of these bare electrodes was constant over five days. As confirmed in the microscopic pictures (Fig.3.6) cells were confluent and viable during the impedance measurements (days 1 and 5).

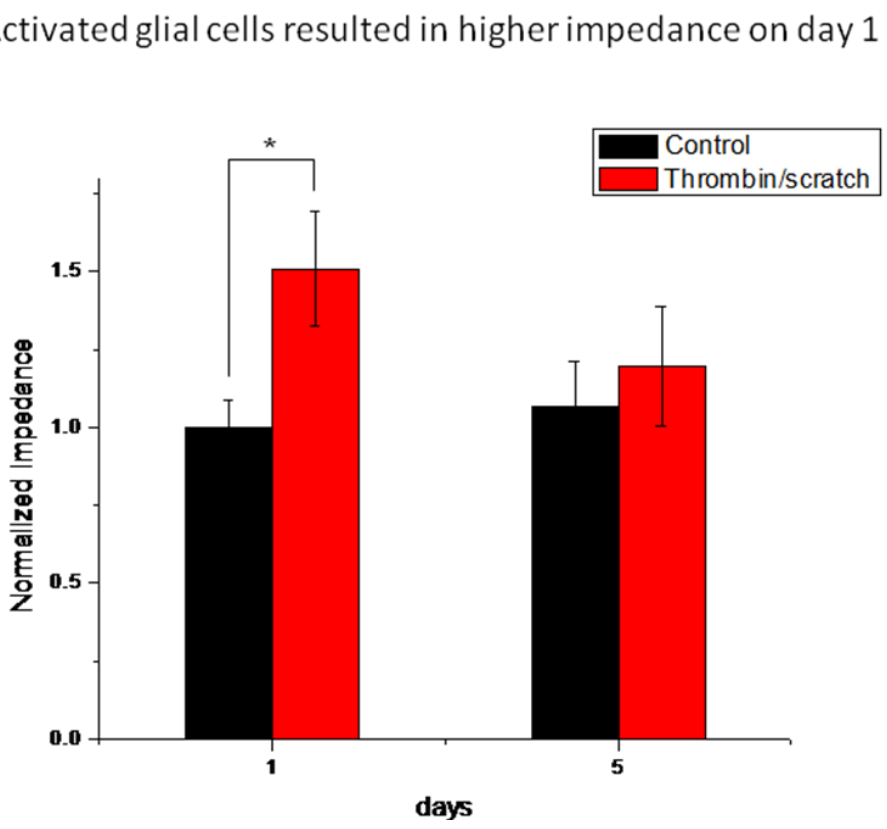

Fig.3.5. Activated glial cells by the injury model (thrombin/scratch) demonstrated higher impedance than control, which was subjected to the same condition except the treatment by thrombin/scratch. The difference was significant on day 1 (p<0.05) but not on day5. Impedance was measured at 1 kHz and normalized to the value of day 1 control group. For each group, samples were from four independent conditions.

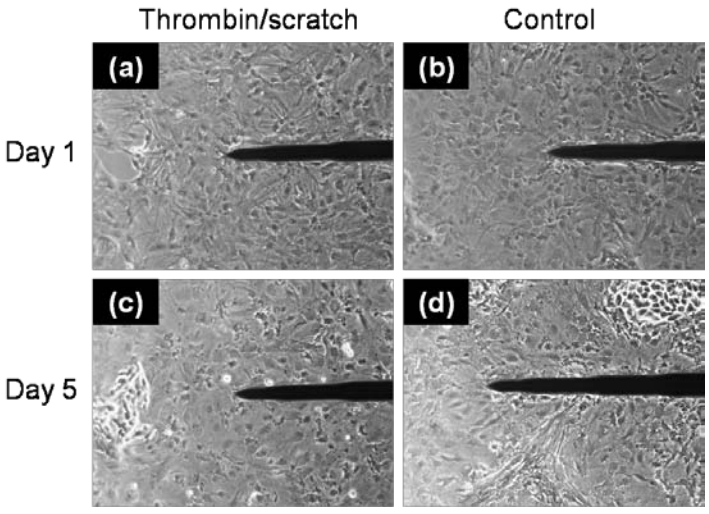

Fig.3.6. Phase contrast microscopic pictures confirmed that glial cells on the setup were viable right before the impedance measurement.

3.1.2. Signature in the impedance spectra

As Johnson et al. and Williams et al. observed in their *in vivo* studies, our *in vitro* results confirmed a 'hump' corresponding to massive encapsulations in the plotted impedance spectra (red line in Fig.3.7) (Johnson, Otto et al. 2005; Williams, Hippensteel et al. 2007). These humps were observed by Johnson et al. using the same type of electrodes we did and by Williams et al. using other types of electrodes. In the Nyquist plots (Fig.3.7), the electrode sites with encapsulation demonstrated a 'hump' (semi-circular arc) in the high frequency range of the impedance spectra. This hump was more pronounced with stronger encapsulation, for electrode sites of channels 4, 12, 5, 15, 2 and 16. The microscopic view (not shown) of these electrode sites confirmed that they were encapsulated by densely clustered cells. However, this hump was not observed for less- or non-encapsulated electrode sites. For bare electrodes at baseline (before cell plating), the Nyquist plots showed a linear relationship between the real and imaginary components (blue line in Fig.3.7).

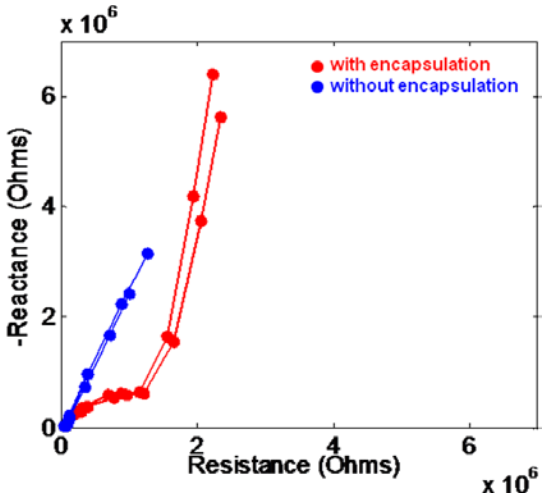

Fig.3.7. Heavily encapsulated electrode sites showed a 'hump' in the low frequency range (red) of the impedance spectra whereas bare or lightly encapsulated sites showed linear profile in the Nyquest plot (blue). Impedance spectra was conducted over 10, 16, 47, 300, 650, 1000, 3000 and 5000 Hz to represent physiological frequencies.

3.2. Glial encapsulation effect on signal recording

3.2.1. Impedance of the plated cells

The initial impedances of the electrodes at 1kHz before plating cells were in good agreement with the values reported previously by other investigators. As shown in Fig.2 day -6, they were in the range of 1.0 Mohm and 1.6 Mohm for 90% of electrodes.

Impedance, after the electrodes were soaked in phosphate buffered saline (PBS), dropped with time. This impedance drop was dominant for the first two or three days and plateaued after four days in all electrode arrays. The impedance changed with time for both control and experimental electrode arrays showing the same trend. Hence the results confirmed the need for a mathematical model to predict the baseline impedance of the experimental electrodes (based on the control group impedance) on a given day. Using the data from the soak test, we built a linear regression model that passes origin; the predictor was the mean of the impedances of the control electrodes and the dependant variable was the mean of the impedances of the experimental electrodes. The R-value of the model was 0.890 with n=4. Then we built a model for each channel of the experimental electrodes; the predictor was the mean of the impedances of the control electrodes and the dependant variable was the impedances of each channel of the experimental electrodes. The R-value of the model for each channel ranged from 0.500 to 0.990 with n=4.

The impedances increased significantly after plating cells on the electrodes in the experimental group whereas this increase did not happen with the control group, i.e., without plated cells; Fig.3.8 shows the impedance over time course. There was a significant difference; 1) between the control and the experimental group and 2) between

the expected impedances and the measured impedances of the experimental group. The impedance of the experimental group was higher than that of the control group by more than five standard deviations. In addition, the measured impedance of the experimental group was significantly higher than the expected values generated by the linear regression model (see section 2.2.3). The difference was more than five standard deviations with $p<0.001$ by a paired student t-test in both cases. Fig.3.8(a) shows the daily impedance changes of the control and experimental electrodes over the entire duration of experiment. Fig.3.8(b) shows the measured impedance of the cell plated group (experimental) normalized to the expected impedance by the linear regression model (LRM). The difference between the expected and measured impedance of an electrode represents the impedance increase caused solely by the plated cells. Error bars in these figures represents the standard error of the mean (SEM).

Some electrodes demonstrated impedance exceeding 5 Mohm as in an open circuit and other electrodes demonstrated impedance as low as 10 kohm as in a short circuit. These unusual impedance values were observed in both cell plated electrodes (experimental group) and bare electrodes (control group). These extremes in impedance were most likely due to device failure, not the effect of the plated cells on the electrode. Therefore, the data from these electrodes were excluded.

3.2.2. Stimulation/recording

The cells plated on the electrode increased the impedance and hence degraded the signal recording performance of the electrode. Electrode performance based on the signal amplitudes recorded from the single sine wave train is shown in Fig.3.9. Fig.3.10 shows the measured signal amplitudes of the cell plated group (experimental) normalized to the

signal amplitudes by the linear regression model (LRM). The difference between the expected and measured signal amplitudes represents the decrease of signal amplitudes caused solely by the plated cells. Error bars in these figures represents the standard error of the mean (SEM). The initial electrode performance in the bare electrodes (the control electrodes for the entire duration and the experimental electrodes before cell plating) showed the same trend of higher impedance coupled with lower performance as shown in Fig.3.8. An electrode with high impedance received the small amplitude of the stimulation signal and an electrode with low impedance received the large amplitude of the signal. After cells were plated on the experimental group, the impedance of these cell plated electrodes increased and hence these electrodes received smaller amplitude of the stimulation signal.

The amplitude of the recorded signal in the cell plated electrode decreased on days 1 and 4 and then plateaued at the value of day 4 (Fig 3.9). These increases between day 0 and each of the subsequent days were statistically significant with $p<0.05$ by paired student t-test.

3.2.3. Immunohistochemistry (IHC)

The plated glial cells formed an evenly distributed tight cell layer on top of the recording electrodes. The cell layers on the electrode array were constructed to model the *in vivo* encapsulation, with the fibroblast surrounding the electrode array and the astrocytes surrounding the fibroblast (Cui, Wiler et al. 2003) as shown in Fig.3.11(A) and (C). The fibroblasts were first plated on the electrode array and then astrocytes in 24 hrs. Both of these cells were plated at the density of $1x10^6$ cells/cm^2; the fibroblasts were stained red and the astrocytes were stained green in Fig.3.11(C). A microelectrode array

was located underneath of the cell layers but it failed to be visualized in the fluorescent microscopy because of the thick cell layer on top of it. Fig.3.11(A) shows the phase contrast microscopic view of the cell layers on the electrodes. Live/dead analysis showed that 90% of both cells in the cell construct on the electrodes were still viable after two weeks of *in vitro* EP tests.

The maximum cell density we could plate on the electrode was $1x10^6$ cells/cm^2; at higher densities, the cell layer was delaminated from the electrode after approximately seven days of testing. To determine the maximum cell density that could be achieved without delamination, glial cells with various densities, ranging from $1x10^4$ to $1x10^6$ cells/cm^2, were plated on test chambers. This delamination is most likely due to insufficient nutrients and oxygen supplied to the cells on the bottom layer. Live/dead analysis showed that more than 90% of cells were viable at cell densities equal to or lower than $5x10^6$ cells/cm^2.

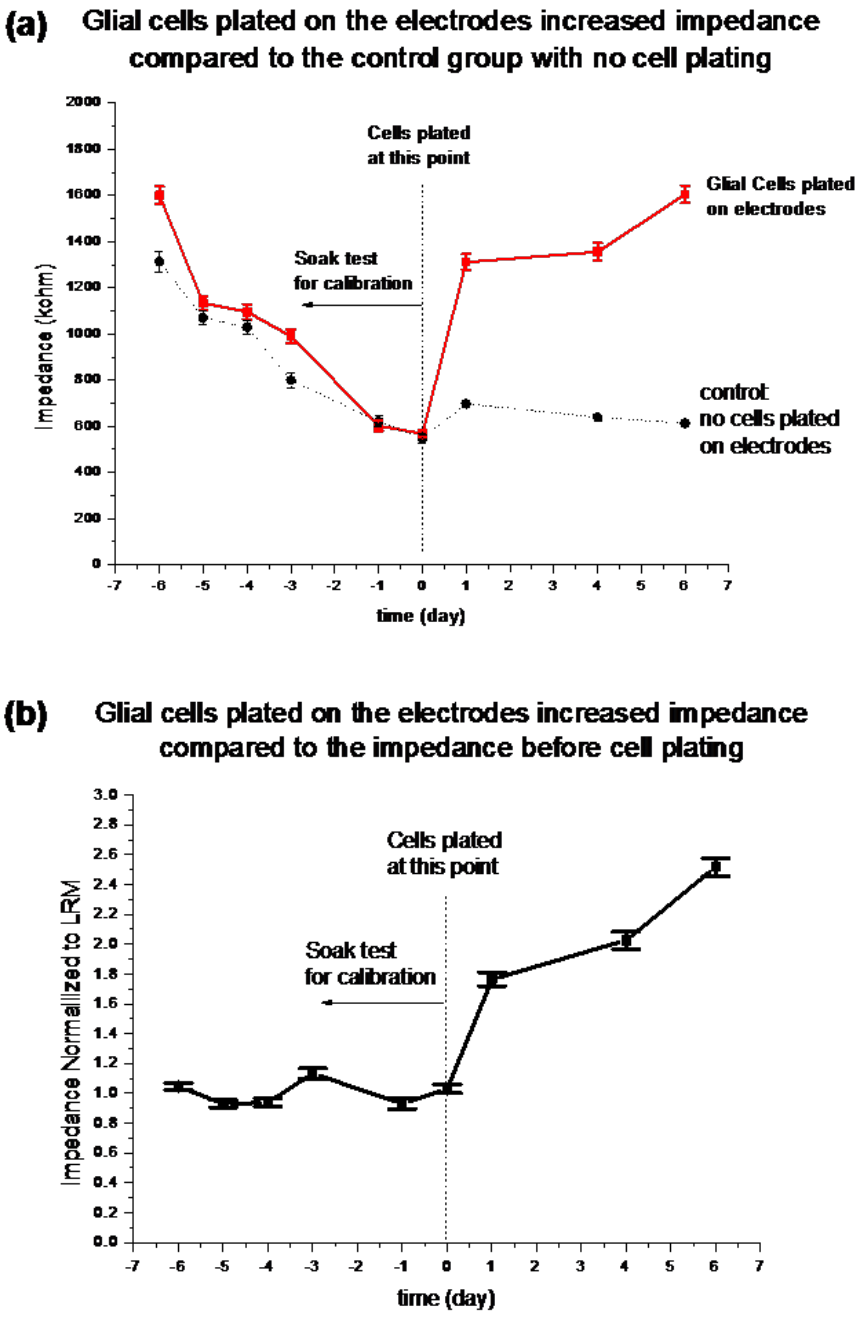

Fig.3.8. Glial cells plated on the electrodes increased impedance in the *in vitro* setup to model cellular encapsulation *in vivo*. The increase was observed in the cell plated electrode whereas there was no significant increase in the control electrodes with no cells (a). In addition, there was a significant increase in impedance between before and after cell plating on the same electrodes (b); the impedances were normalized to the baseline value calculated by the linear regression model (LRM). The error bars indicate the standard error of the mean.

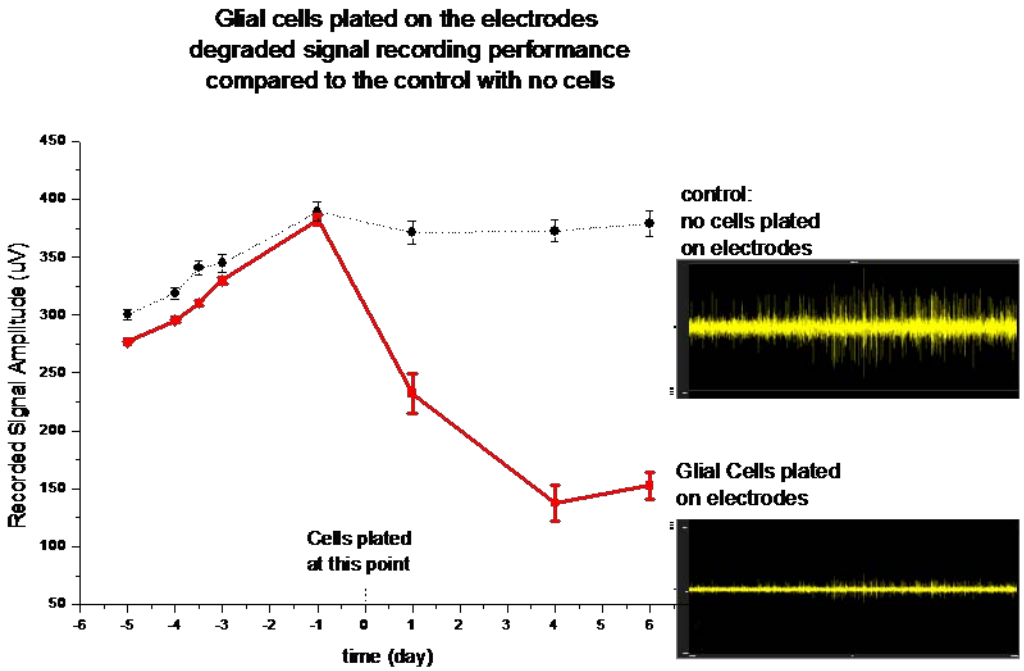

Fig.3.9. Glial cells plated on the electrodes degraded signal recording performance of the electrode compared to the control electrodes with no cells. The recording performance was assessed based on the recorded signal amplitude of the single sine wave train. The signal amplitude increased significantly after plating cells whereas there was no significant increase in the control electrodes. This increase was also demonstrated in the recording of the simulated neuronal spike; upper plot was recorded from the cell plated electrode whereas lower plot was recorded from the control electrode with no cells. Both of the plots were set in the same scale.

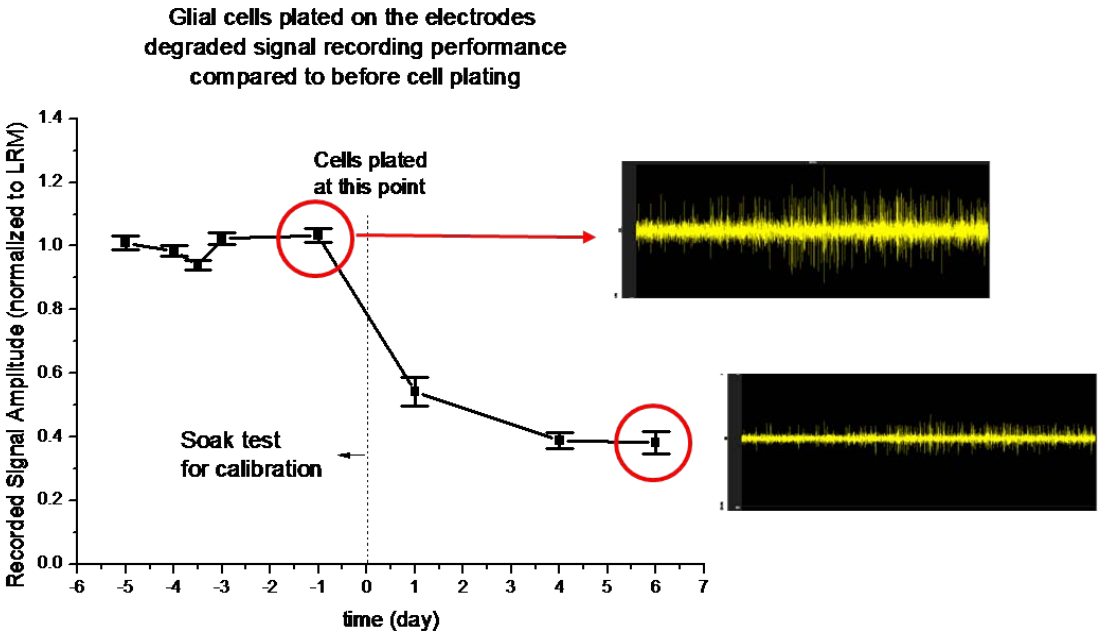

Fig.3.10. There was a significant degradation in the signal recording performance between before and after glial cell plating on the same recording electrode. The signal amplitude increased significantly after plating cells on days 1, 4 and 6. The signal amplitudes of the cell plated electrodes were normalized to the baseline value calculated by the linear regression model (LRM). These increases were also demonstrated in the recording of the simulated neuronal spike; lower plot was recorded before cell plating and the upper plot was recorded after cell plating from the same electrode. Both of the plots were set in the same scale.

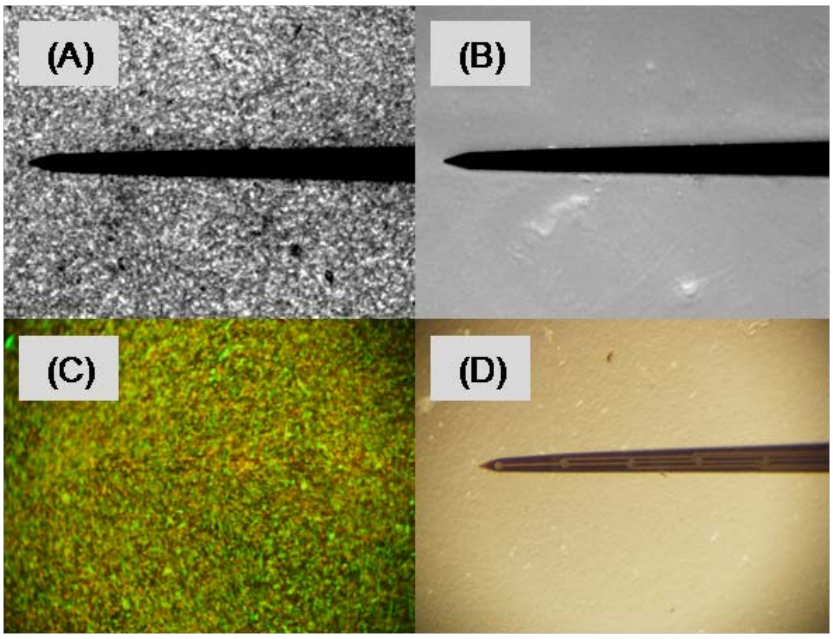

Fig.3.11. The plated glial cells formed an evenly distributed tight cell layer on top of the recording electrodes. Phase contrast micrograph shows the high density living cell layer on the recording electrodes (A) vs. control electrodes without the cell layer (B). Fluorescent micrograph illustrates that the plated cells were evenly distributed over the cell layer (C): 1) meningeal fibroblasts and astrocytes were stained green by vimentin counterstaining, 2) reactive astrocytes were stained red by GFAP counterstaining, and 3) cell nuclei were stained blue by DNA staining using Hoechst. The recording electrode array under the cell layer is shown in the bright field microscopic view (D).

4. Discussion

4.1. Glial activation effect on impedance

Although previous *in vivo* studies were able to provide valuable observations about the increasing impedance over the duration of neural probe implantation, it was not clear whether the impedance increase was directly due to the activation of the glial cells. This impedance increase by activated glial cells in the early inflammatory stage is consistent with *in vivo* impedance increase in the first 3-4 days post implantation (Ludwig, Uram et al. 2006).

Since we learned that the neural probe functionality decreases with the glial activation in the early inflammatory stage, the next question is how to mitigate the inflammation cascade. Possible solutions may involve the introduction of thrombin inhibitors, proinflammatory cytokine inhibitors, or antiinflammatory drugs such as corticosteroids at the probe site.

The signature hump in the impedance spectra that is documented in our study and prior *in vivo* studies could be used as a hallmark in non-invasively detecting glial encapsulation providing a crucial tool for the dynamic control of glial encapsulation necessary for the SRNP (see chapter 1).

The fact that the relative impedance of the injury group (thrombin/scratch) on day 5 was not significantly higher than the control group suggests that the effect of injury (thrombin/scratch) on impedance is the greatest at the early stage of inflammation. This effect may be due to: 1) the activity of cells on day 5 might not be as good as on day 1 due to the fact that cells were in the low serum media (1% FBS) for five days. They may not have had sufficient nutrients for survival. Therefore the intercellular adhesion

became weak and increased electrical permeability. 2) The activation effect by thrombin might be terminated between day 1 and day 5 and no additional activation occurred. We suspect that once an activation effect terminated, intercellular adhesion became weaker. Additional activation might not have occurred after day 1 because thrombin may have degraded after day 1 due to the short half-life, about 35 min (3 NIH U/mL at 37ºC) (Leborgne and Graber 1994). This short half-life of thrombin also explains the smaller expression of some cytokines, CTACK, GM-CSF, IL-2, IL-4, KC, and MCP-1 on day 5 than on day 1 (see protein array results in chapter 2).

The higher impedance in the activated glial cells could be due to the up-regulated intercellular adhesion molecule-1 (ICAM-1). During the early inflammation stage, the activated astrocytes are recruited to the implanted neural probe and form tight intercellular adhesion (Turner, Shain et al. 1999; Szarowski, Andersen et al. 2003). In astrocytes and microglia, the expression of intercellular adhesion molecule-1 (ICAM-1), a mediator of cell-cell and cell-extracellular matrix (ECM), is enhanced by proinflammatory cytokines such as TNF-alpha, IL-1beta, IFN-gamma or also by LPS (Frohman, Frohman et al. 1989; Merrill and Benveniste 1996; Lee and Benveniste 1999). We hypothesized that the ICAM might induce tight astrocyte-astrocyte and/or astrocyte-electode adhesion. These tight adhesions may form a tight seal between astrocyte cells and between asstrocyte and electrode surface, resulting in prevention of the ion diffusion across the cell layer and hence attenuate the signal conduction. One good indicator of the signal conduction across the cell layer is the impedance across it. Vetter et al. observed a correlation between the impedance and recorded signal quality *in vivo* (Vetter, Williams et al. 2004; Ludwig, Uram et al. 2006). When the impedance of the electrodes was high,

signal to noise ratio (SNR) was low. Giaever and Merrill demonstrated that MDCK cells with tight intercellular adhesion showed significantly higher impedance across the cell layer *in vitro* (Giaever and Keese 1993; Merrill and Tresco 2005).

Although LPS induces morphological change from ramified to amoeboid as observed by Beck et al. in cultured mouse microglia (Fig.2.15) (Beck, Penner et al. 2008), the effect of microglial shape change on the impedance is assumed to be small because 1) the portion of microglia in our culture was small (less than 20%) and 2) microglia may not directly adhere to the electrode surface since they sit on top of astrocytes in a mixed culture (Saura 2007).

4.2. Glial encapsulation effect on signal recording

In this paper, we introduced and demonstrated the capability of an *in vitro* stimulation/recording setup to model the *in vivo* cellular encapsulation. By using this setup, we could record simulated signal through the recording electrodes and evaluate the performance of the encapsulated electrodes by analyzing the recorded signal.

With the cellular encapsulation, the performance of the electrodes degraded, as confirmed by both increased impedance and decreased recorded signal quality. In addition, in the recorded neuronal spike signals, not only the amplitude of the spikes was smaller but also they were less discernable in signal received by the cell plated electrodes than by the control group. We suspect the reason for the impedance increase and the signal amplitude decrease on the two initial measurements (days 1 and 4) is due the progression of the cell attachment to the electrode and the formation of intercellular adhesion between the plated glial cells. This phenomenon hinders electrical signal

transmission through the electrical double layer at the electrode and the electrolyte interface. Therefore, specifically, the impedance increased and the signal quality decreased. On the other hand, the plateauing of the impedance and the signal quality after day 4 is most likely due to cell confluence; whereas, the small fluctuations observed in this plateau (Fig 3.8 and Fig 3.9) is most likely due to the metabolite and movement of living cells on the electrodes.

Day to day fluctuation of the impedance and the recorded signal quality due to the electrochemical effect reconfirmed the importance of the linear regression model. For example, the impedance of the experimental group increased between days 4 and 6, however, the impedance decreased in the control group (Fig 3.8). The impedance increase in the control group whereas the decrease in the experimental group indicates that there was a big increase in impedance due to the electrochemical effect (on both experimental and control group) and was a small decrease in impedance due to the cell plating effect (only on the experimental group). We could determine the net effect of cell plating using the LRM otherwise we could have misinterpreted the cell plating effect. In addition, the similar tendency of the two electrode arrays in impedance and the recorded signal amplitude during the soak test before plating cells as shown by the high r-square value (0.900) in the LRM made it possible to build the LRM to calculate the baseline value for the experimental group with reasonable accuracy.

The sensitivity of this *in vitro* stimulation/recording setup makes it possible to quantify the effect of encapsulation and distinguish this effect from electrochemical effect or other artifact. After plating cells on the electrode arrays, the impedance

increased and the signal quality degraded significantly. The statistical significance was more than eight standard error of the mean.

The *in vitro* stimulation/recording setup proved that impedance and recorded signal quality data can be used to quantify the encapsulation. This method, therefore, can be used *in vivo* as well to determine the presence and the degree of encapsulation so that proper remediation can be applied.

References

Beck, A., R. Penner, et al. (2008). "Lipopolysaccharide-induced down-regulation of Ca2+ release-activated Ca2+ currents (I CRAC) but not Ca2+-activated TRPM4-like currents (I CAN) in cultured mouse microglial cells." J Physiol **586**(2): 427-39.

Cui, X., J. Wiler, et al. (2003). "*In vivo* studies of polypyrrole/peptide coated neural probes." Biomaterials **24**(5): 777-87.

Frohman, E. M., T. C. Frohman, et al. (1989). "The induction of intercellular adhesion molecule 1 (ICAM-1) expression on human fetal astrocytes by interferon-gamma, tumor necrosis factor alpha, lymphotoxin, and interleukin-1: relevance to intracerebral antigen presentation." J Neuroimmunol **23**(2): 117-24.

Giaever, I. and C. R. Keese (1993). "A Morphological Biosensor for Mammalian-Cells." Nature **366**(6455): 591-592.

Johnson, M. D., K. J. Otto, et al. (2005). "Repeated voltage biasing improves unit recordings by reducing resistive tissue impedances." Ieee Transactions on Neural Systems and Rehabilitation Engineering **13**(2): 160-165.

Leborgne, S. and M. Graber (1994). "Amidase Activity and Thermal-Stability of Human Thrombin." Applied Biochemistry and Biotechnology **48**(2): 125-135.

Lee, S. J. and E. N. Benveniste (1999). "Adhesion molecule expression and regulation on cells of the central nervous system." Journal of Neuroimmunology **98**(2): 77-88.

Ludwig, K. A., J. D. Uram, et al. (2006). "Chronic neural recordings using silicon microelectrode arrays electrochemically deposited with a poly(3,4-ethylenedioxythiophene) (PEDOT) film." Journal of Neural Engineering **3**(1): 59-70.

Merrill, D. R. and P. A. Tresco (2005). "Impedance characterization of microarray recording electrodes *in vitro*." Ieee Transactions on Biomedical Engineering **52**(11): 1960-1965.

Merrill, J. E. and E. N. Benveniste (1996). "Cytokines in inflammatory brain lesions: helpful and harmful." Trends Neurosci **19**(8): 331-8.

Saura, J. (2007). "Microglial cells in astroglial cultures: a cautionary note." J Neuroinflammation **4**: 26.

Szarowski, D. H., M. D. Andersen, et al. (2003). "Brain responses to micro-machined silicon devices." Brain Research **983**(1-2): 23-35.

Turner, J. N., W. Shain, et al. (1999). "Cerebral astrocyte response to micromachined silicon implants." Experimental Neurology **156**(1): 33-49.

Vetter, R. J., J. C. Williams, et al. (2004). "Chronic neural recording using silicon-substrate microelectrode arrays implanted in cerebral cortex." Ieee Transactions on Biomedical Engineering **51**(6): 896-904.

Williams, J. C., J. A. Hippensteel, et al. (2007). "Complex impedance spectroscopy for monitoring tissue responses to inserted neural implants." Journal of Neural Engineering **4**(4): 410-423.

CHAPTER IV

DYNAMIC CONTROL OF GLIAL ACTIVATION:

AN *IN VITRO* MODEL

1. Introduction

Signal quality for long term stable recording and stimulation is challenged by the low electrical conductivity of glial encapsulation. Efforts made to intervene in this encapsulation problem include injecting voltage pulses (rejuvenation) and delivering corticosteroid systemically and locally (Johnson, Otto et al. 2005; Spataro, Dilgen et al. 2005). These therapeutic agents have been shown to reduce the tissue reaction.

In this study, we propose a concept of a new local drug delivery system with feedback control for dynamic control of the neural environment termed 'Self-Repairing Neural Probe (SRNP)' (Fig. 4.1 and Fig. 4.2) (Moon, Pellinen et al. 2007). The controller of the SRNP will sense the level of encapsulation using its non-invasive sensing method and then will compare the sensed encapsulation level with the target encapsulation level to maintain the desired signal quality of neuronal recording or stimulation given by input value. If the sensed encapsulation level is higher than the target encapsulation level, the controller will inject inactivation agents to reduce the encapsulation, which in turn will prevent reduced signal quality for recording or stimulation.

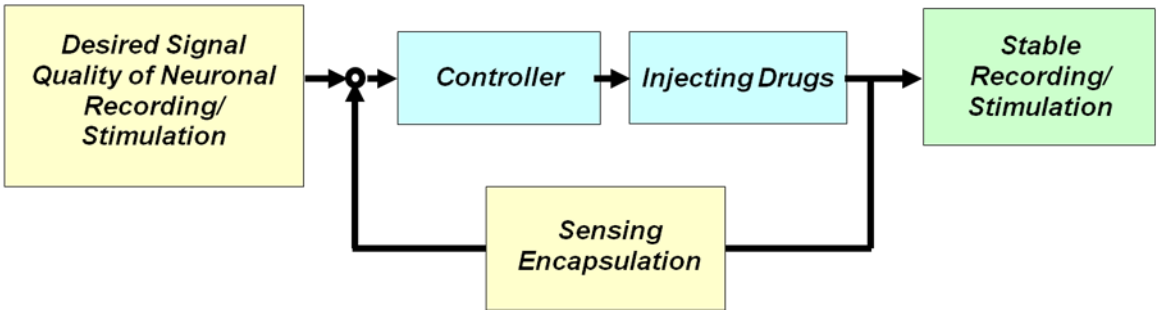

Fig. 4.1. Concept diagram of the self-repairing neural probe. The controller will sense the level of encapsulation using its non-invasive sensing method and then will compare the sensed encapsulation level with the target encapsulation level to maintain the desired signal quality of neuronal recording or stimulation given by input value. If the sensed encapsulation level will is higher than the target encapsulation level, the controller will inject drugs to reduce the encapsulation level and thus acquires desired signal quality for recording or stimulation. In order to build this feedback controlled drug delivery system, two major components are required; sensing part and actuation part. Also we need, neural probe with fluid delivery capability.

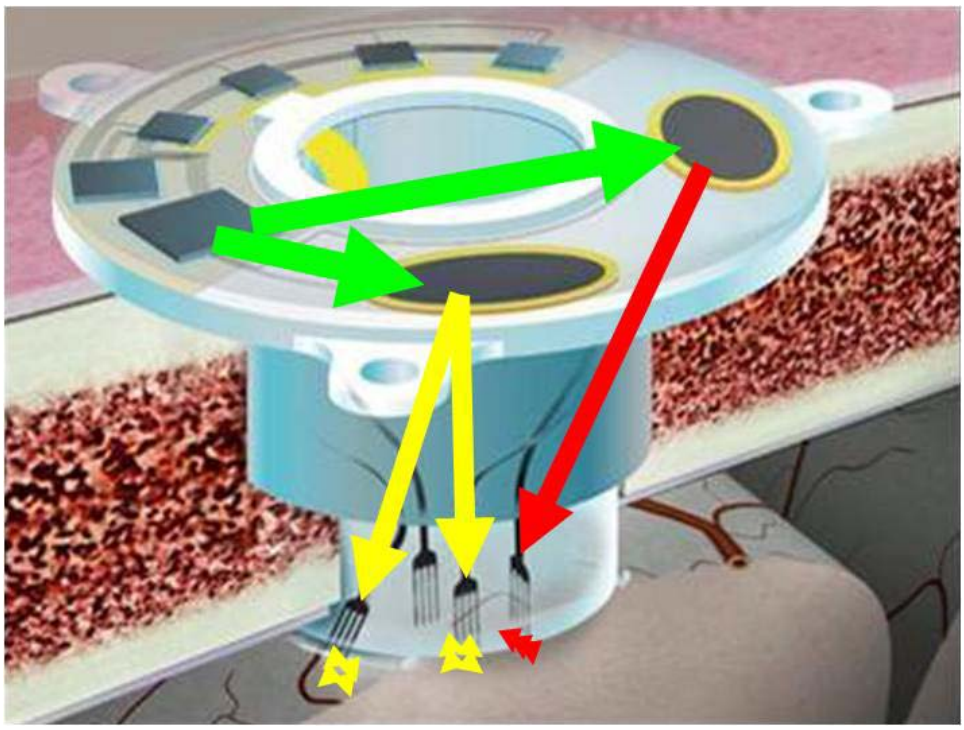

Fig. 4.2. Concept illustration of the implanted self-repairing neural probe (SRNP). The drugs will be delivered locally to the tissues on demand. This local and temporal drug delivery is expected to maximize drug effect whereas minimizing possible toxic effect caused by high drug dosage.

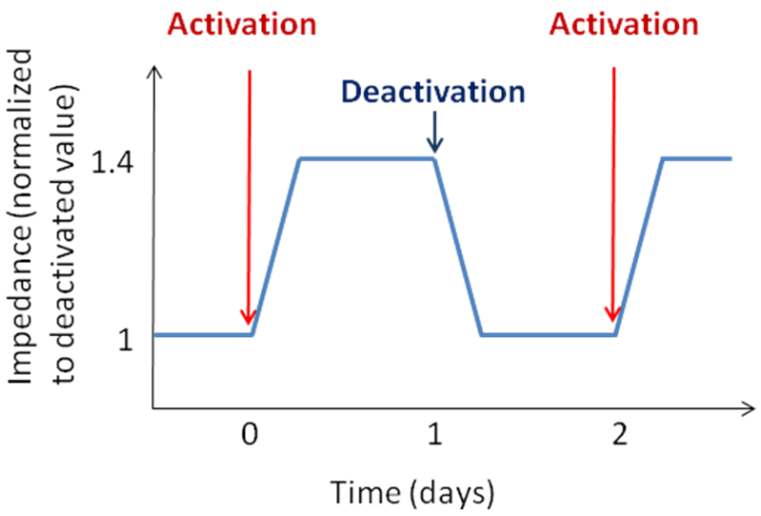

Fig. 4.3. The proof of concept for the dynamic control of the encapsulation level through sequential activation/deactivation of glial cells over a short period of time. The sequential activation/deactivation is conducted every 24 hrs and impedance was measured in 24 hrs after applying each activation/deactivation agents.

The dynamic control capability is crucial to realize the self-repairing neural probe (SRNP). The activation level had to be controlled in a short period of time to obtain stable recordings. Nelson et al. demonstrated that astrocyte culture from mouse brain changed their morphologies when these cells were sequentially treated with thrombin and dbcAMP in a short period of time (Nelson and Siman 1990). Giaever et al. demonstrated that the morphology change of cells on an electrode changed the impedance of the electrode (Giaver 1993).

In this study, we demonstrate the proof of concept for the dynamic control of the encapsulation level through sequential treatments of glial cells with LPS in 10% FBS and dbcAMP in 0% FBS over a short period of time. For each step of the treatment, we investigated the effect of the change of the encapsulation levels on probe functionality by monitoring their impedance. The sequential treatments are conducted every 24 hrs and impedance was measured in 24 hrs after applying each treatment agent (Fig. 4.3).

In addition, we introduce a local drug delivery system for dynamic control of neural environment using parylene-based microelectrodes with a microchannel for drug delivery. In order to build the SRNP, two major functions are required; sensing and actuation (control) of glial encapsulation. The sensing encapsulation, using impedance spectra, was demonstrated in chapter 3. For the control of encapsulation, we need a local drug delivery system to deliver inhibition agent to the place where the encapsulation occurred. We can deliver liquid phase agents using the microchannel and, by using hydrophilic polymer-based nanopoarticles, water insoluble drugs can be loaded in the nanopoarticles and delivered in aqueous emulsion. Also, NP-based release mechanisms enable sustained drug release demonstrated to be important by Spataro and colleagues to suppress the sustained reactive response (Spataro, Dilgen et al. 2005). We propose releasing DEX by diffusion from the microchannel, which is filled with NPs containing DEX. As the NPs are too large and heavy to be transported by diffusion, only the released DEX from NPs will be diffused to the brain tissue (Nicholson 2001). The long (15 mm) and narrow (40 μm x 5 μm) microchannel gives time to transport DEX to the outlet port of the channel. The DEX near the outlet port will diffuse immediately after release from the NPs. However, it will take time for DEX loaded far inside the channel to be released and transported to the outlet port by diffusion. This mechanism would make sustained drug delivery possible.

2. Method

2.1. Dynamic control of glial activation

To demonstrate the proof of concept for the dynamic control of the glial encapsulation level, we developed a model that can treat glial cells sequentially with LPS in 10% FBS and dbcAMP in 0% FBS and monitor their impedance over a short period of time using the impedance monitoring setup described previously (chapter 2).

2.1.1. Experimental setup

Primary glial cells were isolated from fetal mouse brain and plated on a 75 cm^2 tissue culture treated flask as described in chapter 2. These cells were allowed to grow and proliferate for 2-3 weeks based on the state of confluence and then plated on the experimental setup that can monitor impedance as previously described (see chapter 3for more details). These cells were initially plated and cultured in 10% FBS media followed by the treatment with dbcAMP (1mM in 0% FBS for 24 hrs). Then cells were treated with LPS (10 µg/mL in10% FBS for 24 hrs). Finally cells were treated again with dbcAMP (1mM in 0% FBS for 24 hrs).

2.1.2. Morphological change of glial cells due to sequential treatments with LPS in 10% FBS and dbcAMP in 0% FBS

To confirm the morphological change of glial cells induced by the sequential treatments with LPS in 10% FBS and dbcAMP in 0% FBS, before testing the effect of the sequential treatments on impedance, sequentially treated glial cells were monitored their morphologies using high magnification phase contrast microscopy. Phase contrast microscopic pictures of living cells were taken at the end of each treatment periods.

2.1.3. Impedance measurement

Mixed glial cells were plated on a 24-well cell culture plate and treated with LPS in 10% FBS and dbcAMP in 0% FBS sequentially for 24 hr periods. Impedance at 1 kHz was monitored at the end of each treatment period. We used the same protocol used in chapter 3 for the impedance measurements. Briefly, three electrodes were used to measure the impedance: working (microelectrodes), counter (platinum-iridium coil), and reference (miniature Ag/AgCl). HBHS was used as an electrolyte. Phase contrast microscopic pictures were taken right before the impedance measurements to confirm that the cells were confluent and viable during the impedance measurements.

2.2. Local drug delivery system for dynamic control of neural environment using parylene-based neural probe

The drug delivery system to be used for the SRNP should be able to deliver inhibition agent to the exact same tissue where the encapsulation occurred to maximize the efficacy of the drug to the target tissue and, at the same time, minimize the toxicity to the surrounding tissue. To meet this requirement, we developed a local drug delivery system using the multifunctional neural probe with recording and fluid delivery capabilities previously developed in our lab by Pellinen (Pellinen, Moon et al. 2005).

2.2.1. Fluid delivery neural probe

The fluid delivery probe used in this study was designed and fabricated by our group at the Neural Engineering Lab at the University of Michigan (Pellinen, Moon et al. 2005). It is a microfabricated, multi-channel polymer probe capable of selectively delivering chemicals at the cellular level as well as electrically recording and stimulating

neurons *in vivo*. The width and height of the fluidic channel are 40 μm and 5 μm, respectively. The electrical recording sites are located on the top side of the probe – designed to function for both electrical recording and stimulation (Fig. 4.4). The probe is mounted on a custom-built printed circuit board (PCB) with integrated electrical connections. The probe is ball-bonded onto the PCB (Meyer, Stieglitz et al. 2001), on which an electrical connector (Omnetics Connector Co., Minneapolis MN) is soldered. This assembly gives electrical connection between the electrode sites on the microprobe and the electrical signal recording system (Plexon Inc., Dallas, TX). The electrical recording functionality was previously tested and verified as shown in Fig. 4.5.

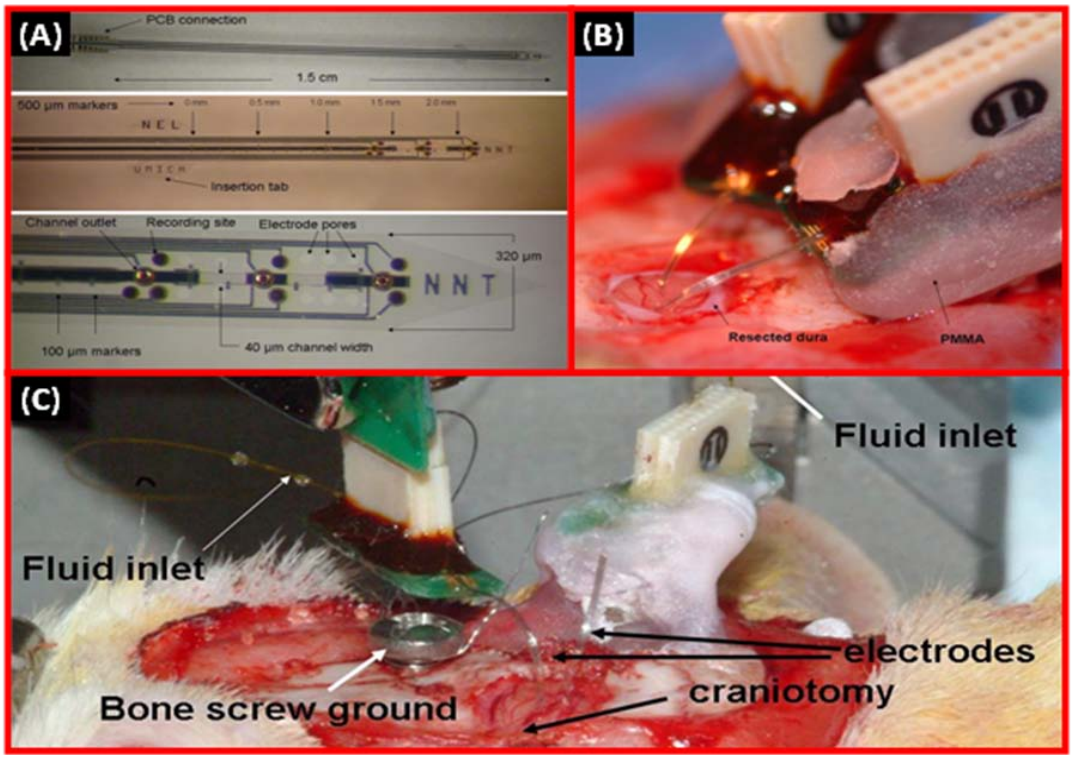

Fig.4.4. (A) Photograph view of the flexible parylene-based microfluidic electrode. The total thickness of the device is nominally 20 μm, with a channel height of 5 μm. (B) Photograph taken during implantation of two neural probes in a rat model. Shown are two neural probes connected to PCBs mounted with Omnetic nano-connectors®. The dura has been resected prior to the implantation. (C) Rat skull with two neural probes implanted during an acute surgery designed to validate the drug delivery capabilities of the electrode.

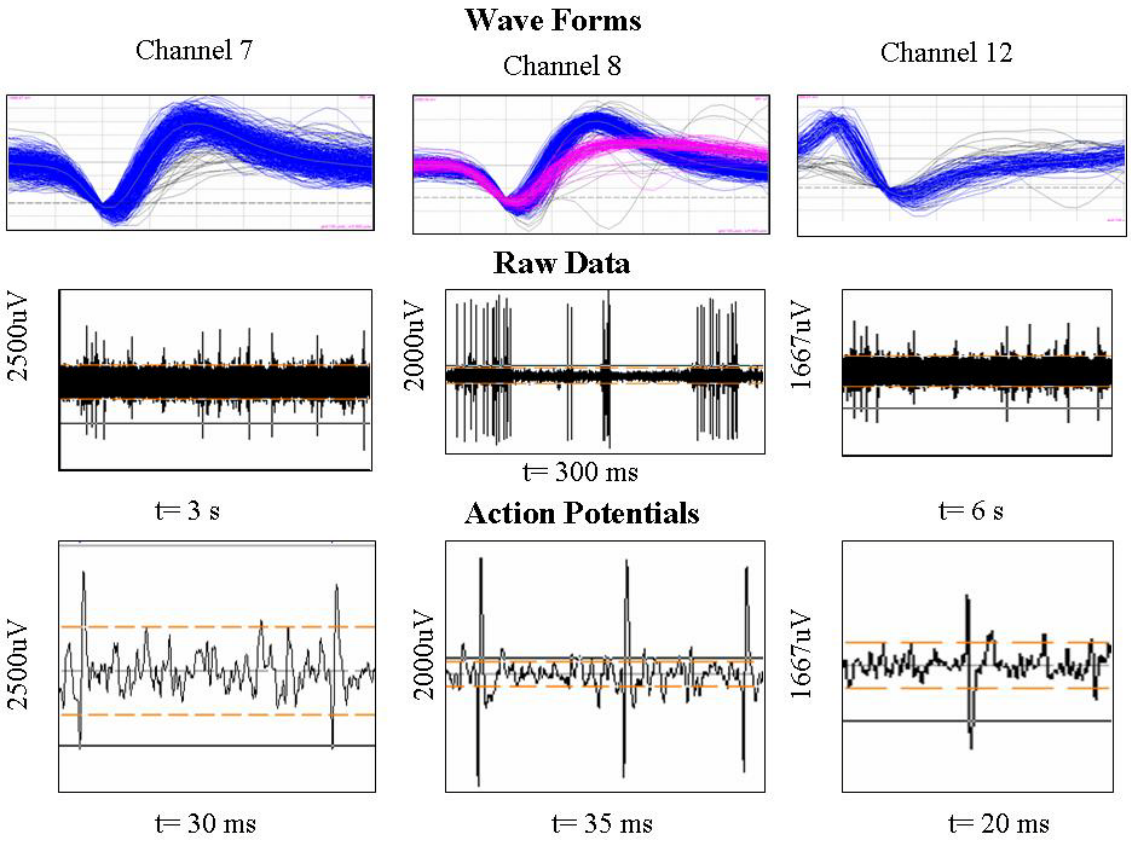

Fig.4.5. Recording capabilities of the neural probe demonstrated with data snapshots: waveforms, raw data samples, and action potentials of 3 different units on 3 different channels on day 4 after the implantation in a rat from (Pellinen, Moon et al. 2005).

2.2.2. Microfluidics

Access to the flow channel is provided through a polyimide tube (A-M systems, Inc.). The flow is driven by a volume flow controlled syringe pump (WPI UltraMicroPump) and a micro syringe (SEG 5 μL). The fluid is initially filtered through a 0.22 μm in-line filter (Corning, Inc.) to remove trace particulates. The connection between the outlet of the syringe and the inlet port of the microprobe is made by polyimide tubing with a 100-μm inner diameter. The fluid enters the inlet port of the

microprobe, and flows through the microchannel inside of the probe until it comes out through the outlet ports, which are placed at the tip of the probe as shown in Fig.4.4. High performance liquid chromatography (HPLC) grade water was injected to visually validate the fluidic line in the device-assembly. If the fluidic line has no clogging or leakage, a water bubble appears at the outlet port of the probe. These outlet ports are placed at the tip of the probe as shown in Fig. 4.4.

2.2.3. Drug embedded nanoparticle

Poly(lactic-co-glycolic acid) (PLGA) nanoparticles loaded with dexamethasone (DEX) were prepared by an oil-in-water emulsion/solvent evaporation method (Arshady 1991; Song, Labhasetwar et al. 1997; Jain 2000). PLGA was dissolved in a dichloromethane (DCM) in 5.3% (w/v) and DEX was dissolved in acetone in 1.3% (w/v). These two organic solutions were mixed together. Then, the mixed solution was added to a 5% (w/v) poly(vinyl alcohol) (PVA) in deionized (DI) water solution. The mixture underwent sonication to form an oil-in-water type emulsion by a probe type sonicator (Ultrasonic processor, CP-750, Cole Palmer). Power of the sonicator was kept at 60 W for 10 min. The emulsion was stirred gently to allow evaporation of the organic solvents over 12 hrs. Nanoparticles were collected by ultracentrifugation at 35,000 rpm for 1 hr (Beckman Couler Optimal L-90K, Beckman, Arlington Heights, IL). The collected nanoparticles were washed three times with DI water to remove PVA residue and unreacted drug. The final product of DEX loaded PLGA nanoparticles were collected by lyophilization (Freezone 4.5, Labcono co., MO).

3. Results

3.1. Dynamic control of glial activation

We demonstrated the concept for the dynamic control of the encapsulation level through sequential treatments of glial cells with LPS in 10% FBS and dbcAMP in 0% FBS over a short period of time as shown in Fig.4.6.

3.1.1. Morphological change of glial cells due to sequential treatments with LPS in 10% FBS and dbcAMP in 0% FBS

Cells treated with LPS in 10% FBS were flat in shape and showed less intercellular space whereas cells treated with dbcAMP in 0% FBS showed thinner processes and more intercellular space as shown in Fig 4.6. This pattern was clearly pronounced during the sequential treatments: (1) cells treated with dbcAMP in 0% FBS on day 1 showed stellate shape (Fig. 4.6(a)), (2) cells treated with LPS in 10% FBS on day 2 was flat shape (Fig 4.6(b)), (3) cells treated with dbcAMP in 0% FBS again on day 3 became stellate again (Fig. 4.6(c)), and (4) cells treated with LPS in 10% FBS again on day 4 became flat again (Fig. 4.6(d)). This data confirms that sequential treatments of glial cells with LPS in 10% FBS and dbcAMP in 0% FBS induce sequential morphological changes.

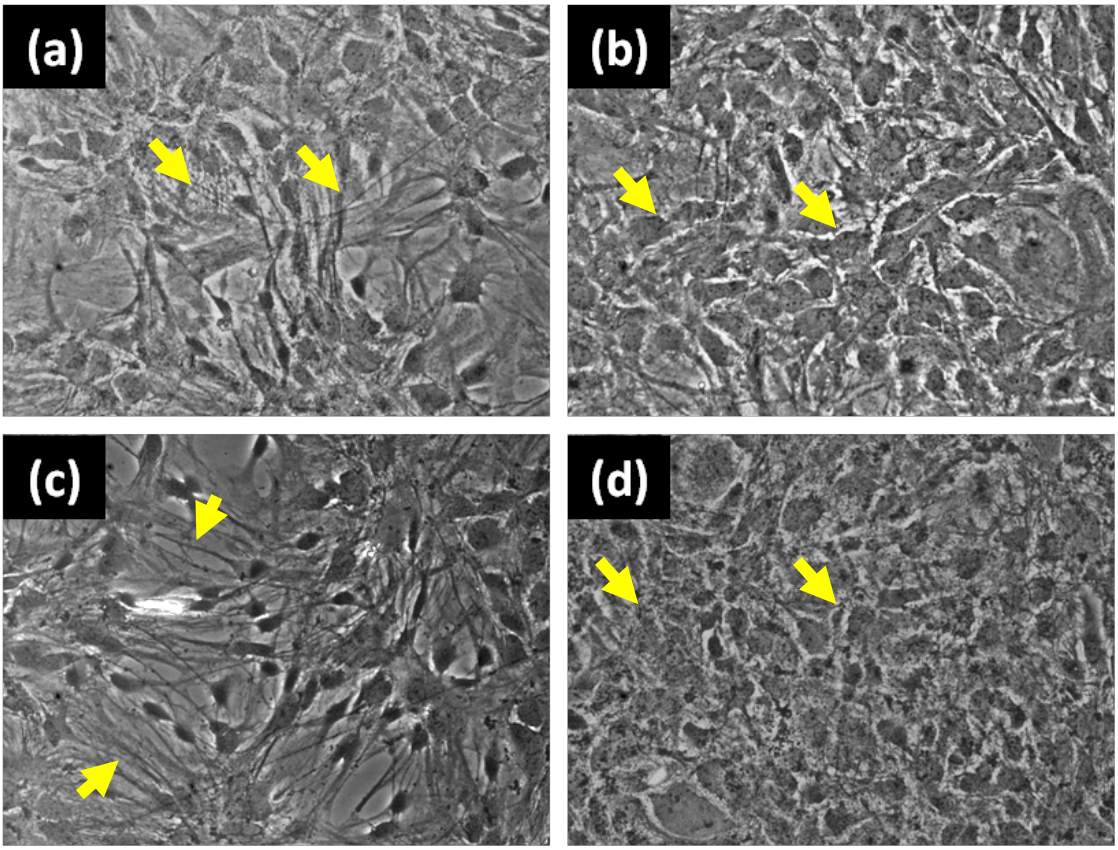

Fig.4.6. Sequential morphological change of glial cells due to sequential treatments of glial cells with LPS in 10% FBS and dbcAMP in 0% FBS: (a) cells were treated with dbcAMP (1mM in 0% FBS for 24 hrs), (b) then cells were treated with by LPS (10 µg/mL in10% FBS for 24 hrs), (c) cells were treated with dbcAMP (1mM in 0% FBS for 24 hrs) again, (d) cells were treated with LPS (10 µg/mL in10% FBS for 24 hrs) again.

3.1.2. Impedance

Impedance and the sequential treatments with LPS in 10% FBS and dbcAMP in 0% FBS demonstrated correlation (Fig.4.7): impedance (1 kHz) increased when cells were treated with LPS in 10% FBS and decreased when cells were treated with dbcAMP in 0% FBS except on days 3 and 4 of the sample in Fig.4.7 (a). Glial cells were plated and cultured in 10% FBS media until they become confluent and then treated with LPS (10µg/mL) in 10% FBS and dbcAMP (1mM) in 0% FBS sequentially. Three

independent probe samples were tested: (a), (b) and (c). Greater impedance changes were found in probe (a), which had the highest cell density. This impedance-treatment correlation varied among different electrode sites in a probe as well as among different probes. This may be due to either overcrowding of the cells in areas of dense encapsulation or sparce cell coverage in low density areas. We suspect that when cells are overcrowded, impedance may not drop even when they are treated with dbcAMP in 0% FBS. On the other hand, when cells are sparce in an area, impedance may not increase even when they are treated with LPS in 10% FBS. However, an important factor to demonstrate this 'dynamic control of glial activation', we found, is to have more than critical mass of cells encapsulating the probe because there should be enough population of cells to make intercellular interaction as previously observed by Nelson and Siman in their *in vitro* study (Nelson and Siman 1990). Inserted pictures of Fig.4.7 show the cell morphology immediately before the impedance measurement of each period of treatment with LPS in 10% FBS or dbcAMP in 0% FBS. As confirmed in the microscopic pictures cells were confluent and viable during each impedance measurement.

Serum also induced higher impedance. Glial cells treated with 10% serum showed higher impedance than the groups treated with 1% FBS (Fig.4.8). Glial cells were plated on day -2 and cultured in 10% FBS media between days -2 and 0. Then the cells were treated with either 1 or 10% FBS on day 0. The cells treated with 10% FBS showed higher impedance than the cells treated with 1% FBS. In addition, please note that the impedance of 1% FBS group dropped dramatically between days 0 and 1 (see Fig. 4.8) when the treatment condition was changed from 10% to 1% FBS. This impedance drop is most likely due to the morphological change from flat to stellate induced by the

treatment with low serum media (1% FBS). In both groups, impedance increased after encapsulation by more than 2 folds and then plateaued up to day 6. This plateau of impedance between days 1 and 6 indicates that our injury model was reliable up to day 6 in both cell layer and electrode surface. Please note that cells used for 10% FBS group was rat astrocytes and fibroblast and for 1% FBS group was mixed mouse brain cells. However, because 1) most of genes are shared between mouse and rat, and 2) in both models, dominant cell type is astrocytes. Therefore, we can deduce the trend of serum effect on impedance.

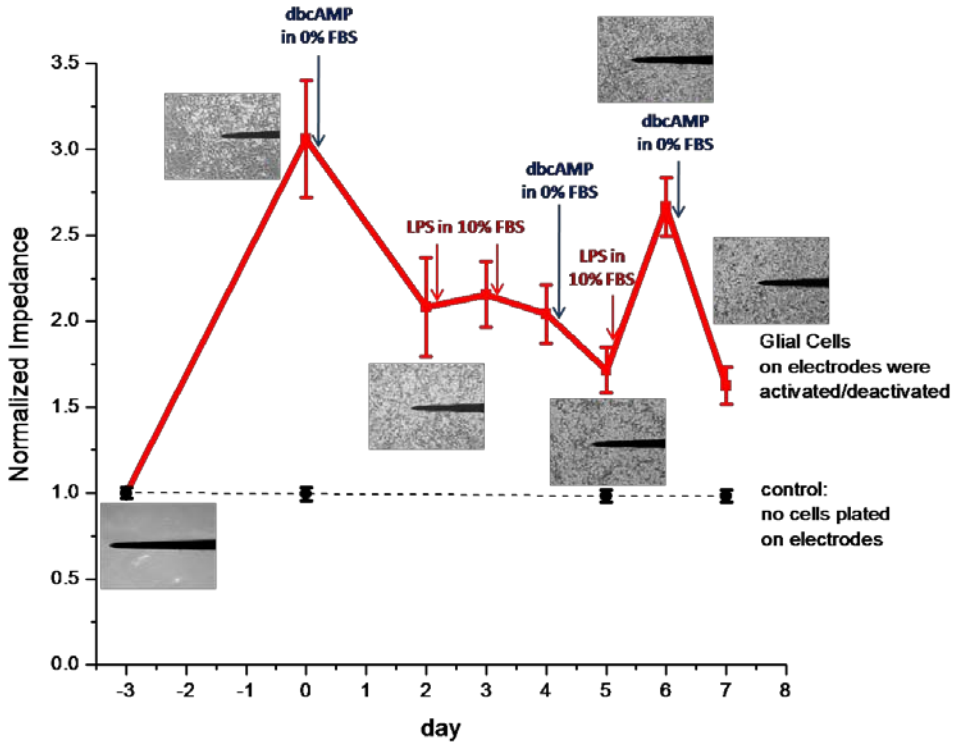

Fig.4.7. Impedance and the sequential treatments with LPS in 10% FBS and dbcAMP in 0% FBS demonstrated correlation: impedance (1 kHz) increased when cells were treated with LPS in 10% FBS and decreased when cells were treated with dbcAMP in 0% FBS except on days 3 and 4 of the sample (a). Glial cells were plated and cultured in 10% FBS media until they become confluent and then treated with LPS (10µg/mL) in 10% FBS and dbcAMP (1mM) in 0% FBS sequentially. Three independent probe samples were tested: (a), (b) and (c). Greater impedance changes were found in probe (a), which had the highest cell density.

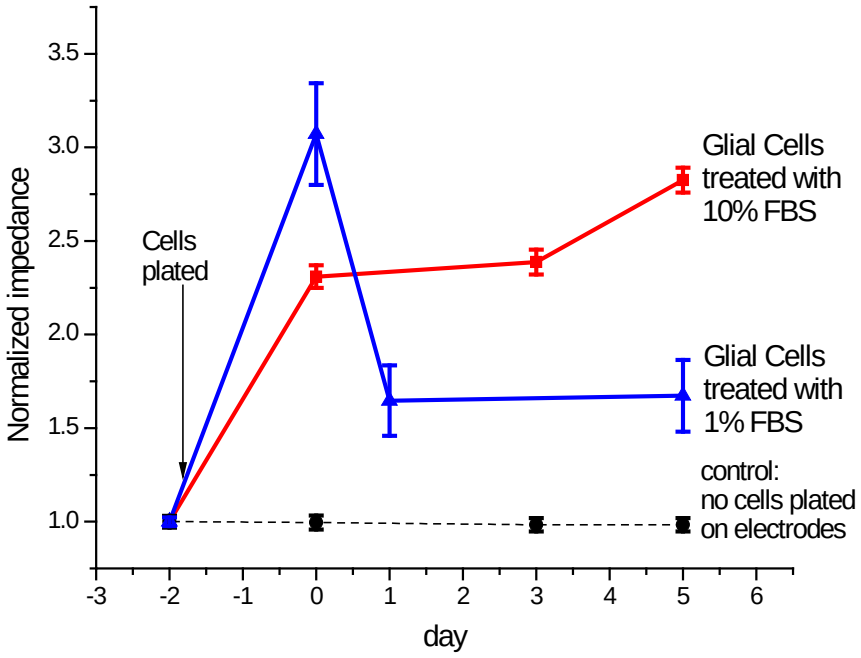

Fig.4.8. Higher serum induced higher impedance. Glial cells were plated and cultured in 10% FBS media between days -2 and 0. Then the cells were subjected to 1% FBS media (blue line) or 10% FBS media (red line) on day 0. Please note that cells used for 10% FBS group was rat astrocytes and fibroblast and for 1% FBS group was mixed mouse brain cells.

3.2. Local drug delivery system for dynamic control of neural environment using parylene-based neural probe

3.2.1. Microfluidics

Fig.4.9 shows a sequential process of a water bubble growing at the fluidic outlet port of the polymer microprobe. HPLC grade water from the syringe pump passed through the fluidic channel in the microprobe and came out through the outlet port of the probe. The water delivered to the tip was detected visually under a bright field microscope.

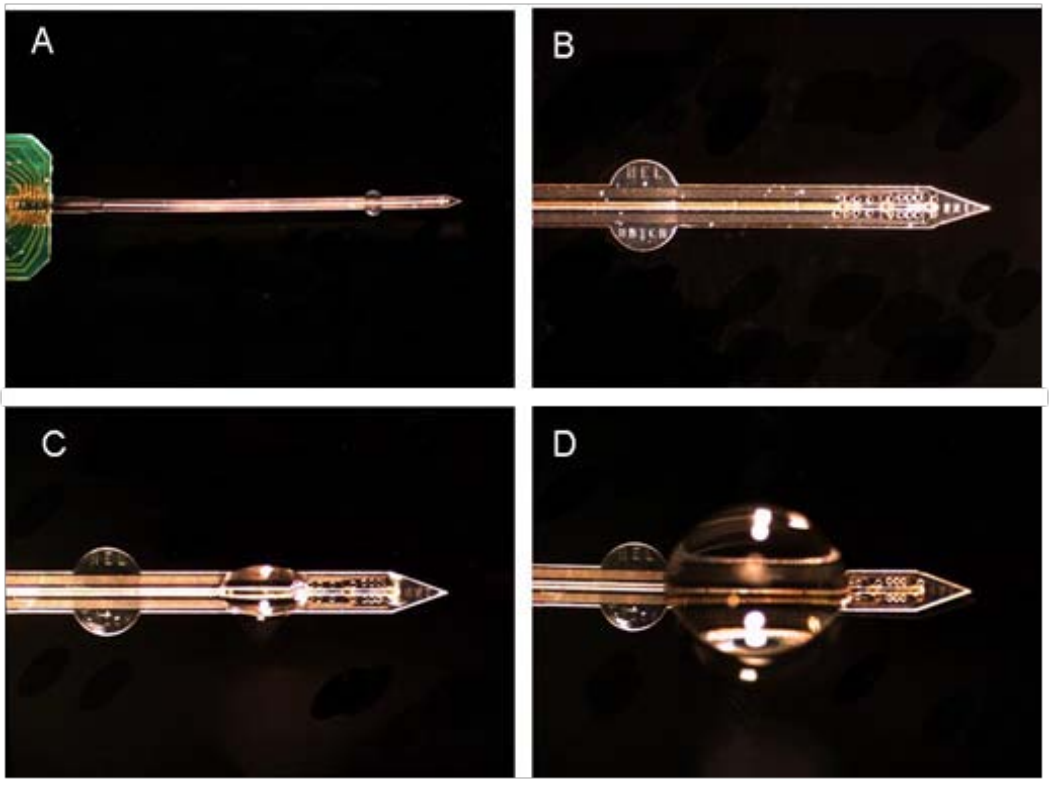

Fig.4.9. Water delivered through a microfluidic neural probe. Figure A shows the whole electrode, up to the bonding pads. The fluid connection (not shown) is to the far left of the probe. Figure B shows the implant portion of the electrode prior to fluid delivery. Figure C show the initiation of flow, which quickly develops into a large bubble of fluid in Figure D.

3.2.2. Drug embedded nanoparticle

Fig 4.10 shows scanning electron micrograph (SEM) of poly(lactic-co-glycolic acid) (PLGA) nanoparticles (NPs) loaded with dexamethasone (DEX) fabricated in neural engineering lab. The NPs were prepared by an oil-in-water emulsion/solvent evaporation method. A box in the picture illustrates the cross sectional size of the microchannel where the NP will be filled.

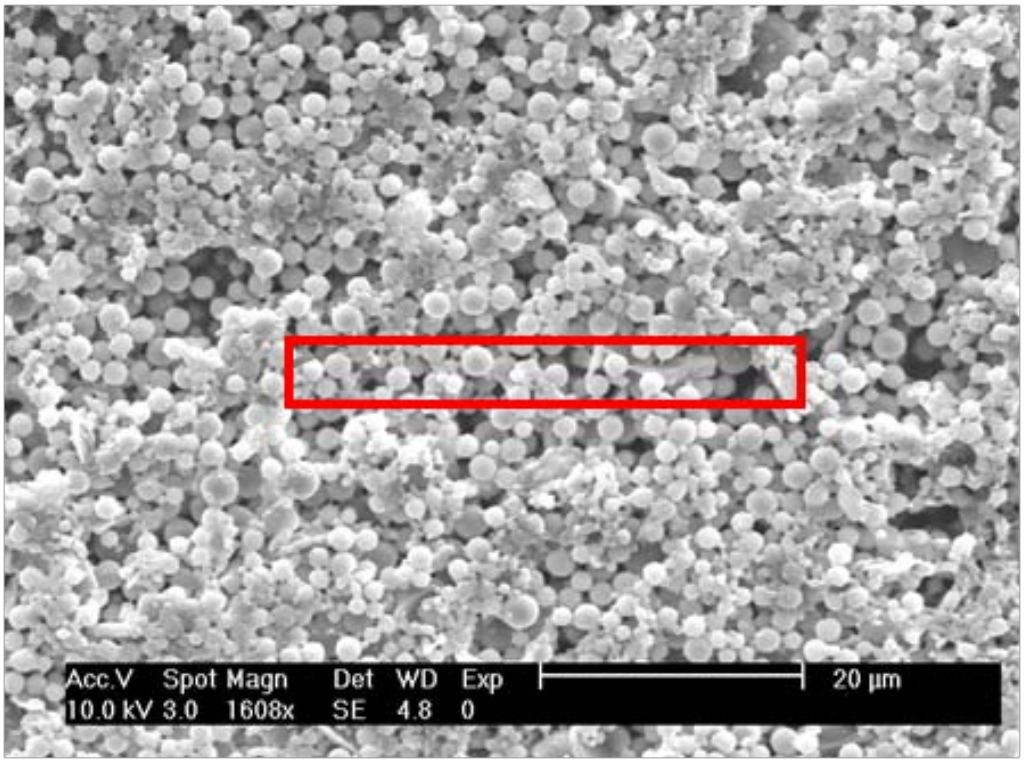

Fig.4.10. Scanning electron microscopy (SEM) picture of the dexamethasone (DEX) embedded nanoparticles (NPs). The red box in the picture illustrates the cross sectional size of the microchannel where the NP will be filled.

4. Discussion

We have successfully demonstrated the proof of concept of dynamic control of glial encapsulation, which is an essential element to realize the SRNP. Although the correlation of our impedance results to probe encapsulation only represent the initial stage in dynamic control of encapsulation, in the long run, this dynamic control could mark the actuation points for the 'Self-Repairing Neural Probe (SRNP)' to reduce the encapsulation maintaining it within an acceptable range for stable signal recording or stimulation.

Glial activation should not only be mitigated at the early stages but also throughout the entire period of probe use to counteract chronic tissue irritation caused by micromotion. This chronic irritation is hypothesized to induce inflammation and activate glial cells (Subbaroyan, Martin et al. 2005).

Since we wanted to achieve morphological changes in a short period of time, we used dbcAMP (1mM) in 0% FBS to induce stellate shape and LPS (10 μg/mL) in 10% FBS to induce flat shape for glial cells. It could be argued, however, that serum could have more roles in morphological changes: cells might have become flat by high (10%) serum contents and have become stellate by no serum contents. Nonetheless, since the goal of this study was to differentiate the impedance between different cell shapes in a short period of time, we wanted to create a set of environments for extreme shifts in cell shapes. To provide more physiological conditions, future studies should include proper pairs of inhibitors and activators such as hirudin/thrombin or proinflammatory cytokines and their inhibitors in a media with the same serum contents.

Parylene based neural probe with microfluidic channel as well as electrical recording/stimulation sites was successfully fabricated and tested for electrical and fluidic functionality in early stage design. Fluidic functionality test showed that the neural probe is sufficiently robust to be used for immediate drug delivery using liquid phase water soluble drugs. NPs were successfully fabricated for Sustained drug delivery using drug-loaded NP-mediated delivery. This feedback controlled drug delivery strategy also could be applied for therapeutic drug delivery application.

References

Agnew, W. F., T. G. H. Yuen, et al. (1986). "Histopathologic Evaluation of Prolonged Intracortical Electrical-Stimulation." Experimental Neurology **92**(1): 162-185.

Arshady, R. (1991). "Preparation of biodegradable microspheres and microcapsules: 2. Polyactides and related polyesters." Journal of Controlled Release **17**(1): 1-21.

Arvin, B., L. F. Neville, et al. (1996). "The role of inflammation and cytokines in brain injury." Neurosci Biobehav Rev **20**(3): 445-52.

Beck, A., R. Penner, et al. (2008). "Lipopolysaccharide-induced down-regulation of Ca2+ release-activated Ca2+ currents (I CRAC) but not Ca2+-activated TRPM4-like currents (I CAN) in cultured mouse microglial cells." J Physiol **586**(2): 427-39.

Beecher, K. L., T. T. Andersen, et al. (1994). "Thrombin receptor peptides induce shape change in neonatal murine astrocytes in culture." J Neurosci Res **37**(1): 108-15.

Biran, R., D. C. Martin, et al. (2005). "Neuronal cell loss accompanies the brain tissue response to chronically implanted silicon microelectrode arrays." Experimental Neurology **195**(1): 115-126.

Bjornsson, C. S., K. L. Smith, et al. (2004). "Brain vascular damage due to neuroprosthetic insertion: casting and quantitative analysis." Journal of Neurochemistry **90**: 67-67.

Coughlin, S. R. and E. Camerer (2003). "PARticipation in inflammation." J Clin Invest **111**(1): 25-7.

Cui, X., J. Wiler, et al. (2003). "*In vivo* studies of polypyrrole/peptide coated neural probes." Biomaterials **24**(5): 777-87.

Dinarello, C. A. (2000). "Proinflammatory cytokines." Chest **118**(2): 503-508.

Edell, D. J., V. V. Toi, et al. (1992). "Factors Influencing the Biocompatibility of Insertable Silicon Microshafts in Cerebral-Cortex." Ieee Transactions on Biomedical Engineering **39**(6): 635-643.

Frampton, J. P., M. R. Hynd, et al. (2007). "Three-dimensional hydrogel cultures for modeling changes in tissue impedance around microfabricated neural probes." Journal of Neural Engineering **4**(4): 399-409.

Frohman, E. M., T. C. Frohman, et al. (1989). "The induction of intercellular adhesion molecule 1 (ICAM-1) expression on human fetal astrocytes by interferon-gamma, tumor necrosis factor alpha, lymphotoxin, and interleukin-1: relevance to intracerebral antigen presentation." J Neuroimmunol **23**(2): 117-24.

Giaever, I. and C. R. Keese (1993). "A Morphological Biosensor for Mammalian-Cells." Nature **366**(6455): 591-592.

Giaver, I. a. K. C. R. (1993). "A morphological biosensor for mammalian cells." **366**(6455): 591.

Giulian, D., J. Woodward, et al. (1988). "Interleukin-1 injected into mammalian brain stimulates astrogliosis and neovascularization." J Neurosci **8**(7): 2485-90.

Goldsack, N. R., R. C. Chambers, et al. (1998). "Moleculs in focus: Thrombin." Int J Biochem Cell Biol **30**(6): 641-6.

Grill, W. M. and J. T. Mortimer (1994). "Electrical-Properties of Implant Encapsulation Tissue." Annals of Biomedical Engineering **22**(1): 23-33.

He, W., G. C. McConnell, et al. (2007). "A novel anti-inflammatory surface for neural electrodes." Advanced Materials **19**(21): 3529-+.

Jain, R. A. (2000). "The manufacturing techniques of various drug loaded biodegradable poly(lactide-co-glycolide) (PLGA) devices." Biomaterials **21**(23): 2475-90.

Jiang, Y., J. Wu, et al. (2002). "Thrombin-receptor activation and thrombin-induced brain tolerance." J Cereb Blood Flow Metab **22**(4): 404-10.

John, G. R., S. C. Lee, et al. (2003). "Cytokines: powerful regulators of glial cell activation." Neuroscientist **9**(1): 10-22.

Johnson, M. D., K. J. Otto, et al. (2005). "Repeated voltage biasing improves unit recordings by reducing resistive tissue impedances." Ieee Transactions on Neural Systems and Rehabilitation Engineering **13**(2): 160-165.

Jones, A. and C. L. Geczy (1990). "Thrombin and factor Xa enhance the production of interleukin-1." Immunology **71**(2): 236-41.

Kipke, D. R. (2004). "Brain-machine interfaces using thin-film silicon microelectrode arrays." 2004 Ieee International Symposium on Circuits and Systems, Vol 5, Proceedings: 497-499.

Leborgne, S. and M. Graber (1994). "Amidase Activity and Thermal-Stability of Human Thrombin." Applied Biochemistry and Biotechnology **48**(2): 125-135.

Lee, S. J. and E. N. Benveniste (1999). "Adhesion molecule expression and regulation on cells of the central nervous system." Journal of Neuroimmunology **98**(2): 77-88.

Lieberman, A. P., P. M. Pitha, et al. (1989). "Production of tumor necrosis factor and other cytokines by astrocytes stimulated with lipopolysaccharide or a neurotropic virus." Proc Natl Acad Sci U S A **86**(16): 6348-52.

Ludwig, K. A., J. D. Uram, et al. (2006). "Chronic neural recordings using silicon microelectrode arrays electrochemically deposited with a poly(3,4-ethylenedioxythiophene) (PEDOT) film." Journal of Neural Engineering **3**(1): 59-70.

Merrill, D. R. and P. A. Tresco (2005). "Impedance characterization of microarray recording electrodes *in vitro*." Ieee Transactions on Biomedical Engineering **52**(11): 1960-1965.

Merrill, J. E. and E. N. Benveniste (1996). "Cytokines in inflammatory brain lesions: helpful and harmful." Trends Neurosci **19**(8): 331-8.

Meyer, J. U., T. Stieglitz, et al. (2001). "High density interconnects and flexible hybrid assemblies for active biomedical implants." IEEE Trans Adv Packaging **24**(3): 366-375.

Moon, T., D. S. Pellinen, et al. (2007). "Local Drug Delivery System for Dynamic Control of Neural Environment using Parylene-Based Microelectrodes." World Congress on Medical Physics and Biomedical Engineering 2006, Vol 14, Pts 1-6 **14**: 3542-3545.

Nelson, R. B. and R. Siman (1990). "Thrombin and its inhibitors regulate morphological and biochemical differentiation of astrocytes *in vitro*." Brain Res Dev Brain Res **54**(1): 93-104.

Nicholson, C. (2001). "Diffusion and related transport mechanisms in brain tissue." Reports on Progress in Physics **64**(7): 815-884.

Nicole, O., A. Goldshmidt, et al. (2005). "Activation of protease-activated receptor-1 triggers astrogliosis after brain injury." J Neurosci **25**(17): 4319-29.

Nicolelis, M. A. L. (2001). "Actions from thoughts." Nature **409**(6818): 403-407.

Normann, R. A. (2007). "Technology Insight: future neuroprosthetic therapies for disorders of the nervous system." Nature Clinical Practice Neurology **3**(8): 444-452.

Obeso, J. A., J. Guridi, et al. (2001). "Deep-brain stimulation of the subthalamic nucleus or the pars interna of the globus pallidus in Parkinson's disease." New England Journal of Medicine **345**(13): 956-963.

Pekny, M. and M. Nilsson (2005). "Astrocyte activation and reactive gliosis." Glia **50**(4): 427-34.

Pellinen, D. S., T. Moon, et al. (2005). "Multifunctional flexible parylene-based intracortical microelectrodes." 2005 27th Annual International Conference of the IEEE Engineering in Medicine and Biology Society, Vols 1-7: 5272-5275.

Polikov, V. S., M. L. Block, et al. (2006). "*In vitro* model of glial scarring around neuroelectrodes chronically implanted in the CNS." Biomaterials **27**(31): 5368-76.

Polikov, V. S., P. A. Tresco, et al. (2005). "Response of brain tissue to chronically implanted neural electrodes." J Neurosci Methods **148**(1): 1-18.

Power, C., S. Henry, et al. (2003). "Intracerebral hemorrhage induces macrophage activation and matrix metalloproteinases." Ann Neurol **53**(6): 731-42.

Ramakers, G. J. and W. H. Moolenaar (1998). "Regulation of astrocyte morphology by RhoA and lysophosphatidic acid." Exp Cell Res **245**(2): 252-62.

Rousche, P. J. and R. A. Normann (1998). "Chronic recording capability of the Utah Intracortical Electrode Array in cat sensory cortex." J Neurosci Methods **82**(1): 1-15.

Rousche, P. J., D. S. Pellinen, et al. (2001). "Flexible polyimide-based intracortical electrode arrays with bioactive capability." Ieee Transactions on Biomedical Engineering **48**(3): 361-371.

Saura, J. (2007). "Microglial cells in astroglial cultures: a cautionary note." J Neuroinflammation **4**: 26.

Sawada, M., N. Kondo, et al. (1989). "Production of tumor necrosis factor-alpha by microglia and astrocytes in culture." Brain Res **491**(2): 394-7.

Schultz, R. L. and T. J. Willey (1976). "The ultrastructure of the sheath around chronically implanted electrodes in brain." J Neurocytol **5**(6): 621-42.

Skaper, S. D., L. Facci, et al. (1986). "Morphological modulation of cultured rat brain astroglial cells: antagonism by ganglioside GM1." Brain Res **390**(1): 21-31.

Song, C. X., V. Labhasetwar, et al. (1997). "Formulation and characterization of biodegradable nanoparticles for intravascular local drug delivery." Journal of Controlled Release **43**(2-3): 197-212.

Spataro, L., J. Dilgen, et al. (2005). "Dexamethasone treatment reduces astroglia responses to inserted neuroprosthetic devices in rat neocortex." Experimental Neurology **194**(2): 289-300.

Stone, S. R. and J. Hofsteenge (1986). "Kinetics of the inhibition of thrombin by hirudin." Biochemistry **25**(16): 4622-8.

Subbaroyan, J., D. C. Martin, et al. (2005). "A finite-element model of the mechanical effects of implantable microelectrodes in the cerebral cortex " Journal of Neural Engineering **2**(4): 103-113.

Suidan, H. S., C. D. Nobes, et al. (1997). "Astrocyte spreading in response to thrombin and lysophosphatidic acid is dependent on the Rho GTPase." Glia **21**(2): 244-52.

Suo, Z., B. A. Citron, et al. (2004). "Thrombin: a potential proinflammatory mediator in neurotrauma and neurodegenerative disorders." Curr Drug Targets Inflamm Allergy **3**(1): 105-14.

Suzumura, A., S. Bhat, et al. (1984). "The isolation and long-term culture of oligodendrocytes from newborn mouse brain." Brain Res **324**(2): 379-83.

Szarowski, D. H., M. D. Andersen, et al. (2003). "Brain responses to micro-machined silicon devices." Brain Research **983**(1-2): 23-35.

Takamiya, M., S. Fujita, et al. (2007). "Simultaneous detections of 27 cytokines during cerebral wound healing by multiplexed bead-based immunoassay for wound age estimation." J Neurotrauma **24**(12): 1833-44.

Turner, J. N., W. Shain, et al. (1999). "Cerebral astrocyte response to micromachined silicon implants." Experimental Neurology **156**(1): 33-49.

Vetter, R. J., J. C. Williams, et al. (2004). "Chronic neural recording using silicon-substrate microelectrode arrays implanted in cerebral cortex." Ieee Transactions on Biomedical Engineering **51**(6): 896-904.

Viswanathan, A. and H. Chabriat (2006). "Cerebral microhemorrhage." Stroke **37**(2): 550-5.

Williams, J. C., J. A. Hippensteel, et al. (2007). "Complex impedance spectroscopy for monitoring tissue responses to inserted neural implants." Journal of Neural Engineering **4**(4): 410-423.

Wolpaw, J. R., N. Birbaumer, et al. (2002). "Brain-computer interfaces for communication and control." Clinical Neurophysiology **113**(6): 767-791.

CHAPTER V

CONCLUSION AND FUTURE DIRECTION

The in vitro models developed in the course of our investigation into the correlation between signal degradation and glial cell encapsulation of neural probes provided evidence of decreasing neural probe functionality with the glial activation, that is, at the very earliest stage of the inflammatory process. Neural probes encapsulated by the activated glial cells activated in the injury model (thrombin/scratch) or the acute inflammation model (LPS) demonstrated higher impedance than the probes encapsulated by the inactivated cells (control). Armed with the evidence of when to intervene in the inflammatory cascade, the next question is how to mitigate the process. Possible solutions may involve the introduction of thrombin inhibitors (hirudin and protease-activated receptor-1 (PAR-1) antagonists), proinflammatory cytokine inhibitors (interleukin-1 receptor antagonist (IL-1RA) and soluble tumor necrosis factor receptor fusion protein (sTNFR:Fc)), antiinflammatory cytokines (IL-10), or antiinflammatory drugs such as corticosteroids (dexamethasone) at the probe site (Stone and Hofsteenge 1986; Eisenberg, Brewer et al. 1991; Balasingam and Yong 1996; Paris, Hickey et al. 1997; Assuma, Oates et al. 1998; Dinarello 1999; Greinacher, Volpel et al. 1999; He, Smith et al. 2005; Spataro, Dilgen et al. 2005). In addition, we can test low dose of thrombin preconditioning during probe insertion, which reduced inflammation and prevented neuronal death induced by intracerebral hemorrhage (Hua, Keep et al. 2003).

Among these deactivation agents, we are more interested in thrombin/cytokine inhibitors rather than steroids because the effect of the inhibitors is specific in blocking the inflammation, therefore, less disrupting the immune system. To block the inflammation chain reaction initiated by the proinflammatory cytokines, we should know which cytokines to target specifically. This specific targeting is important not only to maximize the efficacy of the inhibitors but also to minimize undesired side effects. In addition, we should know how much cytokines and thrombin are secreted to determine the amount of the inhibitors to be used. Therefore identifying and quantifying the cytokines and, also, quantifying thrombin secreted due to the injury are very important.

To identify/quantify cytokines and quantify thrombin, we need to collect and analyze the tissue around the probe insertion site in vivo. The tissue need to be collected and analyzed at different time points to get temporal resolution of the expressed cytokines. Takamiya et al. observed the inflammatory cytokine secretion caused by a traumatic brain injury (Takamiya, Fujita et al. 2007). This temporal trend would be a good reference to the cytokine secretion caused by the injury due to the neural probe insertion. We propose a method: (1) insert neural probes in the brain of animals, (2) collect the tissue around the probe at different time points (30min and 2, 4, 8, 24, 48, 72 and 168 hrs), matching the time scale of cytokine expression, (3) homogenize the tissue to get tissue lysates, (4) analyze the tissue lysates with protein array to screen the expressed cytokines, and (5) analyze the tissue lysates with ELISA to quantify the selected cytokines based on the protein array analysis.

Although blocking inflammation by thrombin/cytokine inhibitors has advantages over steroids, we should note that it might not be as effective as steroids. Since the

inflammation cascade is hypothesized to depend on multiple pathways, blocking just one pathway by a specific cytokine inhibitor might not be enough to block the whole inflammation cascade, which can proceed through another pathway. Therefore, to achieve better efficacy, the efforts should be made to block all the cytokines and thrombin, which involve the inflammation reaction, avoiding interference between inhibitors.

We proposed and verified a novel tissue injury model to activate glial cells, which simulates both mechanical injury and the micro-hemorrhage by the blood vessel rupture. Our results demonstrated that glial cells were well plated on the electrode in the experimental setup and successfully activated. We were able to create both injury (thrombin/scratch) and acute inflammation (LPS) models that mimic the in vivo conditions of neural probe insertion associated with glial activation. The activation observed in our models confirmed the results of previous studies, i.e., that the glial activation induces morphological change and up-regulated inflammatory cytokine expression. These models are expected to be used for further in vitro glial activation studies.

The signature hump in the impedance spectra that is documented in our study and prior in vivo studies could be used as a hallmark in non-invasive and real-time assessment of reactive tissue reaction. We could more precisely assess the glial encapsulation if we employ an equivalent circuit model fit to impedance spectroscopy data (Johnson, Otto et al. 2005; Williams, Hippensteel et al. 2007). By using this model, we can extract the resistive components (Rex and Ren in Fig.5.1) of the encapsulation layer, which are responsible for the impedance increase and precisely represent the signal

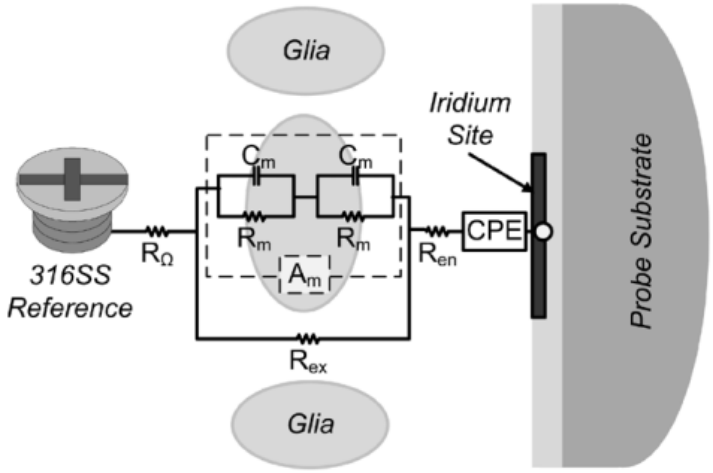

Fig.5.1. The equivalent circuit model fit to impedance spectroscopy data included an iridium microelectrode, an adsorbed resistive layer, and a reactive glial layer. The model includes a sealing resistance (Ren), describing protein adsorption and in some cases a layer of connective tissue. In addition, the model incorporated adjacent cellular layers of glia and macrophages given by a membrane capacitance (Cm), a membrane resistance (Rm) and cellular membrane area (Am) from (Johnson, Otto et al. 2005)

loss due to the encapsulation layer. By using these resistive components, along with the signature hump, we could determine and quantify the glial encapsulation around the neural probe.

We demonstrated the concept for dynamic control of encapsulation level by sequential activation/deactivation of glial cells over a short period of time as shown in Fig 4.5. Although the correlation between the progress of impedance and probe encapsulation represent only the initial stage in dynamic control of encapsulation, in the long run, this dynamic control could mark the actuation points for the 'Self-Repairing Neural Probe (SRNP)' to reduce the encapsulation maintaining it within an acceptable range for stable signal recording or stimulation. Now we would like to move forward to the dynamic control of reactive tissue reaction in vivo. We could test the concept of the

self-repairing neural probe using the prepared local drug delivery system. After implanting a neural probe, watching encapsulation level by monitoring impedance spectra and inject inhibitors at optimal time points to reduce the encapsulation. The reduced encapsulation will be monitored in real-time. Ultimately, we could maintain the encapsulation level within a range in which we can get stable long term recording and stimulation.

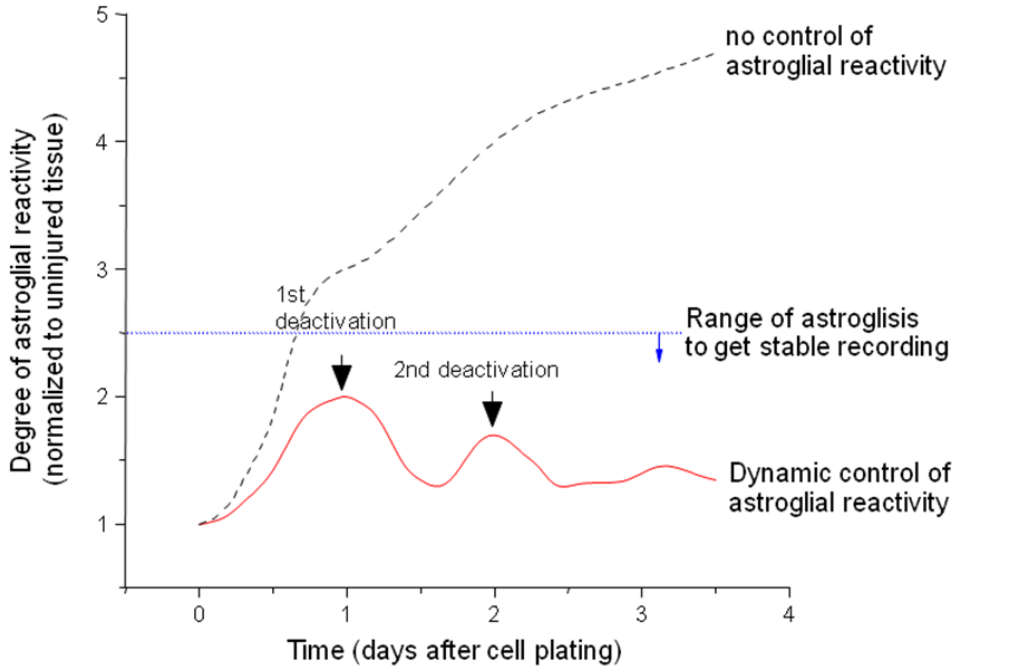

Fig. 5.2. Imaginary plot of dynamic control of glial activation. The goal of this control is to maintain the activation level within a window, in which we can get stable chronic recording.

References

Assuma, R., T. Oates, et al. (1998). "IL-1 and TNF antagonists inhibit the inflammatory response and bone loss in experimental periodontitis." Journal of Immunology **160**(1): 403-409.

Balasingam, V. and V. W. Yong (1996). "Attenuation of astroglial reactivity by interleukin-10." Journal of Neuroscience **16**(9): 2945-2955.

Dinarello, C. A. (1999). "Blocking IL-1 and TNF." Journal of Endotoxin Research **5**(3): 174-176.

Eisenberg, S. P., M. T. Brewer, et al. (1991). "Interleukin-1 Receptor Antagonist Is a Member of the Interleukin-1 Gene Family - Evolution of a Cytokine Control Mechanism." Proceedings of the National Academy of Sciences of the United States of America **88**(12): 5232-5236.

Greinacher, A., H. Volpel, et al. (1999). "Recombinant hirudin (Lepirndin) provides safe and effective anticoagulation in patients with heparin-induced thrombocytopenia - A prospective study." Circulation **99**(1): 73-80.

He, M. M., A. S. Smith, et al. (2005). "Small-molecule inhibition of TNF-alpha." Science **310**(5750): 1022-1025.

Hua, Y., R. F. Keep, et al. (2003). "Thrombin preconditioning attenuates brain edema induced by erythrocytes and iron." Journal of Cerebral Blood Flow and Metabolism **23**(12): 1448-1454.

Johnson, M. D., K. J. Otto, et al. (2005). "Repeated voltage biasing improves unit recordings by reducing resistive tissue impedances." Ieee Transactions on Neural Systems and Rehabilitation Engineering **13**(2): 160-165.

Paris, M. M., S. M. Hickey, et al. (1997). "The effect of interleukin-10 on meningeal inflammation in experimental bacterial meningitis." Journal of Infectious Diseases **176**(5): 1239-1246.

Spataro, L., J. Dilgen, et al. (2005). "Dexamethasone treatment reduces astroglia responses to inserted neuroprosthetic devices in rat neocortex." Experimental Neurology **194**(2): 289-300.

Stone, S. R. and J. Hofsteenge (1986). "Kinetics of the inhibition of thrombin by hirudin." Biochemistry **25**(16): 4622-8.

Takamiya, M., S. Fujita, et al. (2007). "Simultaneous detections of 27 cytokines during cerebral wound healing by multiplexed bead-based immunoassay for wound age estimation." J Neurotrauma **24**(12): 1833-44.

Williams, J. C., J. A. Hippensteel, et al. (2007). "Complex impedance spectroscopy for monitoring tissue responses to inserted neural implants." Journal of Neural Engineering **4**(4): 410-423.